LEVEL

12

TECHNICAL REPORT RG-CR-81-3

RESEARCH ON IMAGE ENHANCEMENT ALGORITHMS

Lewis J. Pinson
Jeffrey P. Lankford
The University of Tennessee
  Space Institute
Tullahoma, TN 37388

DTIC

AUG 2 4 1981

H

May 1981

U.S. ARMY MISSILE COMMAND
Redstone Arsenal, Alabama 35809

81 8   24 004

REPORT DOCUMENTATION PAGE	READ INSTRUCTIONS BEFORE COMPLETING FORM

1. REPORT NUMBER	2. GOVT ACCESSION NO.	3. RECIPIENT'S CATALOG NUMBER
	AD-A103 216	

4. TITLE *(and Subtitle)*	5. TYPE OF REPORT & PERIOD COVERED
Research on Image Enhancement Algorithms	Final Technical Report 7-9-80 to 5-31-81
	6. PERFORMING ORG. REPORT NUMBER

7. AUTHOR(s)	8. CONTRACT OR GRANT NUMBER(s)
L. J. Pinson & J. P. Lankford	DAAH01-80-C-1143

9. PERFORMING ORGANIZATION NAME AND ADDRESS	10. PROGRAM ELEMENT, PROJECT, TASK AREA & WORK UNIT NUMBERS
The University of Tennessee Space Institute Tullahome, TN 37388	

11. CONTROLLING OFFICE NAME AND ADDRESS	12. REPORT DATE
U.S. Army Missile Command Redstone Arsenal, AL 35809	31 May 1981
	13. NUMBER OF PAGES

14. MONITORING AGENCY NAME & ADDRESS *(if different from Controlling Office)*	15. SECURITY CLASS. *(of this report)*
	UNCLASSIFIED
	15a. DECLASSIFICATION/DOWNGRADING SCHEDULE

16. DISTRIBUTION STATEMENT *(of this Report)*

Unlimited Distribution

17. DISTRIBUTION STATEMENT *(of the abstract entered in Block 20, if different from Report)*

18. SUPPLEMENTARY NOTES

19. KEY WORDS *(Continue on reverse side if necessary and identify by block number)*

Image enhancement, real time, man-in-loop, noise cleaning, contrast enhancement, preprocessing, autonomous acquisition, correlation handoff, image quality

20. ABSTRACT *(Continue on reverse side if necessary and identify by block number)*

Six specific image enhancement alforithms are analyzed, simulated and evaluated for potential real-time application to imagery obtained from target acquisition systems. Three processing methods are recommended as operator controlled options for application to the imagery. They are median filtering, gradient processing and locally adaptive gain control. The objective for this effort was to identify and examine methods for enhanced acquisition and handoff for small targets in a complex and cluttered background.

DD FORM 1473 EDITION OF 1 NOV 65 IS OBSOLETE
1 JAN 73

SUMMARY

A major operational need facing the next generation of Scout (ASH) and Attack (AAH) helicopters is to detect targets from nap-of-earth altitudes, on a realistic battlefield in a complex and cluttered scene. The current technology base supports the development of a complement of sensors spanning a region of the spectrum from visible to far infrared. Precision pointing and stabilization has been demonstrated to insure that target detection and recognition requirements can be met. However, the problem for the operator to detect low contrast targets in a complex and cluttered scene at long ranges and minimum exposure time to insure adequate survivability still exists. The targets of interest here are primarily the single, high threat target which will not be contained with the main body of target tanks and will not present many detection cues. This work is oriented primarily for TADS type acquisition systems for airborne missile fire control, although it has general application to any video format imaging system. It holds high potential for improving target signature for seeker lockon and tracking and can possible simplify correlation techniques for missile seeker handoff by preprocessing the seeker and sensor imagery.

Image processing techniques offer potential for improved performance through target acquisition (autonomous or man-in-loop) at greater standoff ranges or in less time and through automatic handoff of identified targets from precision pointing and tracking system to the missile seeker. For this work the emphasis is on man-in-loop target acquisition. Under the constraint of real-time or near real-time operation, specific image processing methods have been identified for analysis and evaluation in terms of improved performance by a human observer seeking to detect/recognize targets in a cluttered background under marginal viewing conditions.

Six specific image enhancement algorithms were analyzed, simulated and
evaluated for potential real-time application to imagery obtained from target
acquisition systems. As a result of this effort, three processing methods
are recommended as operator controlled options for application to the imagery.
One method is a median filter, which reduces noise without blurring edge detail.
The other method is an adaptive edge processor operating on the image gradient.
The third method is local area gain control with a mean dependent gain term.

PREFACE

This final technical report describes the objectives, methods and results of contract DAAH01-80-C-1143 on "Research on Image Enhancement Algorithms" and covers the period 9 July 1980 to 31 May 1981. This effort was conducted by the Gas Diagnostics Research Division of the University of Tennessee Space Institute, Tullahoma, Tennessee 37388. It was sponsored by the Guidance and Control Directorate, U. S. Army Missile Command, Redstone Arsenal, Alabama, 35809.

The authors wish to express their appreciation to Mr. James Baumann and Mr. William Malcolm of MICOM for their technical guidance. Further appreciation is expressed to Mr. James McLean of MICOM for the use of his image display system and special thanks go to Mr. Ed Peters for many hours spent in helping utilize the display system.

TABLE OF CONTENTS

LIST OF ILLUSTRATIONS

LIST OF TABLES

1. INTRODUCTION AND EXECUTIVE SUMMARY

This final technical report describes the objectives, methods and results of contract DAAH01-80-C-1143 on "Research on Image Enhancement Algorithms" and covers the period 9 July 1980 to 31 May 1981. Six specific image enhancement algorithms were analyzed, simulated and evaluated for potential real-time application to imagery obtained from target acquisition systems. As a result of this effort, three processing methods are recommended as operator controlled options for application to the imagery. One method is a median filter, which reduces noise without blurring edge detail. The other method is an adaptive edge processor operating on the image gradient. The third method is local area gain control with a mean dependent gain term.

Details of the six methods investigated and evaluation comparisons are given in the reamining sections of this report.

1.1 <u>Application and relation to performance</u>. A major operational need facing the next generation of Scout (ASH) and Attack (AAH) helicopters is to detect targets from nap-of-earth altitudes, on a realistic battlefield in a complex and cluttered scene. The current technology base supports the development of a complement of sensors spanning a region of the spectrum from visible to far infrared. Precision pointing and stabilization has been demonstrated to insure that target detection and recognition requirements can be met. However, the problem for the operator to detect low contrast targets in a complex and cluttered scene at long ranges and minimum exposure time to insure adequate survivability still exists. The targets of interest here are primarily the single, high threat target which will not be contained with the main body of target tanks and will not present many detection cues. This work is oriented

1

primarily for TADS type acquisition systems for airborne missile fire control, although it has general application to any video format imaging system. It holds high potential for improving target signature for seeker lockon and tracking and can possibly simplify correlation techniques for missile seeker handoff by preprocessing the seeker and sensor imagery.

Image processing techniques offer potential for improved performance through target acquisition (autonomous or man-in-loop) at greater standoff ranges or in less time and through automatic handoff of identified targets from a precision pointing and tracking system to the missile seeker. For this work the emphasis is on man-in-loop target acquisition. Under the constraint of real-time or near real-time operation, specific image processing methods have been identified[1] for analysis and evaluation in terms of improved performance by a human observer seeking to detect/recognize targets in a cluttered background under marginal viewing conditions.

Performance of an observer in acquiring a target is usually given in terms of probabilities of specific subjective decisions by the observer[2]. Target acquisition is taken to mean the detection and/or recognition of potential target classes by a human observer viewing a display of the imaged scene. Performance in terms of detection probability and recognition probability can be related to quantifiable system performance measures for the sensor system.

$$P_{D,R} = P_1 \cdot P_2 \cdot P_3 \cdot P_4$$

where P_1 is a search-term probability which depends on scene clutter

P_2 depends on contrast

P_3 depends on resolution

P_4 depends on noise.

Based on this model, image processing methods which improve contrast, resolution or signal-to-noise are candidates for application to the target acquisition problem. Definitions and properties for the six processing methods are given in Section 2. Subjective and quantitative evaluation measures are discussed in Section 3.

```
┌──────────────────────┐        ┌────────────────────────────┐
│ INPUT IMAGERY        │        │ PROCESSORS                 │
│                      │        │                            │
│ •Sine & Square Wave  │───────▶│ 1.  LAGC         Contrast  │
│ •TGT on Uniform BKGD │        │ 2.  HIST. MOD.   Resolution│
│ •TADS Imagery        │        │ 3.  EDGE-WINDOW  Enhancement│
│ •Noise               │        │                            │
│                      │        │ 4.  MEDIAN                 │
│                      │        │ 5.  ADAPTIVE LPF   Noise   │
│                      │        │ 6.  WINDOW-SMOOTH  Reduction│
│                      │        │                            │
│                      │        │ - Parallel/Serial Comginations│
└──────────────────────┘        └────────────────────────────┘
```
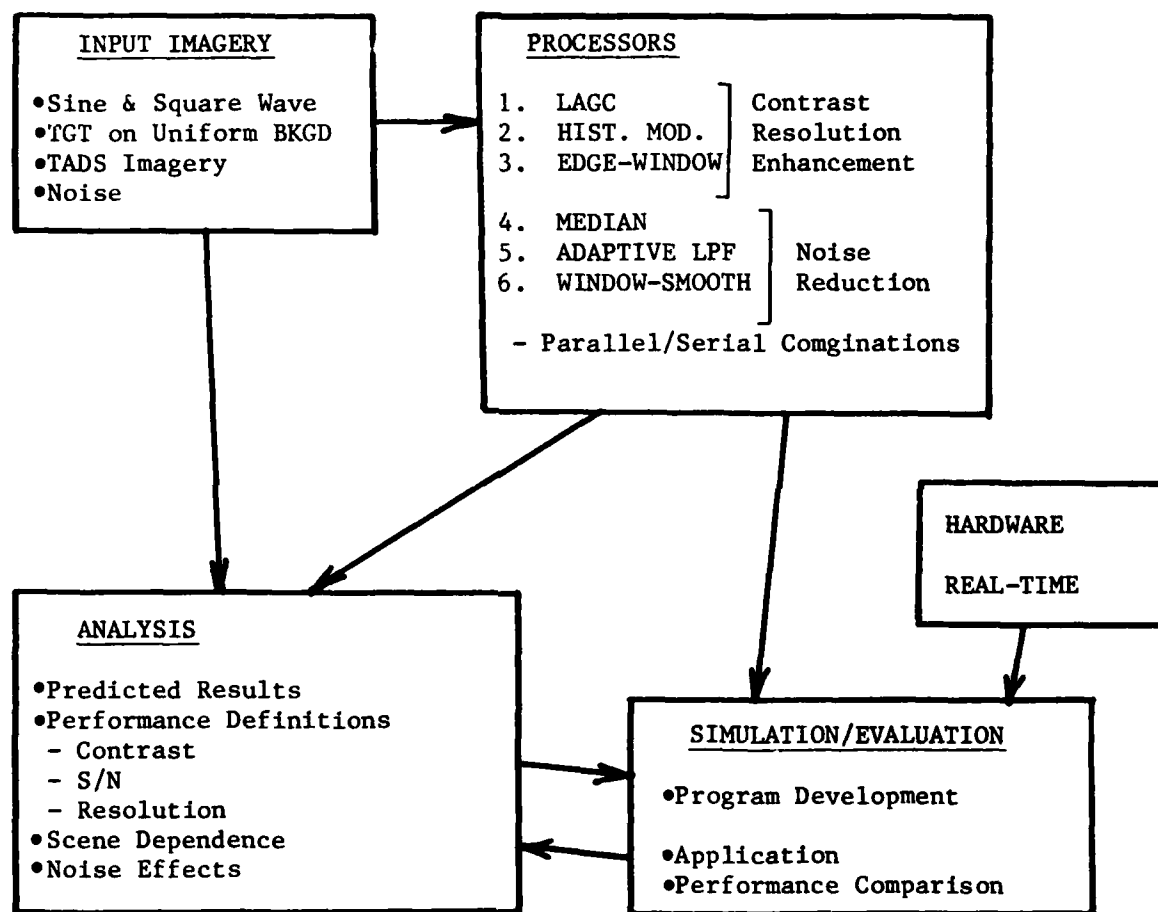
FIGURE 1.1 Elements of image enhancement research

INPUT IMAGERY
•Sine & Square Wave
•TGT on Uniform BKGD
•TADS Imagery
•Noise

PROCESSORS
1. LAGC   Contrast
2. HIST. MOD.   Resolution
3. EDGE-WINDOW   Enhancement
4. MEDIAN
5. ADAPTIVE LPF Noise
6. WINDOW-SMOOTH Reduction
- Parallel/Serial Comginations

HARDWARE
REAL-TIME

ANALYSIS
•Predicted Results
•Performance Definitions
 - Contrast
 - S/N
 - Resolution
•Scene Dependence
•Noise Effects

SIMULATION/EVALUATION
•Program Development
•Application
•Performance Comparison

1.2 <u>Methods investigated and overall plan</u>. The overall effort is outlined graphically in Figure 1.1. It consisted of analysis, simulation and evaluation of six image processing methods: 1. local area gain control (LAGC), 2. histogram modification (HIST), 3. edge detection (EDGE), 4. median filtering (MED), 5. adaptive lowpass filtering (ALPF), and 6. window smoothing (WIND).

Each processing method was evaluated individually to determine the effect of different parameter values on the resultant processed image. Additionally, the processors were evaluated in various serial and parallel combinations to determine if more than one process should be considered for implementation.

Quantitative measures of target-to-background contrast, signal-to-noise ratio, target to clutter ratio and resolution were defined and computed for the imagery before and after each processing step. Subjective evaluation was accomplished in terms of relative clarity of known target boards and/or vehicles in the imagery. A detailed description of the imagery and the processor simulations is given in Section 4.

1.3 <u>Significant results and recommendations</u>. Of the methods investigated for noise reduction median filtering offers the least amount of image blurring. It is therefore recommended for implementation. Further, the noise reduction processing should be done first in the processing sequence. From that point it is recommended that further processing be done and combined in parallel with the median filtered image. Thus a serial-parallel processing system (median — parallel processing) is recommended.

Options for additional processing include LAGC (with mean dependent gain) and gradient/edge processing. The LAGC option with gain $= \frac{1}{\sigma}$ was found to introduce excessive clutter. Edge detection threshold based on

4

statistics in a local window produced results which showed promise for identifying low-contrast objects. Window size for threshold calculation was found to be very important and should be operator selectable.

Further details of the processers and performance are given in subsequent sections of this report. A recommended processor implementation is diagrammed in section 5.

2. IMAGE PROCESSING ALGORITHMS-DEFINITION AND PROPERTIES

The following six processing methods were evaluated as part of this effort:

1. Local area gain control - an adaptive contrast enhancement method,

2. Histogram modification - both histogram equalization and histogram hyperbolization were evaluated for expected contrast enhancement,

3. Edge detection - binary edge maps dependent on a threshold applied to the gradient image,

4. Median filtering - a non-linear filter for improving signal, to noise with a passband which is adaptive to scene content,

6. Window smoothing - a simple averaging window for reducing noise.

2.1 <u>Local area gain control</u> (LAGC) - LAGC is a non-linear adaptive processor which is designed to enhance low-contrast sub-regions in an image without causing high contrast regions to saturate the display dynamic range. It thus seeks to avoid the major problem encountered with simple linear contrast stretching. LAGC is a method whereby the gain applied to the center pixel within a window varies with the statistics of all pixel values in the window. Gain must be re-computed for each pixel as the window moves across the image.

If the input image $f(x,y)$ is processed to give output image $g(x,y)$ then LAGC is defined by

$$g(x,y) = G\left[f(x,y) - m_{AB}(x,y)\right] + km_{AB}(x,y) \tag{2-1}$$

5

where: $-m_{AB}(x,y)$ is the mean pixel value within an A x B window centered

about pixel location (x,y)

- $G = C/S_{AB}(x,y)$ is the adaptive gain

- $S_{AB}(x,y)$ is the standard deviation of pixel values within the

A x B window centered at pixel location (x,y)

- C and k are constants which control the gain magnitude and

relative mean value added back to the signal.

The method is diagrammed in Figure 2.1
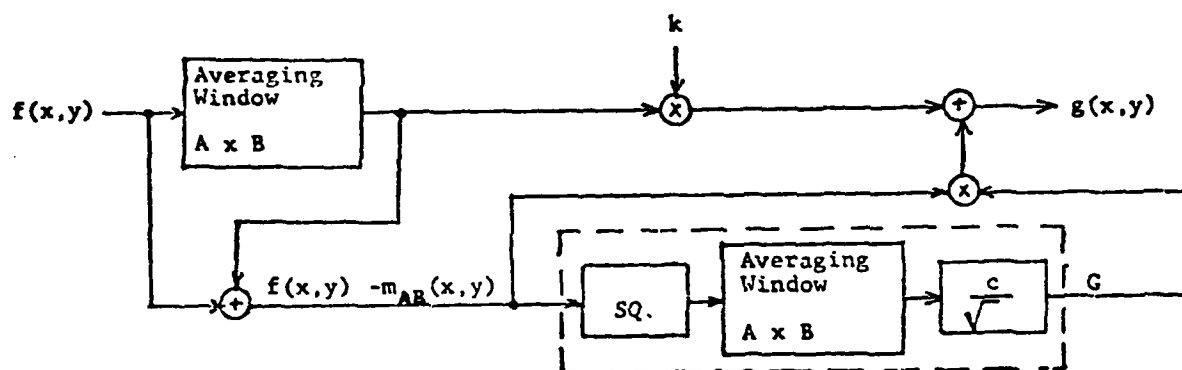
FIGURE 2.1 Local area gain control (LAGC) method.

An alternate version of the LAGC method uses $G = Cm_{AB}(x,y)/S_{AB}(x,y)$ as

the gain term in (2-1). Both versions were simulated.

For this effort, simulations were done for square windows only (A=B).

Window sizes of (3 x 3), (5 x 5) and (15 x 15) were implemented and evaluated.

An analysis of expected contrast transfer for the LAGC method was done.

Results of this analysis are given in Appendix A.

2.2 Histogram modification. Histogram modification is a point intensity

transformation which is designed to enhance image contrast based on global

statistics for the image. The procedure is as follows.

If the input image f(x,y) has an intensity histogram p(f), and the out-

put image g(x,y) is to have the desired histogram p(g) then g(x,y) is obtained

from

$$g(x,y) = r^{-1} \left[s \left\{ f(x,y) \right\} \right] \qquad (2-2)$$

where: $r^{-1} \left[\bullet \right]$ is the inverse function of $r \left[\bullet \right]$, and

$$s(f) = \int_{-\infty}^{f} p(f)df \qquad (2-3)$$

$$r(g) = \int_{-\infty}^{g} p(g)dg \quad . \qquad (2-4)$$

Thus s(f) is the cummulative distribution function for intensities in

f(x,y), and r(g) is the cummulative distribution function for intensities in

g(x,y). These functions are implemented digitally as

$$s(m) = \sum_{i=0}^{m} P_{i,f} \qquad (2-5)$$

$$r(n) = \sum_{j=0}^{n} P_{j,g} \qquad (2-6)$$

for m,n = 0, 1, 2 --- 255 (8 bit images). Then the transformation (2-2) is

implemented with a look-up table.

2.2.1 Equalization. Histogram equalization is the process whereby the output

histogram p(g) has a uniform density (ie, a flat histogram). The resultant

equalized image exhibits maximum entropy.

The equalization process is accomplished by first computing the discrete

histogram $P_{i,f}$ for i = 0, 255 of the imput image f(x,y). Then s(m) is calculated

using (2-5). The equalized output image is then obtained from

$$g(f) = s(f) \bullet \frac{255}{KL} \qquad (2-7)$$

where KL is the total number of pixels in the image.

2.2.2 **Hyperbolization.** This method produces an output image whose histogram has an hyperbolic shape which emphasizes the lower pixel values. It's importance is derived from models for human visual response. The transformation for hyperbolization is given by[3]

$$g(f) = c \left\{ \exp \left[\ell n \left(1 + \frac{255}{c} \right) \frac{s(f)}{KL} \right] - 1 \right\} \qquad (2\text{-}8)$$

where c is a specified parameter (larger values of c provide more emphasis of low pixel values).

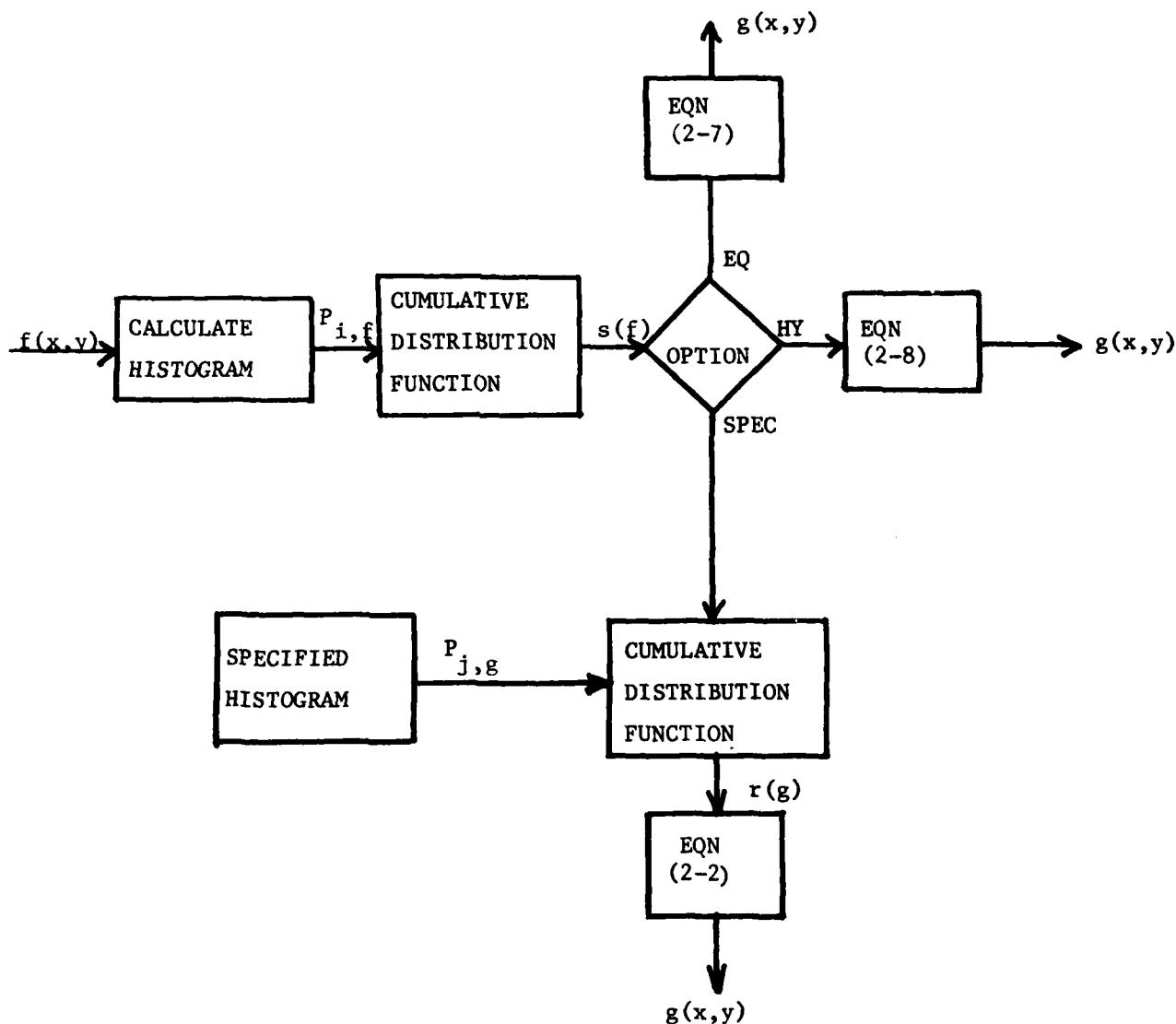The histogram modification method is outlined in Figure 2.2

Figure 2.2 Histogram modification

8

2.3 <u>Median filtering</u>.   A median filter is one which replaces the center pixel within a window with the median in the window.   It is a non-linear processor which reduces noise and blemishes in the image without as much edge blurring as results from low pass and related smoothing windows.   The procedure is outlined in Figure 2.3
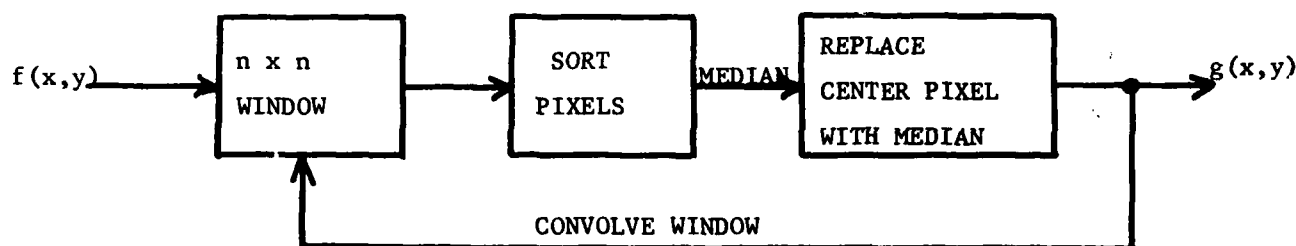

Figure 2.3 Median filter

For an n x n window, n^2 pixels must be sorted at each window position. For this effort window sizes of (3 x 3) and 5 x 5) were implemented.

2.4 <u>Adaptive low pass filtering</u>.   This method applies a linear smoothing filter to the image and adjusts the filter passband adaptively dependent on the image statistics in a local window.

Consider the input image modeled in one direction as

$$f(x) = a + bx + cx^2 + dx^3 \qquad (2-9)$$

filtered by a low pass (averaging) window of width L

$$g(x) = \frac{1}{L} \sum_{n = -\frac{L-1}{2}}^{\frac{L-1}{2}} f(n) \qquad (2-10)$$

Then the error at the center pixel due to smoothing is

$$\varepsilon = \left| \frac{g(o) - f(o)}{f(o)} \right| = \frac{L^2}{12} \left| \frac{c}{a} \right| \qquad (2-11)$$

9

For a specified error in the center pixel value it is possible to calculate the required filter width L

$$L = \left[12 \left| \frac{a}{c} \right| \varepsilon \right]^{\frac{1}{2}} \tag{2-12}$$

where a and c are computed as least square error estimates using[4]

$$a = \frac{7g_a - g_c}{21} \tag{2-13}$$

$$c = \frac{g_c - 4g_a}{84} \tag{2-14}$$

where:

$$g_a = \sum_{i=-3}^{3} f(i)$$

$$g_c = \sum_{i=1}^{3} \left[f(i) + f(-i) \right] i^2 \tag{2-15}$$

based on a seven pixel window $\left| \frac{c}{a} \right|$ is calculated for 0°, 90°, $\pm 45^o$. The largest $\left| \frac{c}{a} \right|$ determines the maximum filter size L.

For this effort, smoothing windows of (3 x 3) and (5 x 5) averages were applied non-adaptively to the imagery. Since significant blurring was noticeable for both window sizes, and since (3 x 3) is the smallest practical averaging window size, it was suspected that the adaptive window would not give different results (eg. it would essentially always choose the smallest window (3 x 3)).

The above hypothesis was tested by computing the maximum values for L across the image using equations (2-12), (2-13), (2-14) and (2-15) for selected errors. Except for a few isolated pixels, the value of L was always less than three and often equal to one. As a result, it was felt that any averaging window applied to the image would degrade image quality. Therefore, the median filtering window was used for subsequent noise reduction processing.

2.5 Windowing. Windowing is a technique whereby the input image is convolved with an n x n (n odd) array of coefficients. Smoothing or gradient operations

differ only in the choice of coe-ficient magnitudes and signs. For the
pixel position (x,y) at the center of the window, the output is

$$g(x,y) = k \sum_{i=-\frac{n-1}{2}}^{\frac{n-1}{2}} \sum_{j=-\frac{n-1}{2}}^{\frac{n-1}{2}} C_{ij} \, f(x+i, y+j) \qquad (2\text{-}16)$$

A number of different sets of coefficients have been examined in the literature.
For this effort two smoothing windows and four gradient operators were
implemented.

2.5.1 <u>Smoothing</u>. Image smoothing was implemented as an averaging window
convolved with the input image. Two window sizes (3 x 3) and (5 x 5) were
used. The algorithm is

$$g(x,y) = \frac{1}{n^2} \sum_{i=-\frac{n-1}{2}}^{\frac{n-1}{2}} \sum_{j=-\frac{n-1}{2}}^{\frac{n-1}{2}} f(x+i, y+j) \qquad (2\text{-}17)$$

for n = 3 and n = 5 .

2.5.2 Gradient Processing.

2.5.2.1 <u>Gradient images</u>. One option on this processing method is to simply
display the gradient image as the output. There are of course several options
on which gradient operator to use. For this effort, four different methods
were used to compute gradient images.

    1. Prewitt –

$$g_1(x,y) = f(x,y) * \begin{bmatrix} 1 & 0 & -1 \\ 1 & 0 & -1 \\ 1 & 0 & -1 \end{bmatrix} \qquad (2\text{-}18)$$

$$g_2(x,y) = f(x,y) * \begin{bmatrix} -1 & -1 & -1 \\ 0 & 0 & 0 \\ 1 & 1 & 1 \end{bmatrix} \qquad (2\text{-}19)$$

$$g(x,y) = \max \left| g_1(x,y), \, g_2(x,y) \right| \qquad (2\text{-}20)$$

2. Sobel –

$$g_1(x,y) = f(x,y) * \begin{bmatrix} 1 & 0 & -1 \\ 2 & 0 & -2 \\ 1 & 0 & -1 \end{bmatrix} \qquad (2\text{-}21)$$

$$g_2(x,y) = f(x,y) * \begin{bmatrix} -1 & -2 & -1 \\ 0 & 0 & 0 \\ 1 & 2 & 1 \end{bmatrix} \qquad (2\text{-}22)$$

$$g(x,y) = \max \left| g_1(x,y), \; g_2(x,y) \right| \qquad (2\text{-}23)$$

3. Unsharp mask – subtract smoothed image from original

$$g(x,y) = f(x,y) - f(x,y) * \frac{1}{9} \begin{bmatrix} 1 & 1 & 1 \\ 1 & 1 & 1 \\ 1 & 1 & 1 \end{bmatrix} \qquad (2\text{-}24)$$

$$\text{and } g(x,y) = f(x,y) - f(x,y) * \frac{1}{25} \begin{bmatrix} 1 & 1 & 1 & 1 & 1 \\ 1 & 1 & 1 & 1 & 1 \\ 1 & 1 & 1 & 1 & 1 \\ 1 & 1 & 1 & 1 & 1 \\ 1 & 1 & 1 & 1 & 1 \end{bmatrix} \qquad (2\text{-}25)$$

4. Symmetric – a single pass gradient operator

$$g(x,y) = f(x,y) * \begin{bmatrix} -c & -b & -c \\ -b & a & -b \\ -c & -b & -c \end{bmatrix} \qquad (2\text{-}26)$$

2.5.2.2 Edge maps. The gradient images may be thresholded to produce a binary edge map.

$$\begin{aligned} g(x,y) &= 255 \quad \text{if} \quad g(x,y) \geq T \\ &= 0 \quad\;\; \text{if} \quad g(x,y) < T \end{aligned} \Bigg] \qquad (2\text{-}27)$$

This was done using two methods.

1. Global threshold –

$$T = \mu + k\sigma \qquad (2\text{-}28)$$

where μ and σ are the mean and standard deviation of the total image.

2. Local threshold (adaptive) –

$$T_{AB} = \mu_{AB} + k\sigma_{AB} \qquad (2\text{-}29)$$

where μ_{AB} and σ_{AB} are statistics in a local A x B window. The locally

adaptive threshold provides for detection of less distinct edges that would have been suppressed by the sharp edges using a global threshold. The window size A x B must be chosen as a parameter. For this effort, local statistics were computed for (3 x 3), (5 x 5) and (15 x 15) windows.

2.6 Output image combinations. Several options were exercised on combinations of processed images and the original image for output display.

2.6.1 Original plus gradient or edge. For this option, two images were combined into one in a way to produce an output image which utilized the full dynamic range of gray levels (0-255). One method was to simply add the two images and rescale the sum as indicated in Figure 2.4
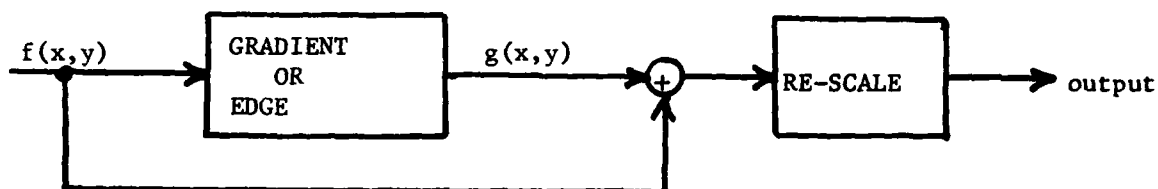

Figure 2.4 Rescaled sum output image.

The problem with this method is that the re-scaling is biased by large gradient values. The result is a darker original image with bright edges. To maintain the same range of gray levels in the original image but with bright edges, an edge replacement output option was used as indicated in Figure 2.5
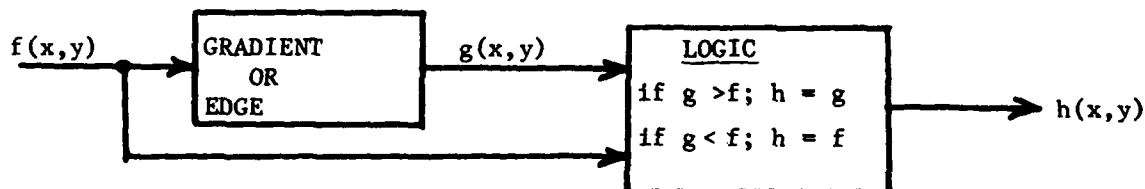

Figure 2.5 Original with edge replacement

13

2.6.2 <u>Serial combinations</u>. For a number of simulation runs the input image was
subjected to two or three processors applied serially. In these cases the
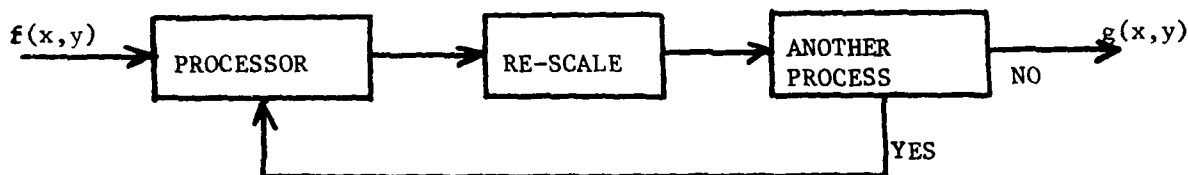image was re-scaled to (0-255) after each process as indicated in Figure 2.6.

Figure 2.6   Serial processing

2.6.3 <u>Parallel combinations</u>. For the case of parallel combinations of
multiple processors, the procedure outlined in Figure 2.7 was followed using
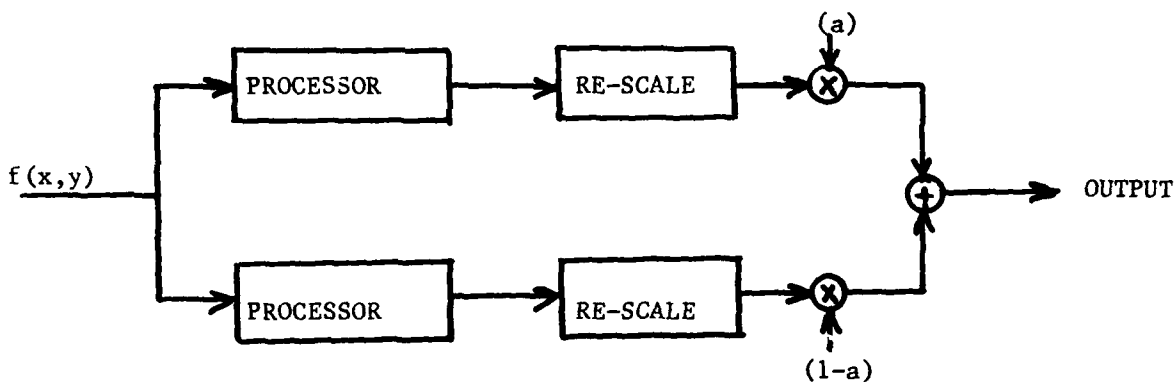various values for the parameter "a".

Figure 2.7   Parallel combinations

Re-scaling to a gray level range of 0-255 was accomplished as shown. For
the case of three processors combined in parallel, the multiplication weights
were equal $\left(\frac{1}{3}\right)$ for each image.

3.   EVALUATION MEASURES

3.1 <u>Subjective methods</u>. Results of the various processing combinations are
evaluated by subjective comparisons and comments as given in this report.
(Sections 4.and 5.)

3.2 <u>Quantitative methods</u>. The objectives for any quantitative evaluation

14

measures are that they be directly relatable to improved performance. For target acquisition by a human observer looking at a CRT display, performance is related to four quantitative image quality measures: S/N, resolution, contrast and scene clutter. For autonomous acquisition and correlation systems, performance is also relatable to these image quality measures. The following definitions may require modification depending on the application; however, they served as first cut image quality definitions for this effort.

3.2.1 <u>Contrast.</u> Contrast transfer is defined as the ratio of contrast in the processed image (output) to that of the same area in the unprocessed (input) image. For this application both peak and average values of modulation contrast over a specified target/background area were calculated.

$$\text{Peak Contrast Transfer } C_p = \frac{M_p(\text{output})}{M_p(\text{input})} \qquad (3\text{-}1)$$

$$\text{Average Contrast Transfer } C_a = \frac{M_a(\text{output})}{M_a(\text{input})} \qquad (3\text{-}2)$$

where M is modulation contrast defined by

$$\text{Peak: } M_p = \frac{\left| f_{max} - f_{min} \right|}{f_{max} + f_{min}} \qquad \text{Average: } M_a = \frac{\left| f_1 - f_2 \right|}{f_1 + f_2} \qquad (3\text{-}3)$$
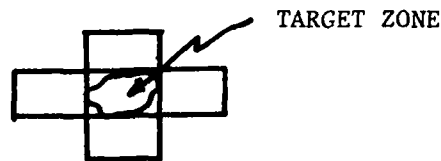
where:

<u>for target on background:</u>
f_{max} = maximum value on target

f_{min} = minimum value on background

f_1 = average target value

f_2 = average background value

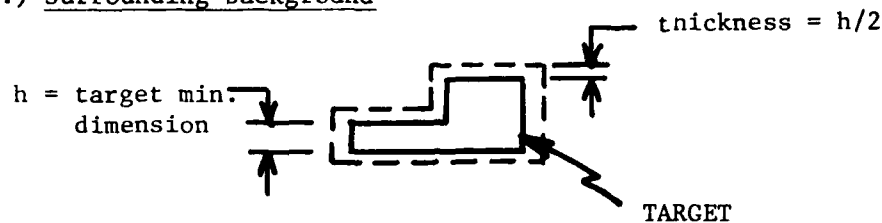There are several options on how to define the background values including the following three:

15

a.) side by side

Adjacent Background
Zone of Equal Size

TARGET ZONE
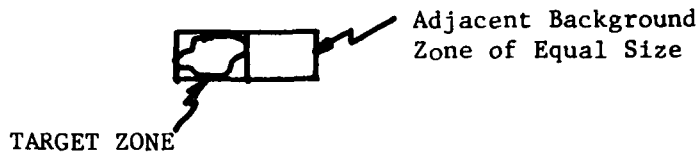
b.) 4 neighbor average background

TARGET ZONE

c.) surrounding background

tnickness = h/2

h = target min.
dimension

TARGET

background consists of band of pixels

bordering the target and with a thickness

one-half the target minimum dimension

For the simulation runs with images which contained targets the procedure
was to locate the target, specify its size, then choose a background option
and compute equations (3-1) thru (3-3). Contrast transfer was meaningless
for image segments without definite targets (eg. tree background or field
background only).

3.2.2 Resolution. Resolution is typically specified most completely by a
relative frequency response. For linear operators this is in the form of an
MTF for circular symmetric systems and a 2-D transfer function for more
general processors. Unfortunately, only the adaptive low pass filter and the
convolutional window are linear processors. LAGC, HIST, EDGE, and MEDIAN are

non-linear processors and will generate new frequencies in the output image which were not present in the input image. An effective transfer function (plot of gain vs frequency) can be computed for the non-linear processors; however, interpretation may be difficult.

Resolution measures given as single parameter values such as "limiting resolution", MTFA or "resolvable lines across the target minimum dimension " have been defined for simple resolution comparisons. For relative ease of comparison and because it is the resolution parameter used in many performance models, resolvable lines across the target minimum dimension, N_R , was used for quantitative comparison of the various processing combinations. More detailed understanding of what a given processor does to the image in terms of frequency content can be evaluated by comparison of the image Fourier spectrum, before and after processing.

The procedure shown in Figure 3.1 for evaluating resolution enhancement was implemented. Resolution improvement was then computed as the ratios

$$R_r = \frac{N_R'}{N_R} \qquad \text{(limiting resolution)} \qquad (3\text{-}4)$$

$$R_a = \frac{\int_0^{N_R'} G(\beta) \, d\beta}{\int_0^{N_R} F(\beta) \, d\beta} \qquad \text{(resolution area)} \qquad (3\text{-}5)$$
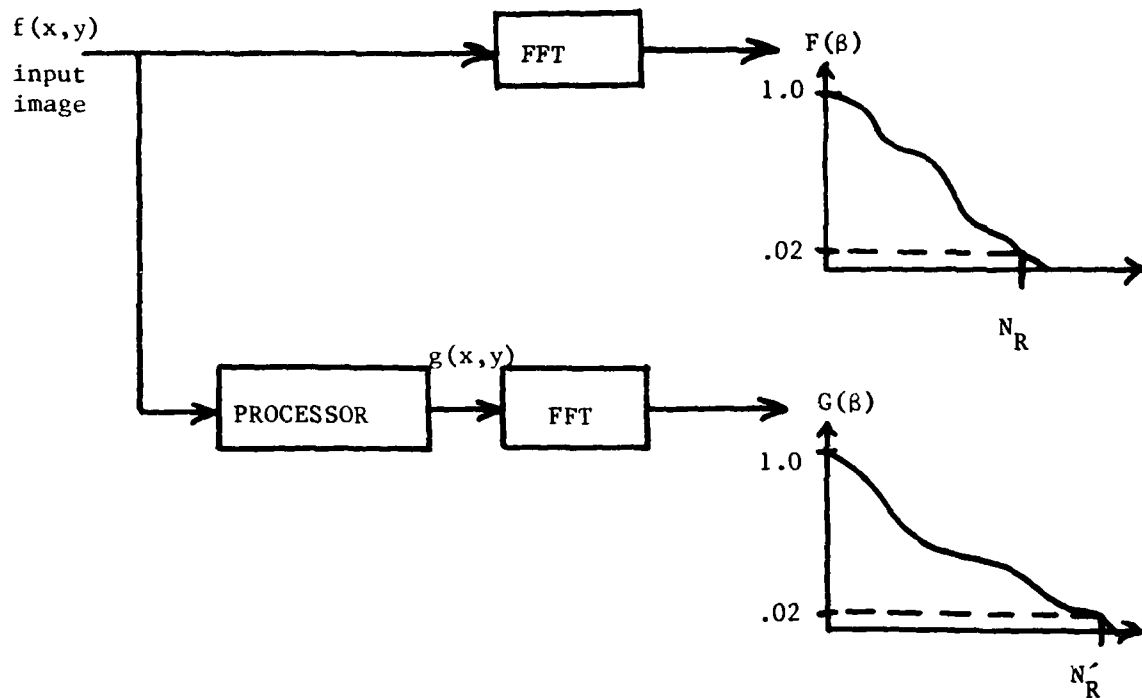
Figure 3.1   Evaluation of Resolution

3.2.3 Signal -to-noise ratio. A total signal model was used which included additive gaussian noise.

$$r(x,y) = f(x,y) + n(x,y) \tag{3-6}$$

The noise term, $n(x,y)$, was generated by an approximation to a random gaussian with zero mean and specified standard deviation. This number was added on a pixel by pixel basis to $f(x,y)$. Each processor was then applied to $r(x,y)$ and $n(x,y)$. If $f(x,y)$ and $n(x,y)$ are statistically independent, then their variances add to give the variance of $r(x,y)$.

$$\sigma_r^2 = \sigma_f^2 + \sigma_n^2 \tag{3-7}$$

The procedure for computing S/N improvement is outlined in Figure 3.2 and given by

$$SNI = \text{Improvement} = \frac{(S/N) \text{ output}}{(S/N) \text{ input}} \tag{3-8}$$

$$SNI = \frac{\sigma_g / \sigma_{n'}}{\sigma_f / \sigma_n} \tag{3-9}$$

where σ_g is the standard deviation of the output image with no noise.

σ_f – computed from input image

σ_n – specified (or computed to verify)

$\sigma_{n'}$ – computed from processor application to noise only

σ_g – computed from $\sigma_{gn}^2 = \sigma_g^2 + \sigma_n^2$, where σ_{gn} is computed

from processor application to signal plus noise.
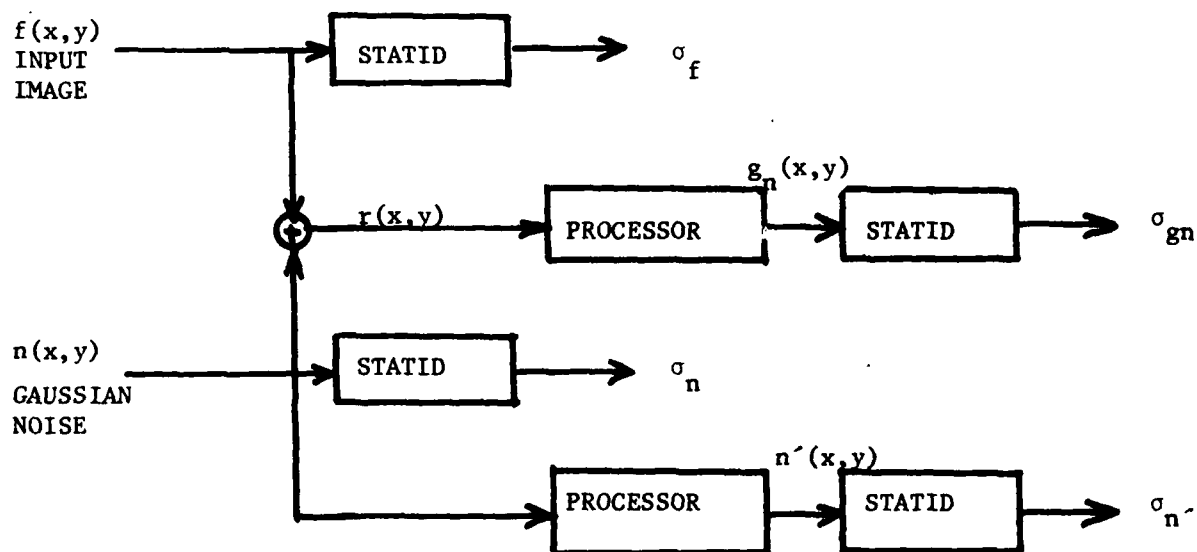
Figure 3.2 Signal-to-noise ratio improvement

3.2.4 <u>Signal to clutter ratio</u>. The definition of signal to clutter ratio is complicated by difficulties in defining and measuring clutter. This parameter was included primarily to emphasize the fact that it will affect detection and recognition probabilities. For this effort a very simple definition was used

$$S/C = \frac{|\mu_t - \mu_b|}{\sigma_s} \qquad (3-10)$$

where μ_t is the target mean value, μ_b is the background mean value and σ_s is the standard deviation for a total segment or image as applicable.

4. SIMULATION RESULTS

4.1 <u>Overview</u>. A number of single, serial and parallel processing mathods were simulated and applied to typical TV and FLIR imagery. The simulation plan and processor combinations are described in 4.1.1 and the imagery is described in 4.1.2 .

4.1.1 <u>Simulation plan</u>. The six processing methods were loosely grouped into three categories:

1. Noise reduction (MEDIAN, ALPF, WINDOW-SMOOTH);
2. S/N, Contrast enhancement (LAGC, HIST. MOD, WINDOW-GRADIENT);
3. Clutter reduction (EDGE).

Actually EDGE does not just reduce clutter; it produces an edge image which has a significantly reduced information content.

The rationale for various serial and parallel combinations of the processors was that processors which do the same thing (eg. reduce noise) should not be combined nor should processors which have opposing effects be combined (eg. a smoothing window and a gradient window).

Figure 4.1 gives a simple flow chart of the steps in simulation evaluation of each individual processor. To reduce computation costs, many simulations were done on smaller image segments. After initial evaluation, the better processors were applied to the total image.

The images and sub-images were characterized statistically, plotted and measured in terms of the four quantitative evaluation measures described in 3. After being processed, the images were again characterized and compared both subjectively and quantitatively with the unprocessed images. The resultant images were written onto digital tape in a format compatible with the MICOM display system. Processed sub-images were re-inserted into the larger image to provide easy comparison between the original and processed results.

Simulation results shown in this report are photographs taken of images displayed on the MICOM system. Some image quality is lost in the photographic process; however, relative comparisons can still be made. With some exceptions, all photographs in this report were taken during a single session to ensure equal gain and contrast settings for the display system.

```
┌─────────────────────────┐              ┌──────────────────┐
│ IMAGERY                 │─────────────▶│ PROCESSOR        │
│ -TADS TV & FLIR         │              └──────────────────┘
│   (407 x 392 pixels)    │
│ -IMAGE SEGMENTS         │
│   (64 x 64 pixels)      │
└─────────────────────────┘

┌─────────────────────────┐    ┌──────────────────────────────────┐
│ - COMPARATIVE EVALUATION│◀───│ IMAGE CHARACTERZATION            │
│ -PARAMETER SELECTION    │    │                                  │
└─────────────────────────┘    │ - STATID - MOMENTS               │
                               │ - FFT2D                          │
     Additional                │ -HISTOGRAM - PLOT                │
     Processing                │ -SIGNAL/NOISE                    │
┌─────────────────────────┐    │ -SIGNAL/CLUTTER                  │
│ -WRITE DIGITAL TAPE     │◀───│ -RESOLUTION                      │
│ -REINSERT SEGMENTS      │    │ -TARGET/BACKGROUND CONTRAST      │
└─────────────────────────┘    └──────────────────────────────────┘

     Display
     & Photo
```
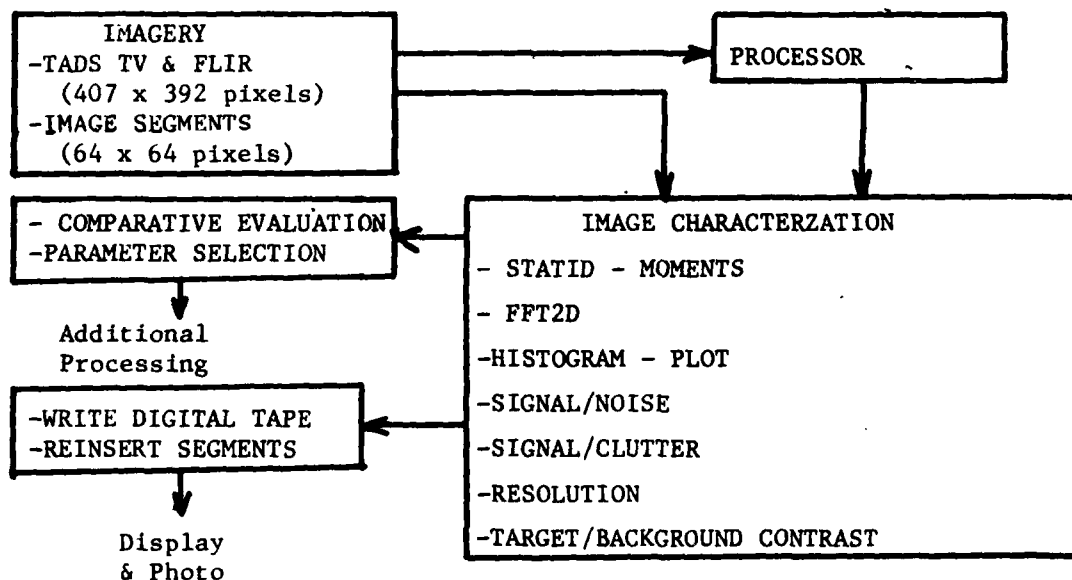
Figure 4.1 Evaluation of single processors

21

4.1.2 Image descriptions. Initial processing was applied to 64 x 64 pixel image segments from the POS B TADS TV WFOV TGT2 silicon TV imagery. Six different image segments were chosen representing various target and background conditions (different scene content). Total image processing was applied to POS B TV and FLIR imagery and to POS D TV and FLIR imagery. Table 4.1 lists the images and sub-images.

Further descriptions of the imagery are given in Figures 4.2 thru 4.11. Photographs of each image are given. Additionally the histogram and moments are given.

```
                Table 4.1   Imagery for processor simulation.


    1   -   POS B TADS TV WFOV TGT 2
                (407 x 392 pixels - TV image)

    2   -   IMAGE SEGMENTS (64 x 64 pixels) FROM IMAGE 1
                - TARGET/FIELD BACKGROUND
                - TARGET/TREE BACKGROUND
                - TARGET/TREE-FIELD MIXED BACKGROUND
                - TREE BACKGROUND
                - FIELD BACKGROUND
                - TARGET BOARDS/TREE-FIELD BACKGROUND

    3   -   POS D TADS TV WFOV TGT 2
                (407 x 392 pixels - TV image)

    4   -   POS D TADS FLIR NFOV TGT 2
                (407 x 392 pixels - FLIR image)
                          (white hot)
```

Statistical characterization and quantitative evaluation parameters for each simulation are listed in Table 4.2.
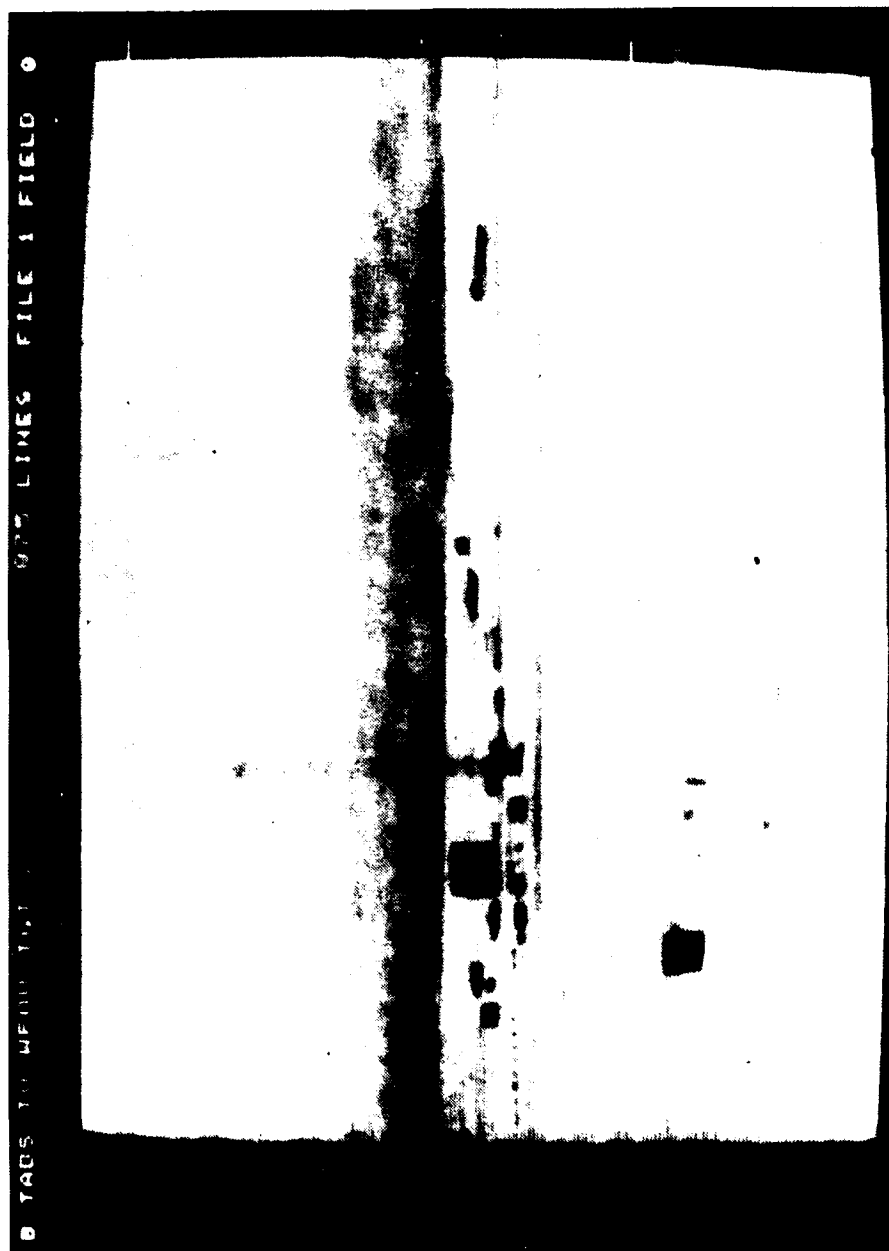
Figure 4.2 Original – POS B TADS TV WFOV TGT 2

23

MEAN   = 206.4331
STD   = 57.15028
SKEW   = -2.596792
KURTOSIS = 9.476180
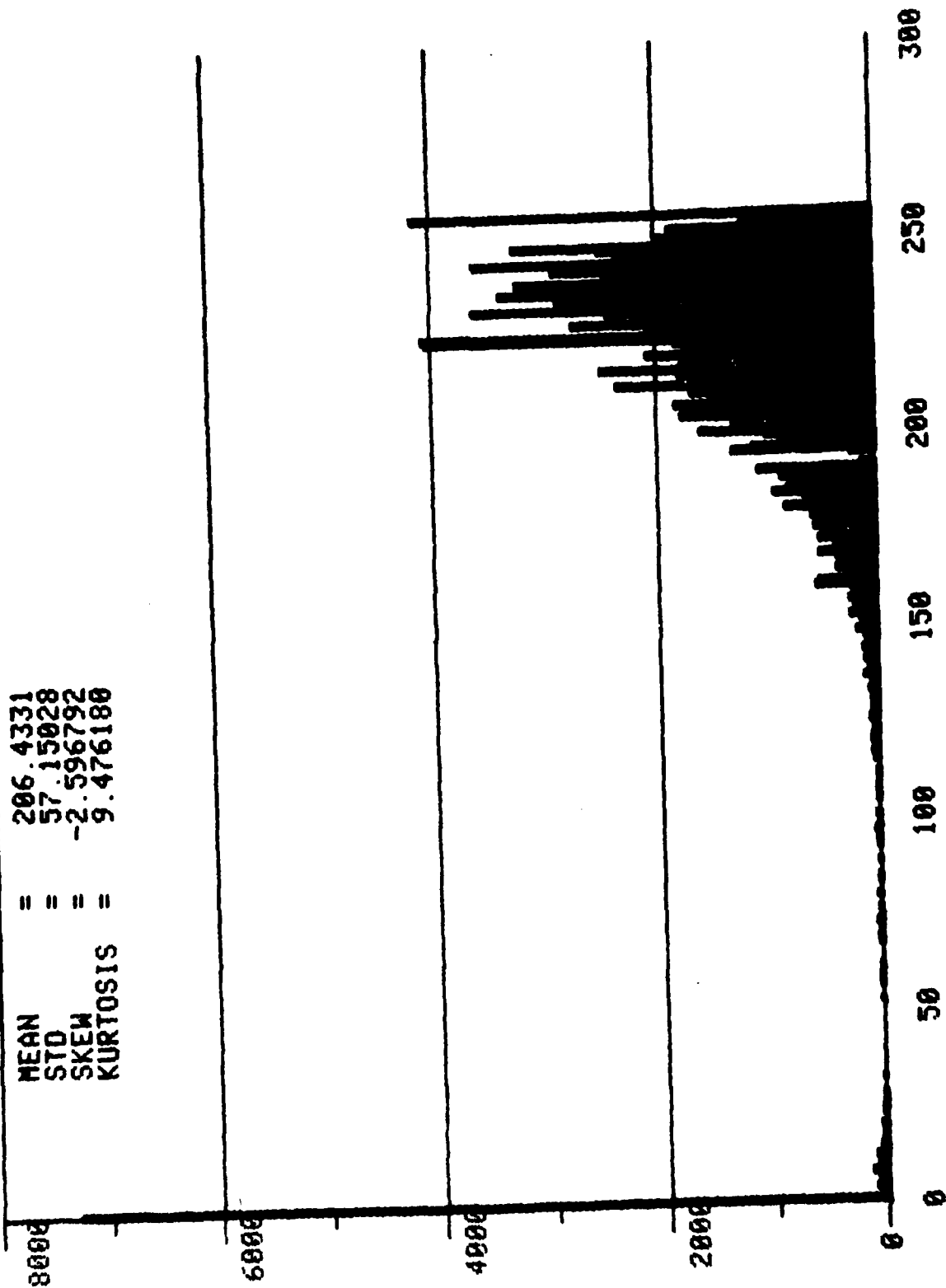
Figure 4.3 Histogram - POS B TADS TV WFOV TGT 2
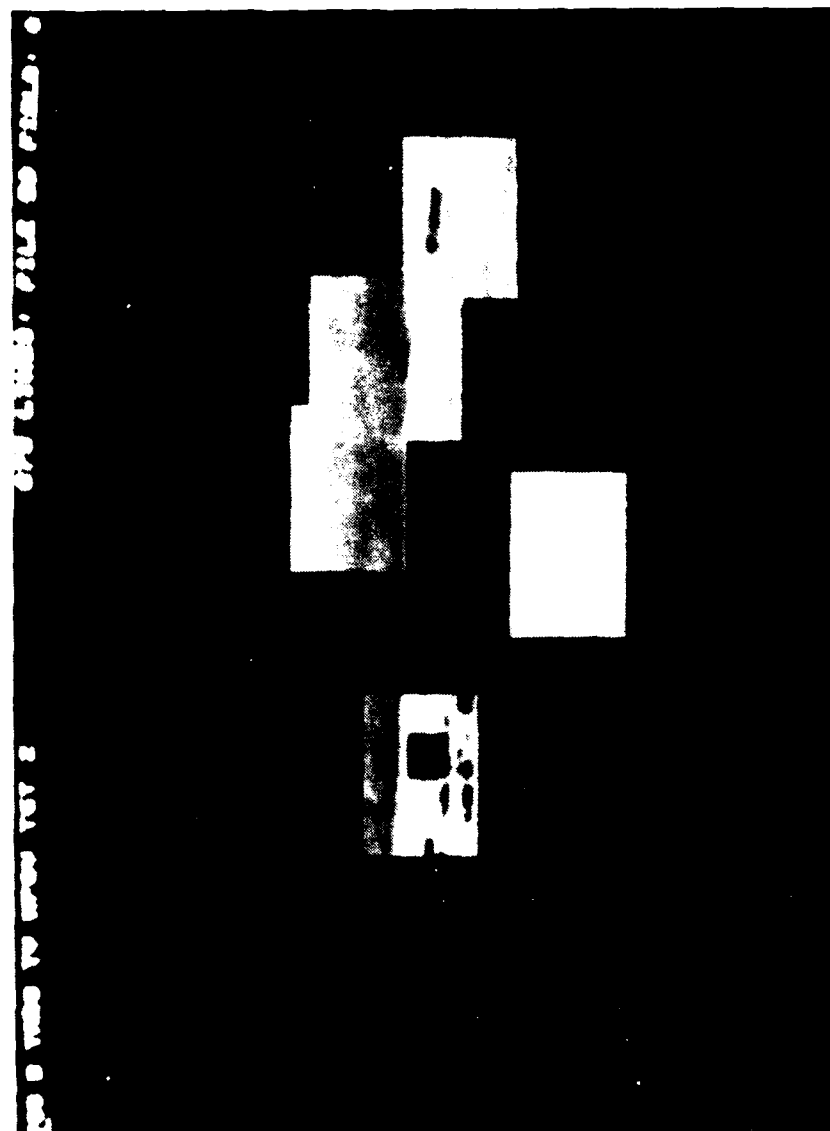
Figure 4.4 Original - Image Segments
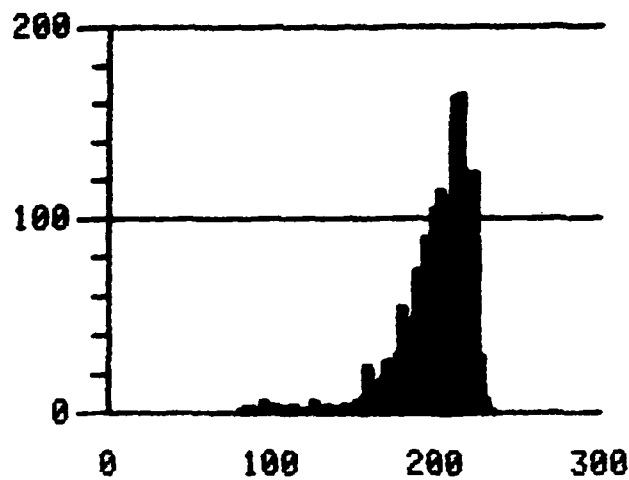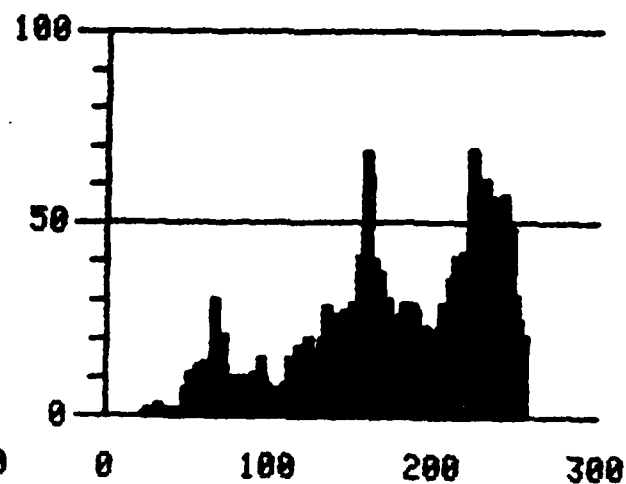
a) Target/tree background
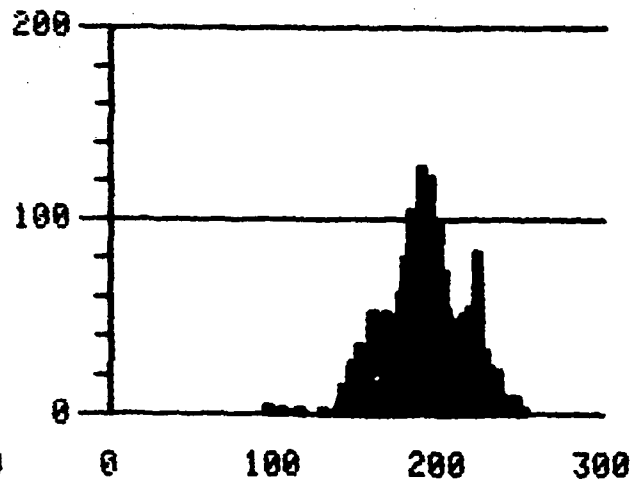
b) Target/field background
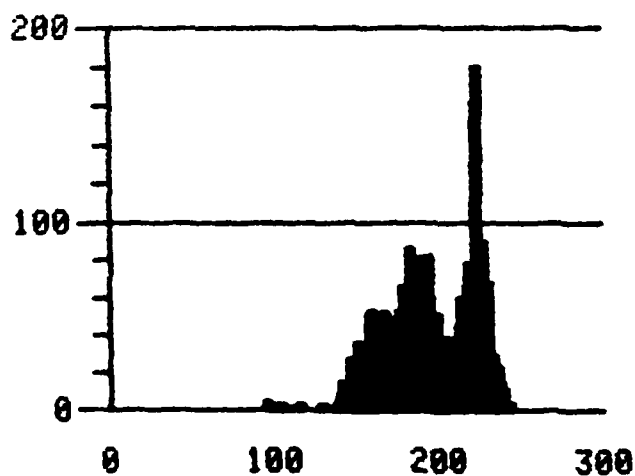
c) Target/mixed background
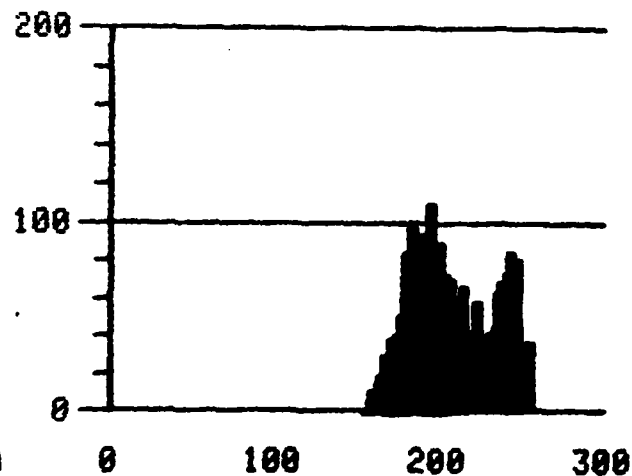
d) Tree background
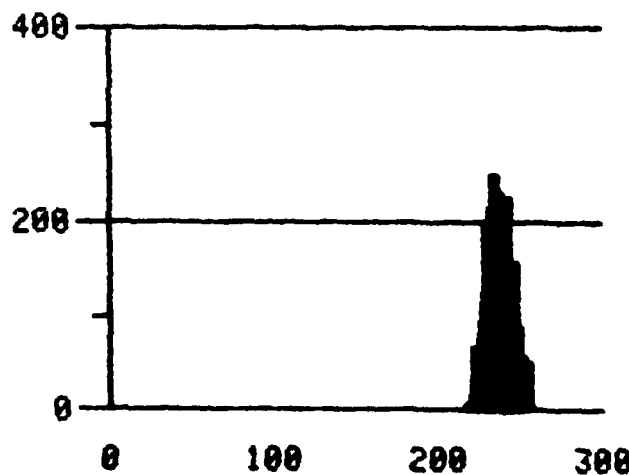
e) Field background

f) Large target board

Figure 4.5   Histogram - Image Segments
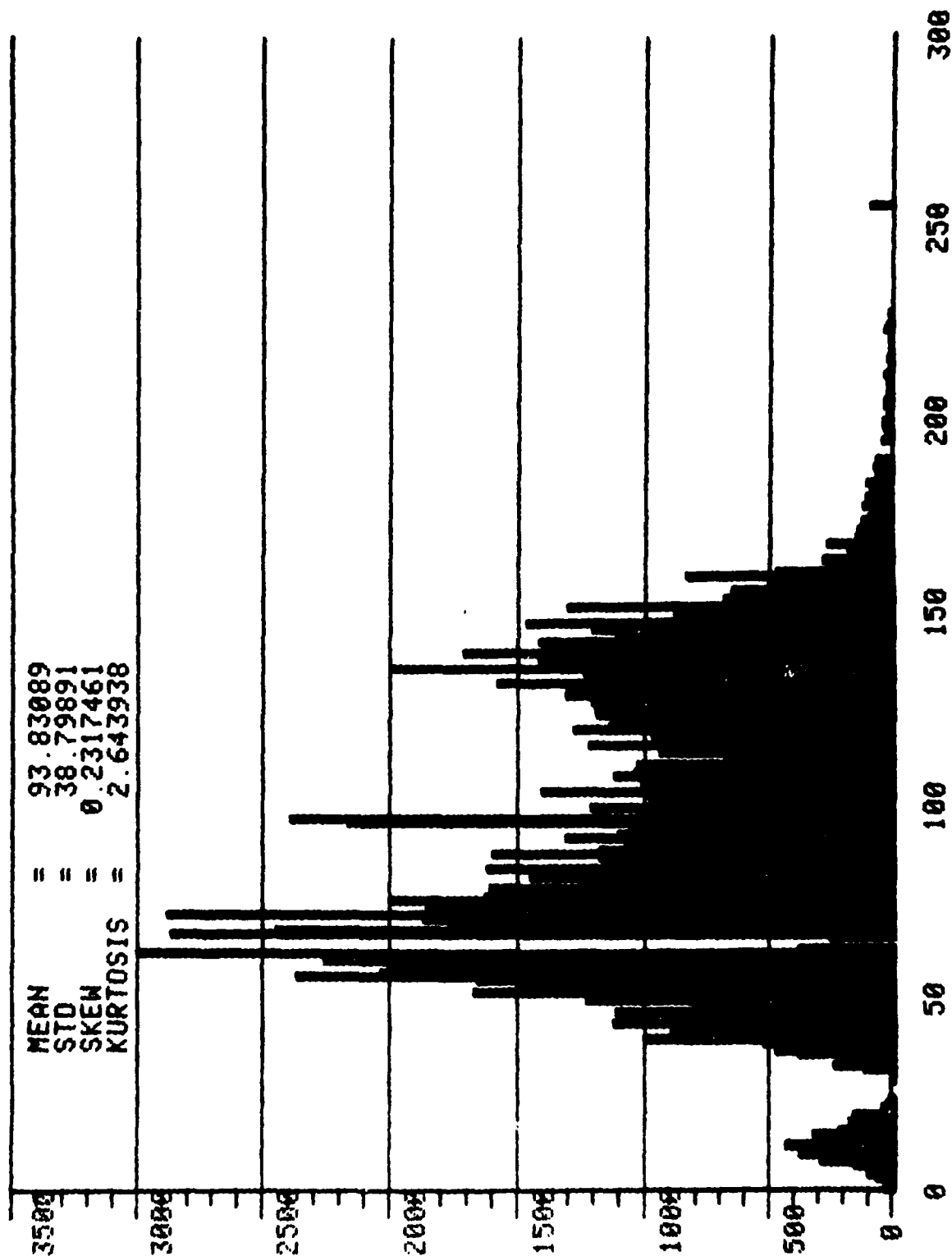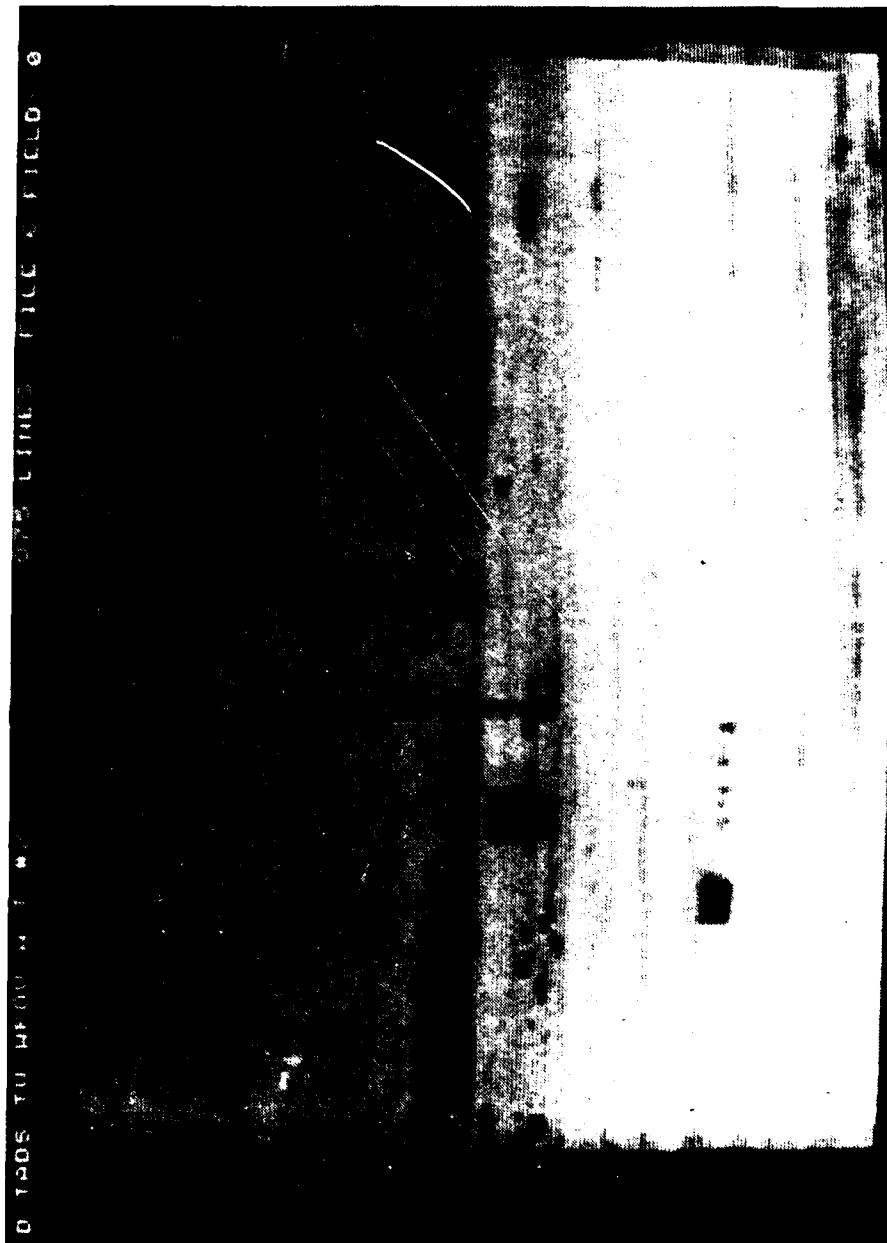
26

Figure 4.6 Original - FLIR

27

Figure 4.7 Histogram - FLIR

Figure 4.8 Original - POS D TADS TV WFOV TFT 2
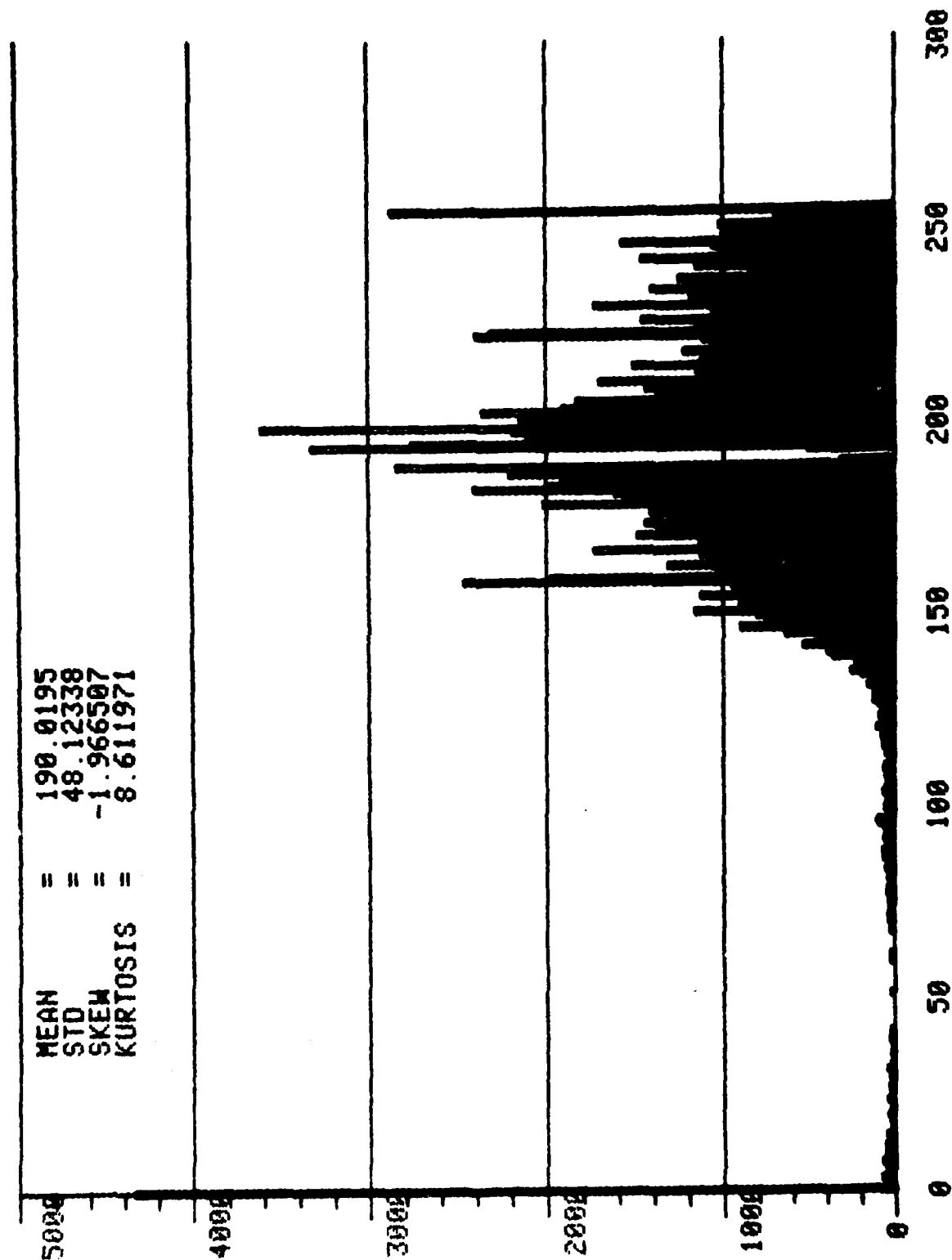
Figure 4.9 Histogram - POS D TADS TV WFOV TFT 2

MEAN   =   190.0195
STD   =   48.12338
SKEW   =   -1.966507
KURTOSIS   =   8.611971
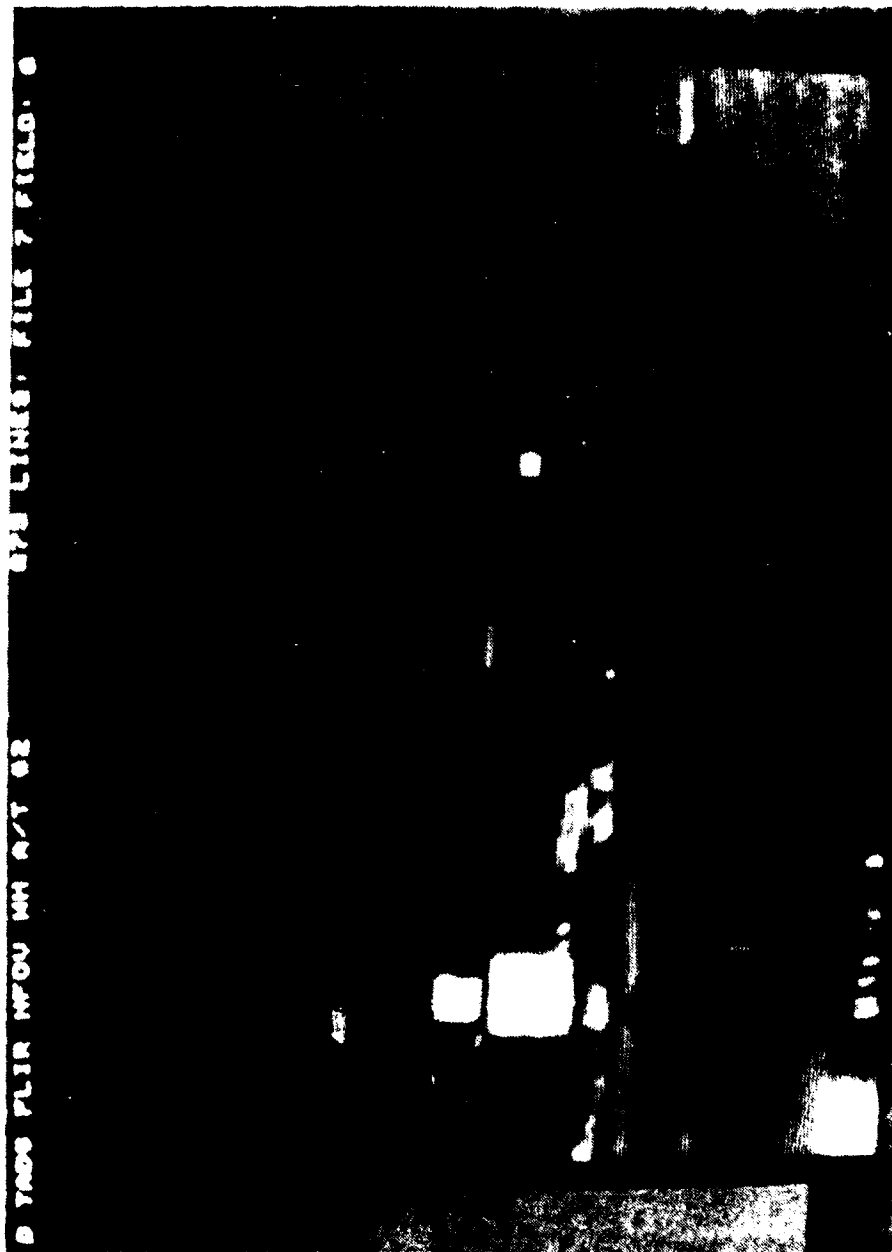
Figure 4.10 Original - POS D/TADS FLIR NFOV TGT 2 WH

31
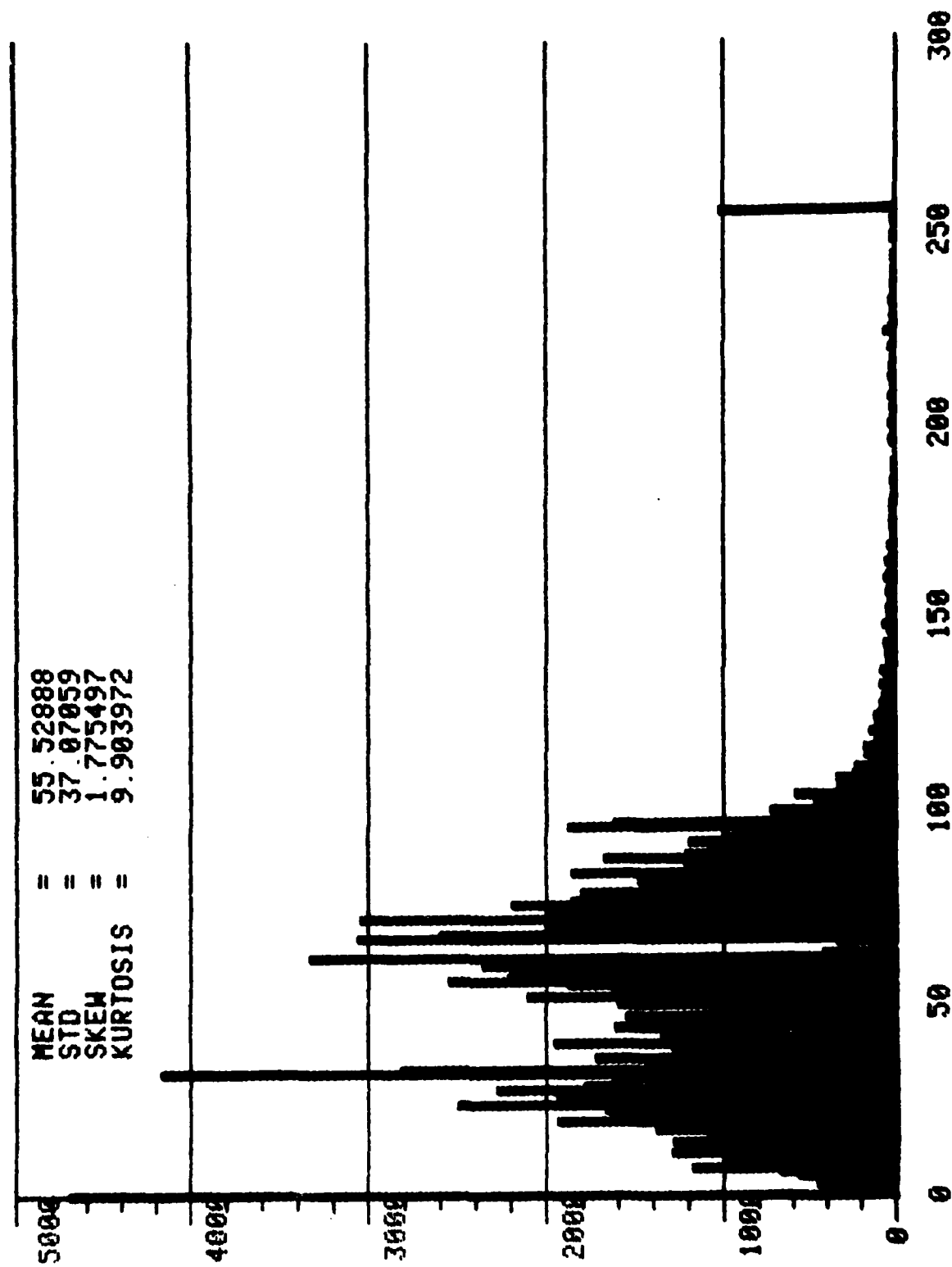
Figure 4.11 POS D TADS FLIR NFOV TGT 2 WH

TABLE 4.2 IMAGE CHARACTERIZATION

| IMAGE | MEAN | STATISTICS | | | SIGNAL/ NOISE | SIGNAL/ CLUTTER | FFT RESOLUTION | CONTRAST | FIGURE |
		STD	SKEW	KURTOSIS					
				UNPROCESSED					
1. B-TV (Total)	206.4	57.2	-2.6	9.5	4.99	5.02	6	0.74	4.2
2. B-TV (Segments)									
A. TARGET/FIELD	200.6	22.4	-2.2	9.7	4.8	5.99	7	0.72	
B. TARGET/TREES	190.8	25.3	-0.29	3.25	5.34	4.14	4	0.78	
C. TARGET/FIELD-TREES	195.5	27.8	-0.48	2.64	5.98	4.17	4	0.79	
D. TREE BACKGROUND	207.9	25.5	0.174	1.83	X	X	3	X	
E. FIELD BACKGROUND	237.9	7.37	8.0E-2	2.53	X	X	22	X	
F. LARGE TARGET BOARD	180.1	53.8	-0.668	2.58	11.1	3.38	8	0.89	
3. B-FLIR (Total)	98.8	38.8	0.23	2.64	5.25	4.37	5	0.76	4.6
4. D-TV (Total)	190.0	48.1	-1.97	8.61	5.02	4.96	6	0.75	4.8
5. D-FLIR (Total)	55.5	37.1	1.78	9.90	5.30	4.31	5	0.75	4.10

4.1.3 <u>List of processors</u>. A number of initial iterations for the processors was designed to evaluate the effect of parameters and combinations of processors. A total of more than 200 processing steps were simulated, and the results are available on digital tape. For this report representative simulation results were chosen to illustrate parameter effects and to provide inter-processor comparisons.

Table 4.3 lists image statistics and quantitative evaluation parameters for selected simulations. Pictorial results for each processor   listed in Table 4.3 are included in Sections 4.2 and 4.3.

4.2 <u>Single Processors</u>.

4.2.1 <u>Noise cleaning</u>. Noise cleaning algorithms included averaging windows, median filtering and adaptive low pass filtering. Results are illustrated in Figures 4.12 thru 4.17.

Figure 4.12 illustrates comparative results of median filtering and window averaging techniques applied to image segments from POS B TV. In the figure, b.) and c.) are median filtered and d.) and e.) are averaged. Further, b.) and d.) used a 3 x 3 window while c.) and e.) used a 5 x 5 window. Blurring is more evident in the averaging technique as expected. This effect is illustrated further by Figure 4.14 where 5 x 5 median and averaging techniques were applied to the total B - TV and FLIR images. Figure 4.16 shows the 5 x 5 median processed B - TV & FLIR images along with the originals for comparison.

Corresponding histograms for all images are given in figures immediately following the image figures.

4.2.2 <u>Contrast enhancement</u>. Contrast enhancement techniques included histogram equalization, histogram hyperbolization and LAGC. Figures 4.18 thru 4.23 illustrate results of these simulations. Histogram equalization and hyper-bolization are illustrated in Figure 4.18 a.) and b.). This result along

34

with other simulations indicated that histogram modification did not produce desired results. This was a subjective evaluation based on relative ease in identifying known target objects in the image. Figure 4.18 c.) is a 3 x 3 LAGC applied to B-TV segments and d.) is a 5 x 5 LAGC applied to the total image. Figure 4.18 f.) is a 5 x 5 LAGC applied to B-FLIR. The gain factor for LAGC was $G = \frac{1}{\sigma}$ for these simulations.

The LAGC method ($G = \frac{1}{\sigma}$) enhances image detail; however, it generates high frequency noise which makes the image look grainy. This is illustrated further in Figure 4-20 c.) and d.) for the D - TV and FLIR images. Increasing the window size to 15 x 15 in 4.20 e.) and f.) gave expected results, ie, contrast is enhanced most for object sizes equal to the window size. The resultant images still exhibit confusing graininess.

An alternate gain factor ($G = \frac{\mu}{\sigma}$) was used in the LAGC method. Results are shown in Figure 4.22 c.) and d.) for D - TV and FLIR using a 5 x 5 window and in e.) and f.) using a 15 x 15 window. The 5 x 5 window appears to give slight contrast enhancement and does not exhibit the graininess observed with $G = \frac{1}{\sigma}$. However, window size for this algorithm becomes more critical as illustrated by excessive blurring for the 15 x 15 window.

4.2.3 Gradient and edge processors.

4.2.3.1 Gradient images. A number of different gradient processors were evaluated. The results of four processors applied to B-TV segments are shown in figure 4.24 a.) 3 x 3 Prewitt, b.) 3 x 3 Sobel, c.) 3 x 3 unsharp masking, and d.) 5 x 5 unsharp masking. Strong gradients are easily detected by all methods. Further results are given in Figures 4.26 and 4.28 for 3 x 3 Prewitt and 3 x 3 unsharp masking applied to B-TV and FLIR images and D-TV and FLIR images respectively.

These gradient images would certainly be useful for identifying distinct objects or for image registration; however, without further processing they offer little help in identifying obscured, low-contrast targets.

4.2.3.2 Thresholded edge images. One method for emphasizing edges is to simply apply a threshold to the gradient image and represent all edges above threshold by a single brightness level. The threshold is typically based on global (total) image statistics and chosen in terms of either percentiles or mean and standard deviation.

Results of global edge detection with a mean threshold are shown in Figure 4.30 a.) Prewitt (3 x 3) and b.) Sobel (3 x 3). Again, sharp edges are easily detected and weaker edges missed.

An approach which offered promise for detecting low contrast edges was to choose a threshold which was locally adaptive and based on statistics within a specified window about each pixel. Results of this local edge detection using the mean value in a 3 x 3 window as threshold are shown in Figure 4.30 c.) Prewitt and d.) Sobel. This method produced almost 50% edges as would be expected from choosing the mean of a 3 x 3 array as a threshold. Low contrast edges were identified however, they were obscured by noisy edges.

To pursue the local edge detection method further, simulations were done with varying thresholds and window sizes for threshold statistics. Figure 4.32 shows the result of varying threshold in a 3 x 3 window for D-TV and FLIR images (thresholds are a.) and b.) $T = \mu + .5\sigma$; c.) and d.) $T = \mu + \sigma$; e.) and f.) $T = \mu + 2\sigma$). Increasing the threshold does reduce the number of edge points; however, as illustrated in 4.32 e.) and f.) it eliminates good edge points and noise edge points equally. The conclusion was that simply increasing the threshold would not produce desirable results.

Figures 4.34 and 4.36 show the effect of window size for statistical calculation of three different thresholds for D-TV and D-FLIR respectively. In both images the parameters are 7 x 7 window: a.) $T = \mu$ c.) $T = \mu + .5\sigma$ e.) $T=\mu + \sigma$ and 15 x 15 windows: b.) $T = \mu$ d.) $T = \mu +.5\sigma$ f.) $T = \mu + \sigma$. Comparison of these figures with 4.32 indicates that improved results were obtained using the larger window sizes for threshold calculation.

Further improvements in the edge detection results could be accomplished by edge thinning and edge connectivity algorithms; however, these methods do not operate in near real-time.

4.2.3.3 <u>Original plus edges or gradients</u>. It was felt that a potentially optimum output display would result from a combined original scene with edge or gradient images superimposed. Figure 4.38 shows the B-TV images (segments and full images) with Prewitt and Sobel gradients added. For this figure the images were summed and rescaled to (0-255). Unfortunately, this biased the resultant image by setting the largest gradient value to 255 and thus suppressed the original image gray levels. This effect was corrected by using an edge re-placement method instead of summing the images. Figure 4.40 shows the original D-TV and FLIR images with edge replacement using the Prewitt local threshold $T =\mu +\sigma$ edge images for 3 x 3: a.) b.) ; 7 x 7: c.) d.); and 15 x 15: e.) f.) window sizes.

4.3 <u>Multiple processors</u>. Serial and parallel combinations of processors were implemented in an effort to gain in more than one quality measure (ie. reduce noise, enhance contrast, improve resolution).

4.3.1 <u>Serial combinations</u>. A number of serial combinations were investigated. It was found that the errors introduced by one method were generally carried through subsequent processing steps. Examples of serial processors are given

in Figure 4.42 a.) 5 x 5 LAGC followed by 5 x 5 median filtering, b.) 5 x 5 averaging window followed by histogram equalization, c.) and d.) 5 x 5 median followed by 5 x 5 LAGC.

4.3.2 <u>Parallel processing</u>. Parallel combination of selected processors seemed to produce the better (subjective) images. Examples are given for B-TV in Figure 4.44 a.) unprocessed b.) 5 x 5 median plus 5 x 5 LAGC plus Prewitt gradient c.) 5 x 5 median (25%) plus 5 x 5 LAGC (75%) d.) 5 x 5 median (75%) plus 5 x 5 LAGC (25%), and for B-FLIR in Figure 4.46 a.) unprocessed b.) 5 x 5 median plus 5 x 5 LAGC plus Prewitt gradient c.) 5 x 5 median (25%) plus 5 x 5 LAGC (75%) d.) 5 x 5 median (75%) plus 5 x 5 LAGC (25%).
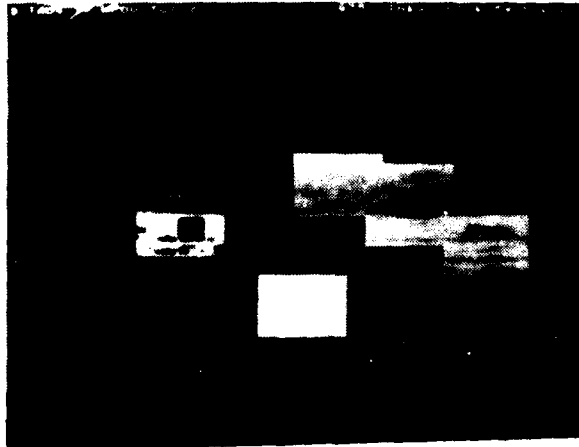
a) TV - segments (unprocessed)

b) Median (3 x 3)

c) Median (5 x 5)

d) Average (3 x 3)

e) Average (5 x 5)

Figure 4.12 B - TV Segments - noise cleaning algorithms

THIS PAGE INTENTIONALLY LEFT BLANK

Figure 4.13 Histograms for figure 4.12
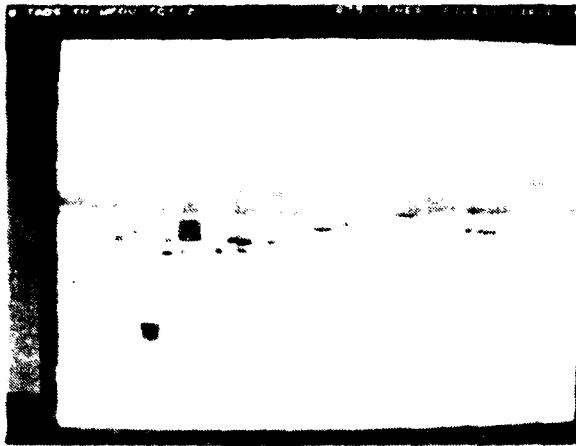
a) B-TV Original
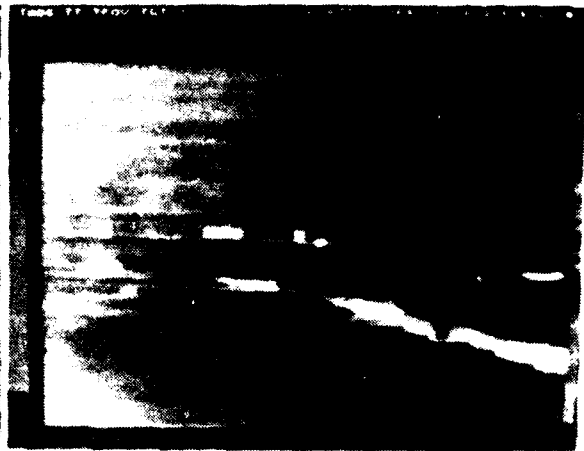
b) B-FLIR Original
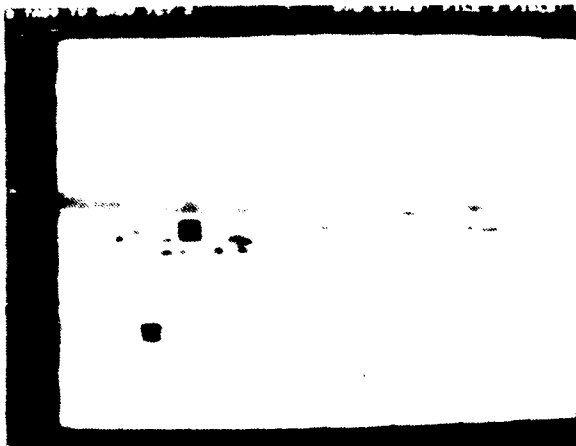
c) Median (5 x 5)
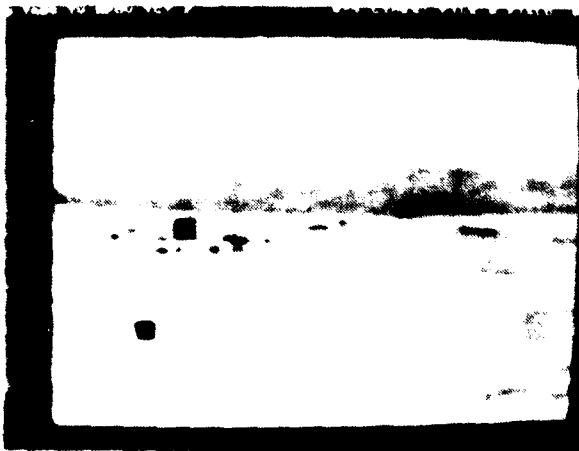
d) Median (5 x 5)

e) Average (5 x 5)

f) Average (5 x 5)

Figure 4.14   B-TV & FLIR - noise cleaning algorithms

41
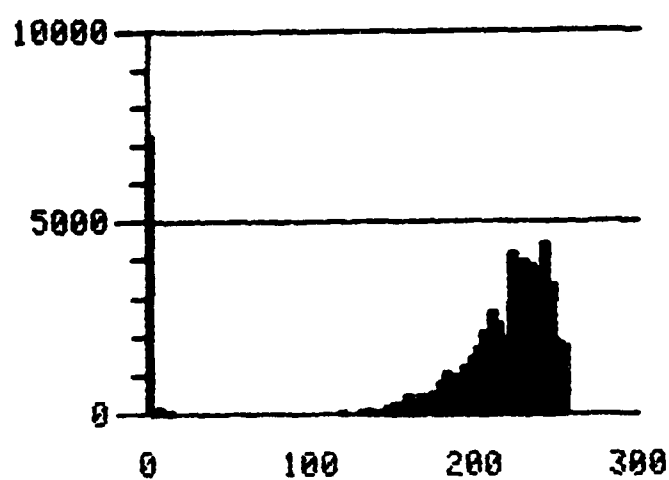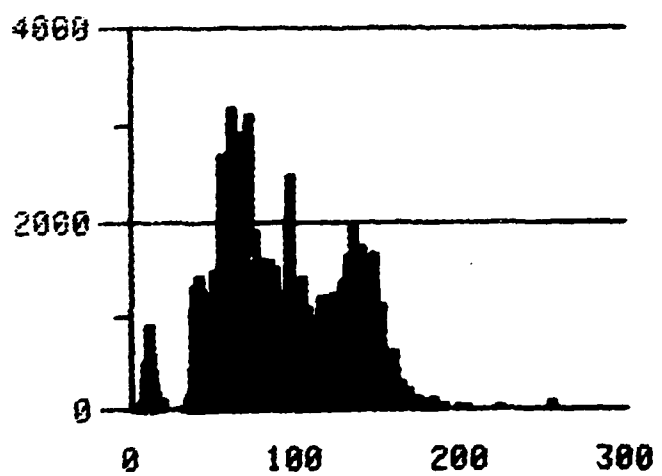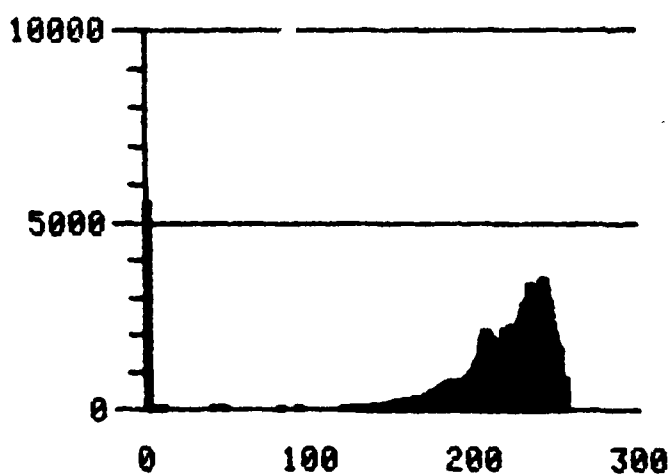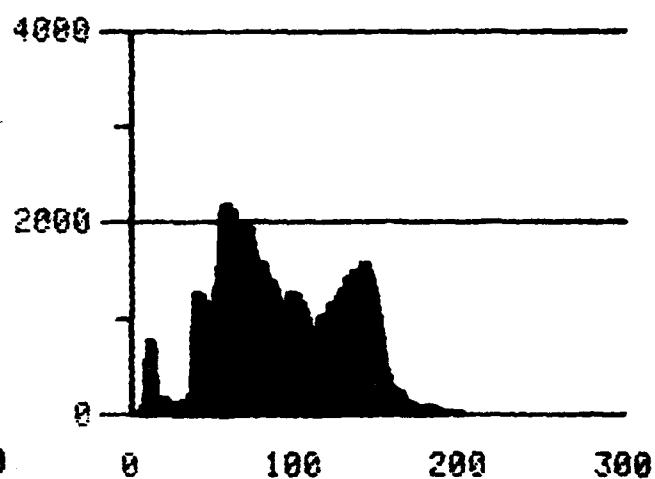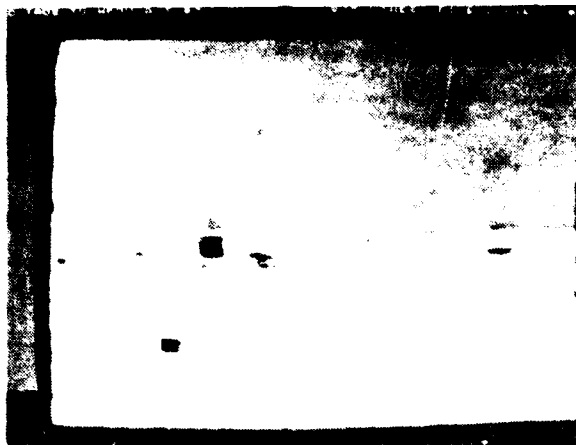
Figure 4.15 Histograms for figure 4.14

42
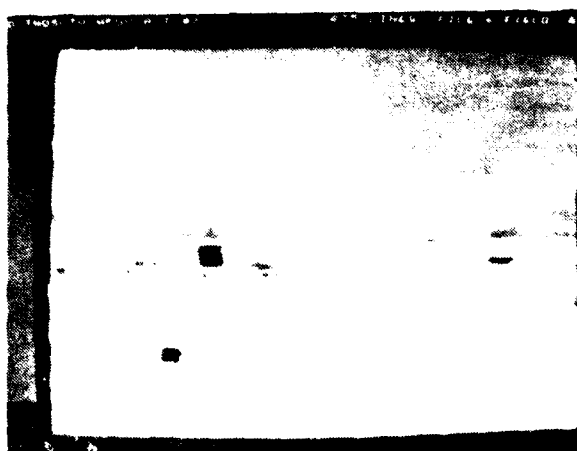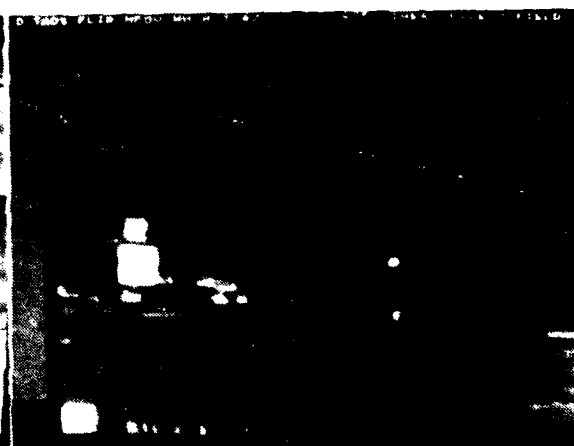
a) D-TV Original   b) D-FLIR Original
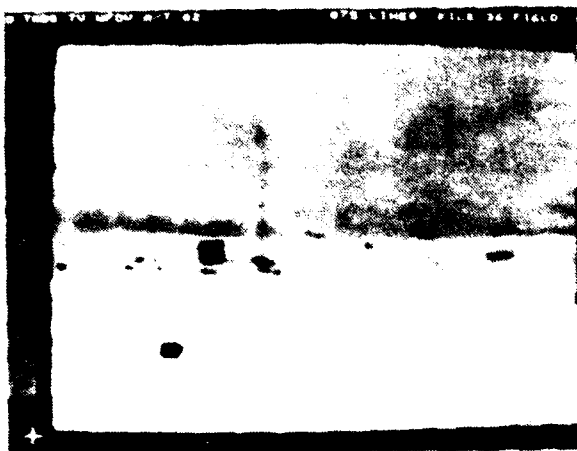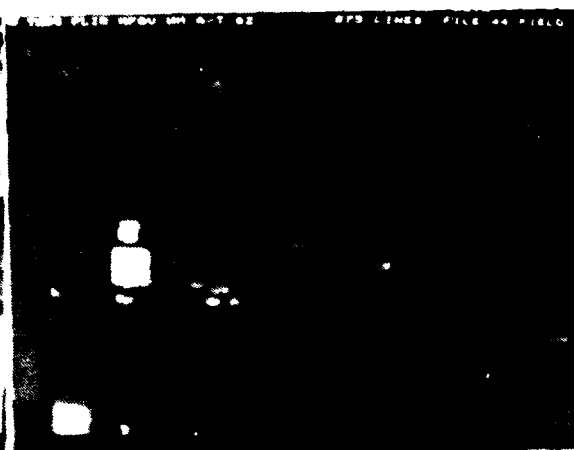
c) Median (5 x 5)   d) Median (5 x 5)

Figure 4.16   D - TV & FLIR median filtered images

43
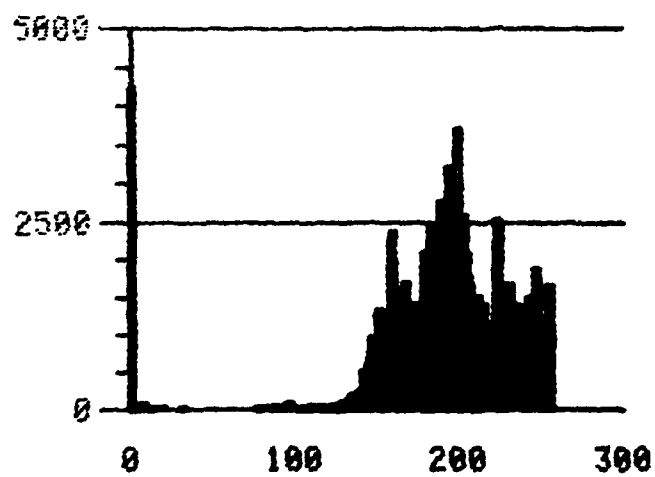
c)
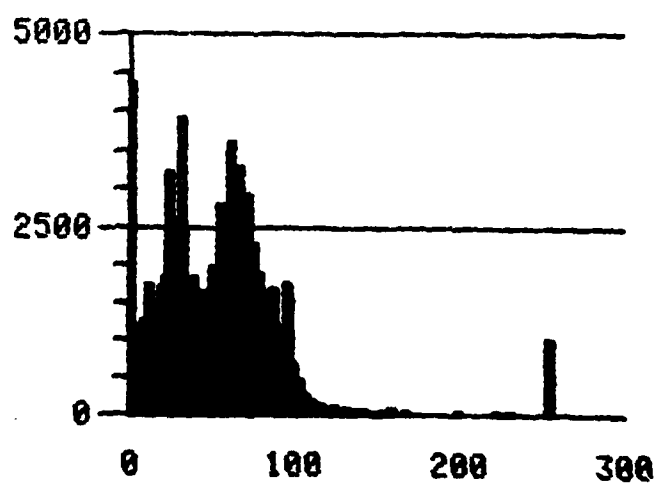
d)

Figure 4.17   Histograms for figure 4.16

44
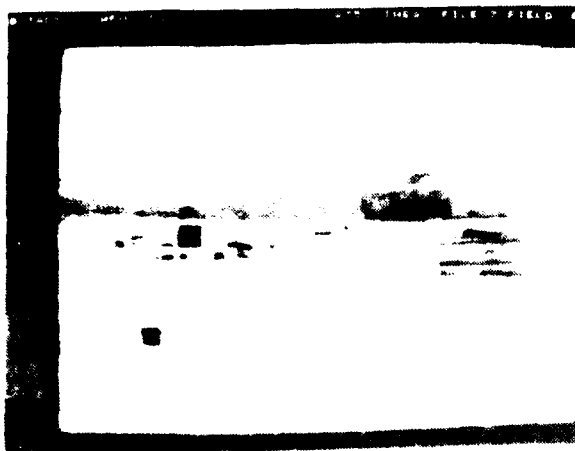
a) Histogram equalization   b) Histogram hyperbolization
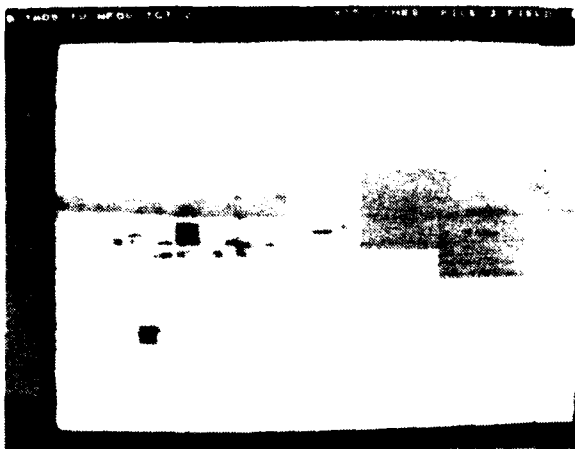
c) LAGC (3 x 3, $G = 1/\sigma$)   d) LAGC (5 x 5, $G = 1/\sigma$)
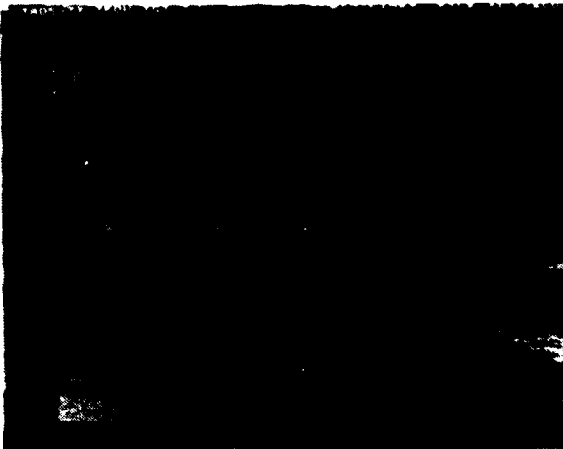
e) B-FLIR original   f) LAGC (5 x 5, $G = 1/\sigma$)

Figure 4.18   Histogram modification and LAGC ($G = 1/\sigma$
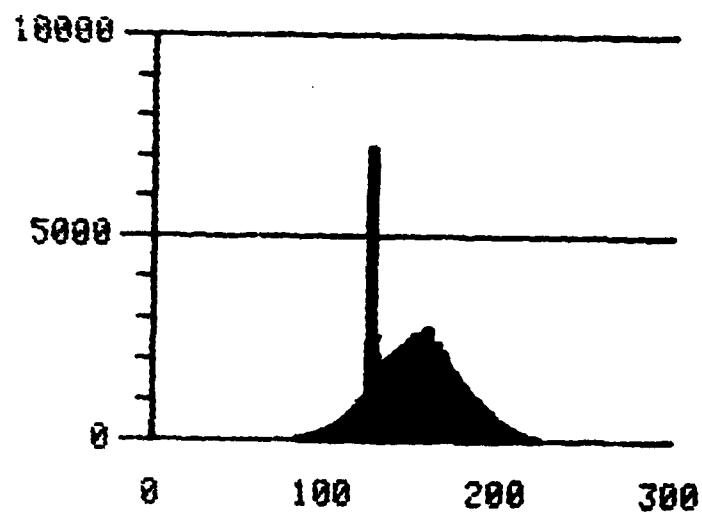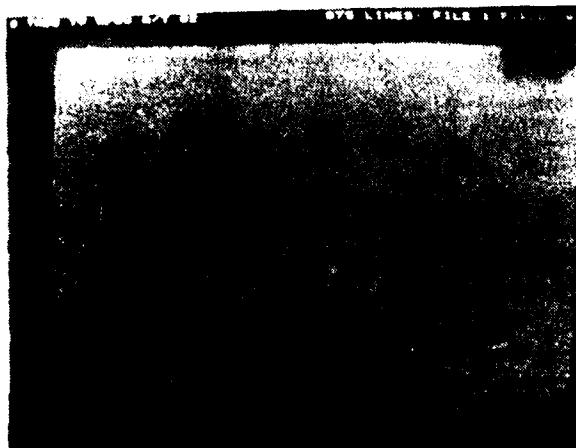
d)
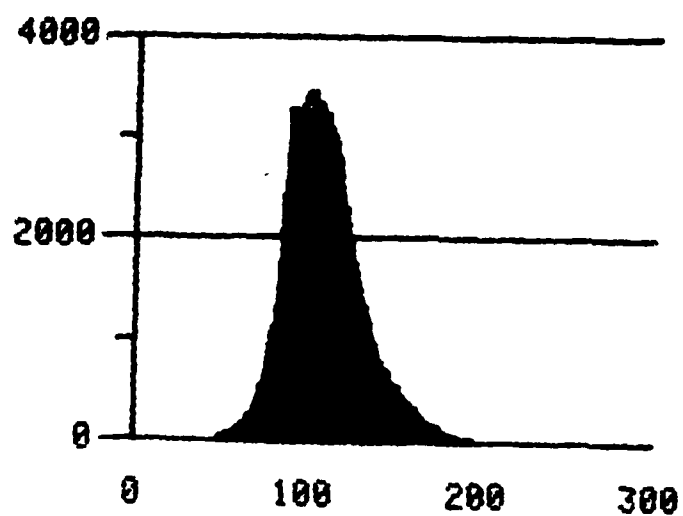
f)

Figure 4.19   Histograms for figure 4.18
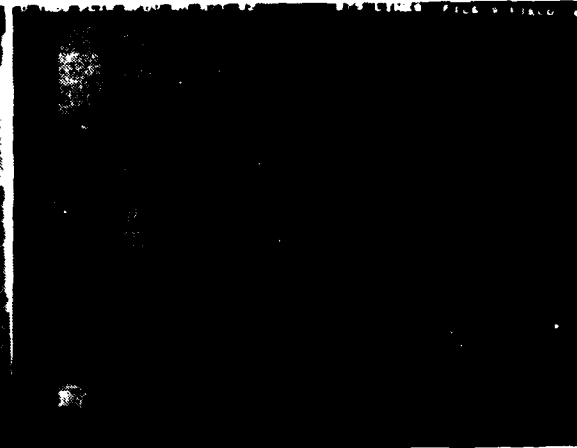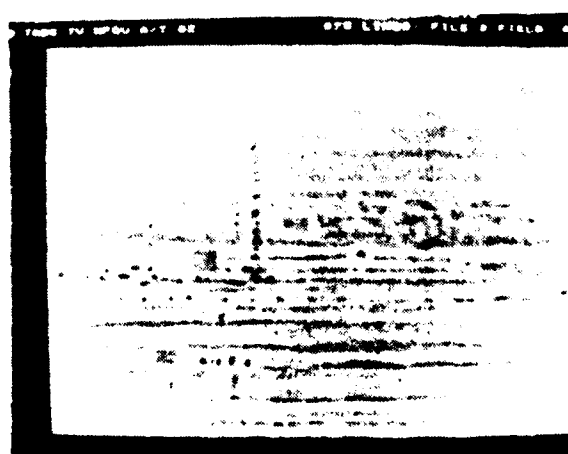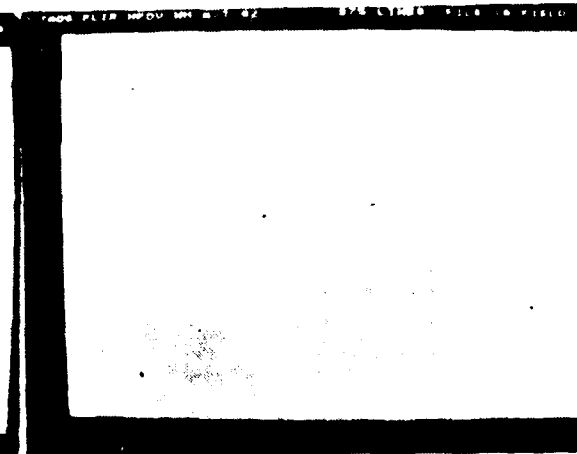
46

a) D-TV original
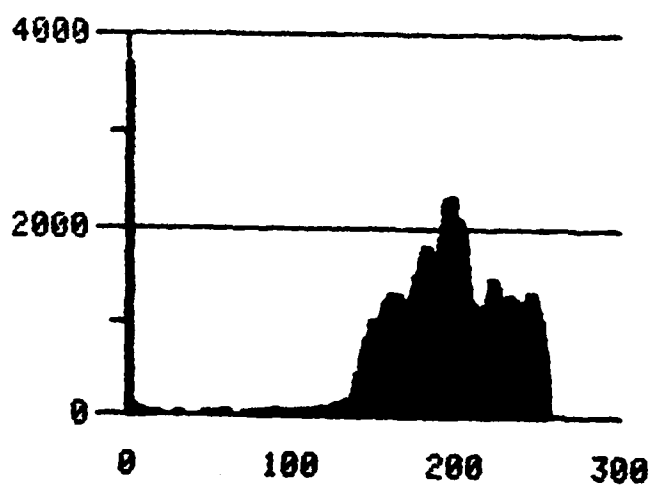
b) D-FLIR original

c) LAGC (3 x 3, G = 1/σ)

d) LAGC (3 x 3, G - 1/σ)

e) LAGC (15 x 15, G = 1/σ)

f) LAGC (15 x 15, G = 1/σ)

Figure 4.20   D-TV & FLIR LAGC (G = 1/σ) (L = 3 & 5)
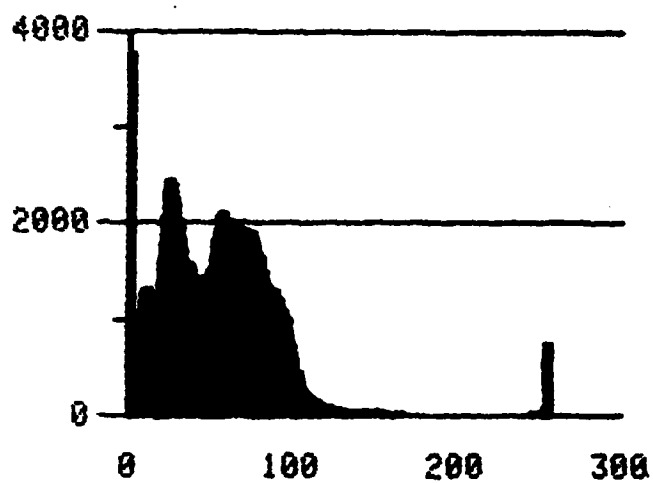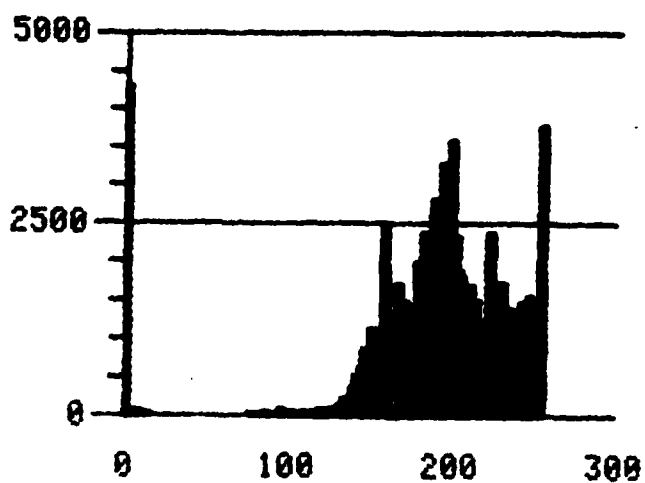
Figure 4.21   Histograms for figure 4.20

48

a) D-TV original
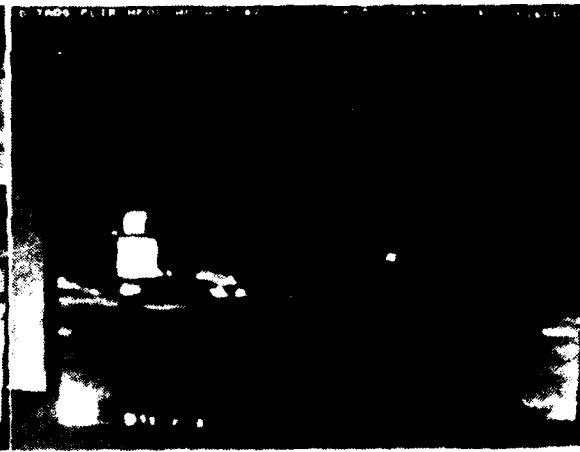
b) D-FLIR original
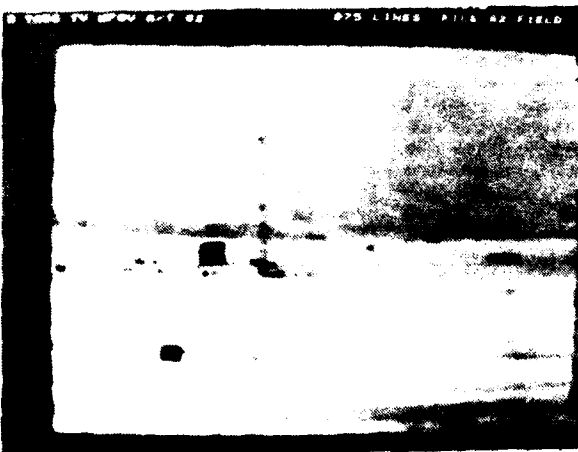
c) LAGC (5 x 5, G = μ/σ)

d) LAGC (5 x 5, G = μ/σ)
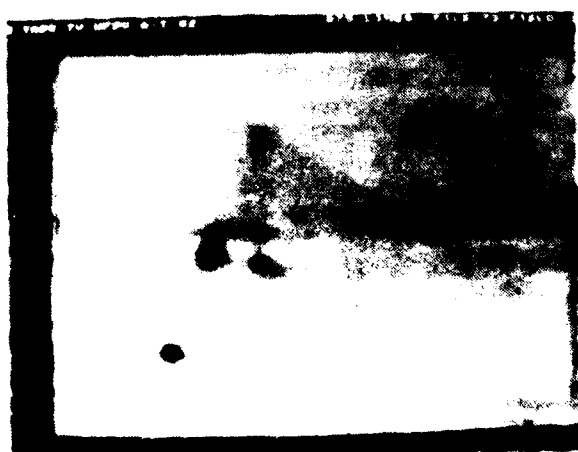
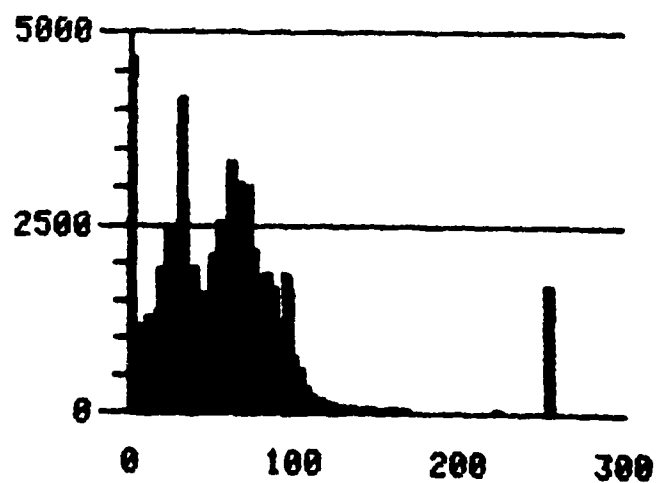e) LAGC (15 x 15, G = μ/σ)

f) LAGC (15 x 15, G = μ/σ)

Figure 4.22   D-TV & FLIR   LAGC (G = μ/σ) (L = 5 & 15)

49
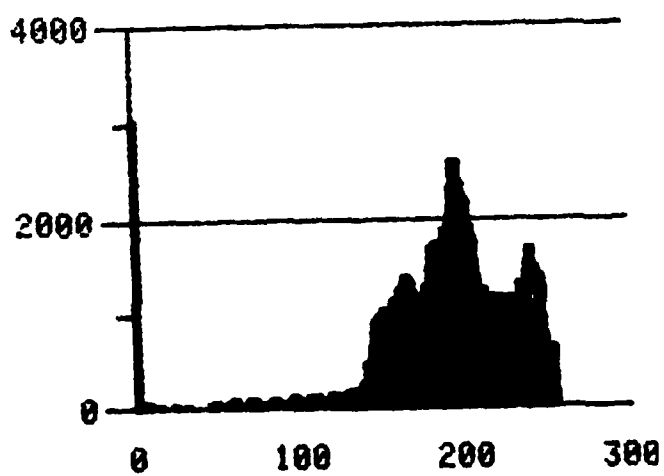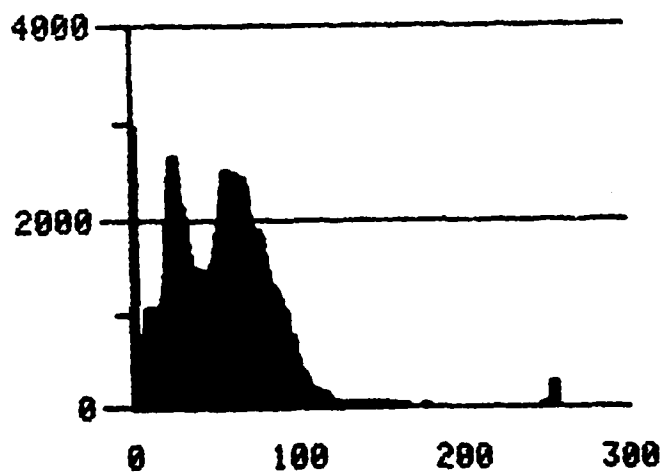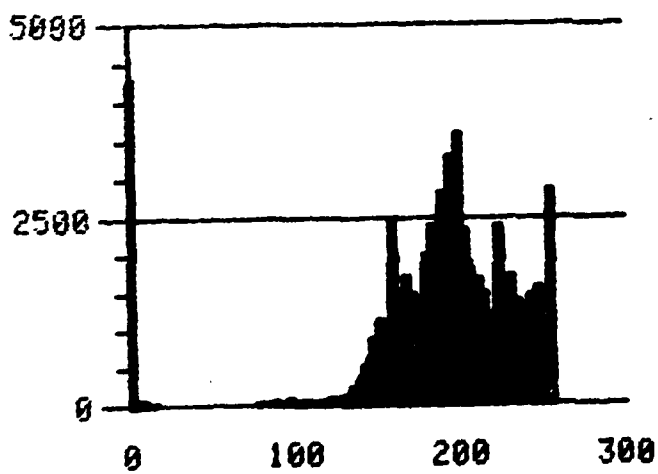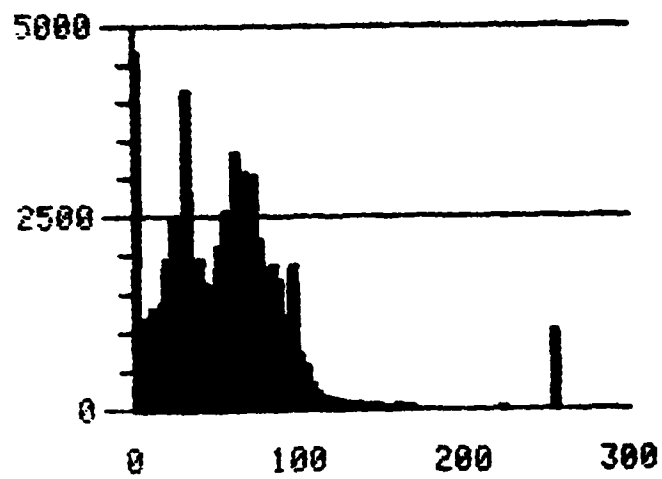
Figure 4.23   Histograms for figure 4.22

50
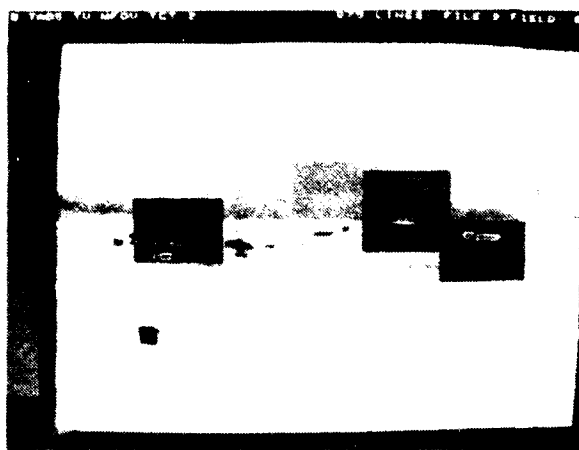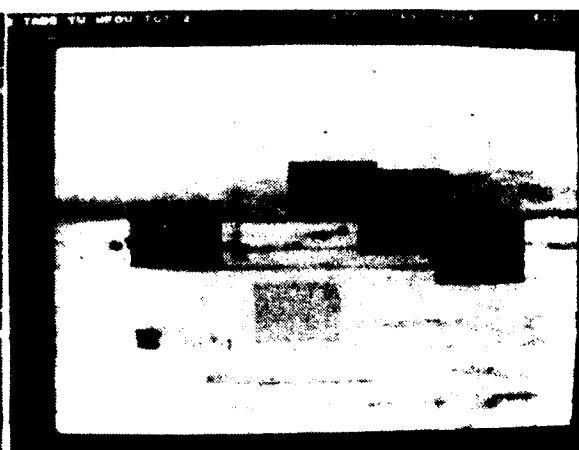
a) Prewitt (3 x 3)

b) Sobel (3 x 3)
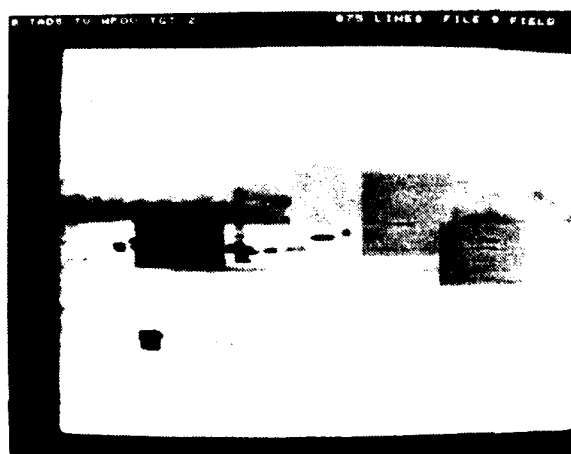
c) Unsharp mask (3 x 3)
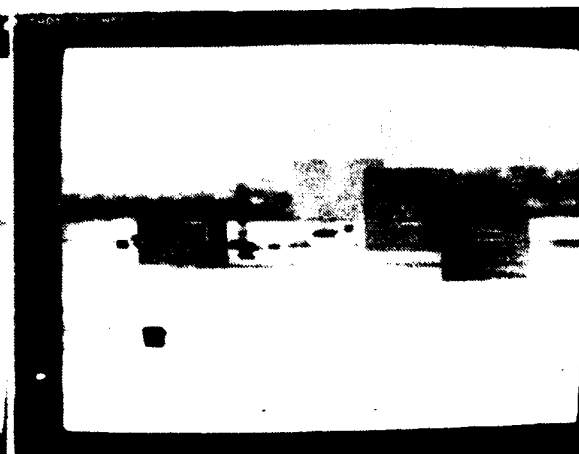
d) Unsharp mask (5 x 5)

Figure 4.24 Gradient processor comparisons

THIS PAGE INTENTIONALLY LEFT BLANK

Figure 4.25 Histograms for figure 4.24

a) B-TV original   b) B-FLIR original
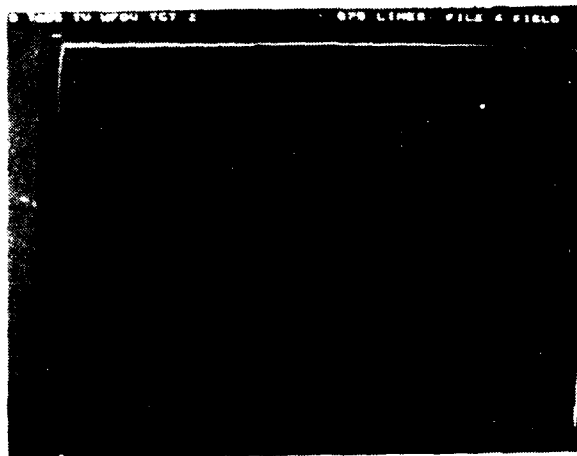
c) Prewitt (3 x 3)   d) Prewitt (3 x 3)
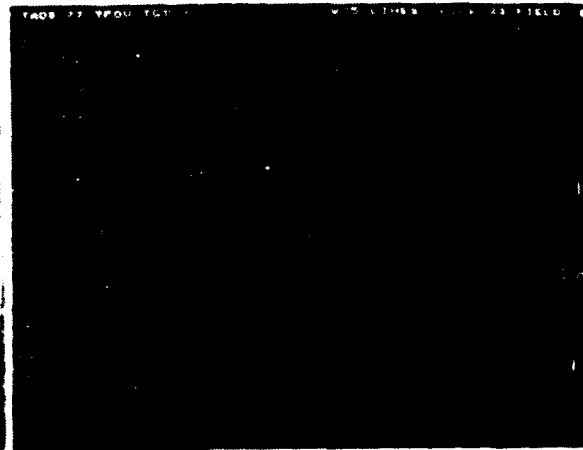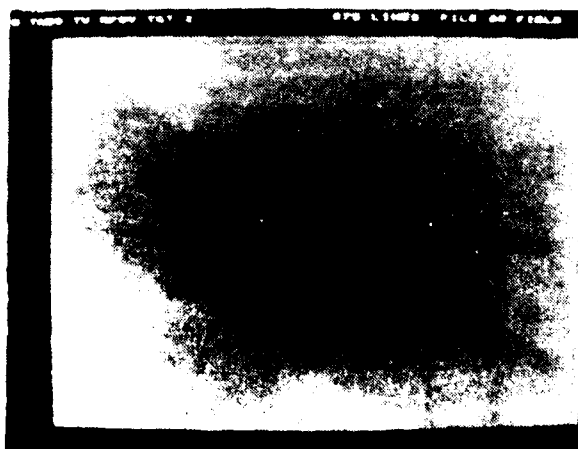
e) Unsharp mask (3 x 3)   f) Unsharp mask (3 x 3)
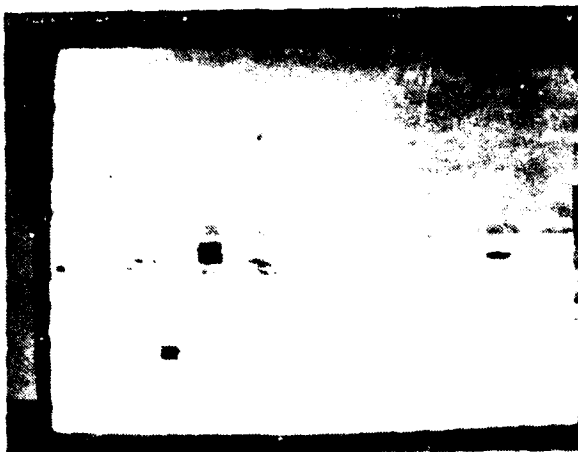
Figure 4.26   B-TV & FLIR image gradients
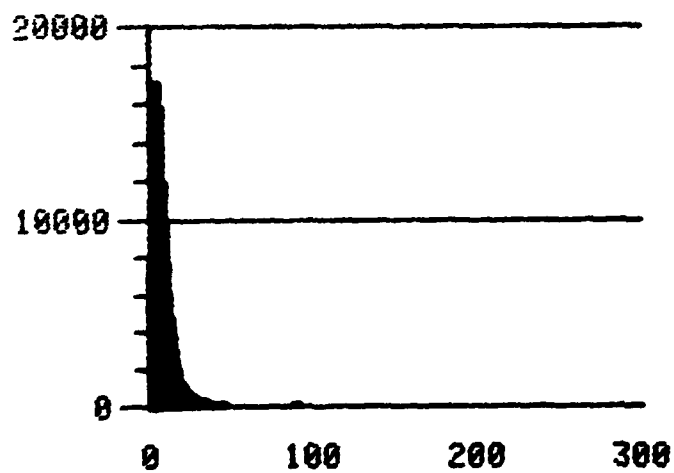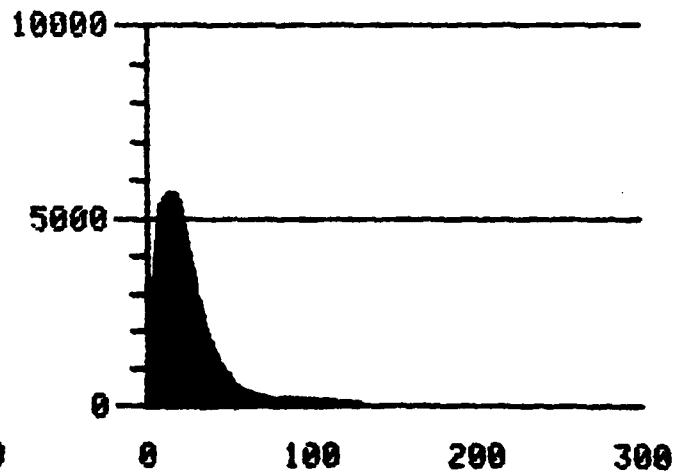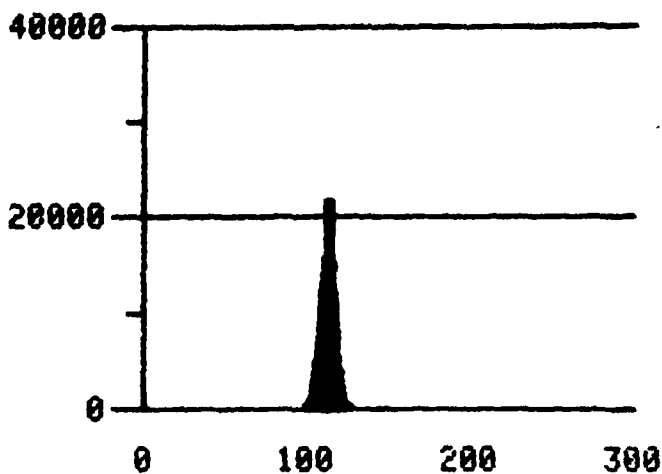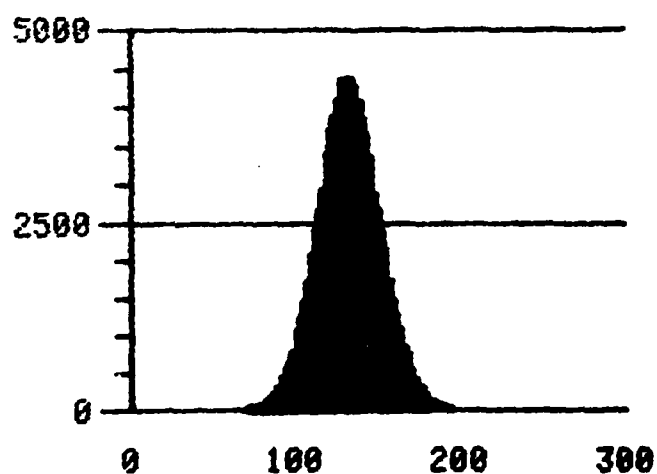
Figure 4.27 Histograms for figure 4.26
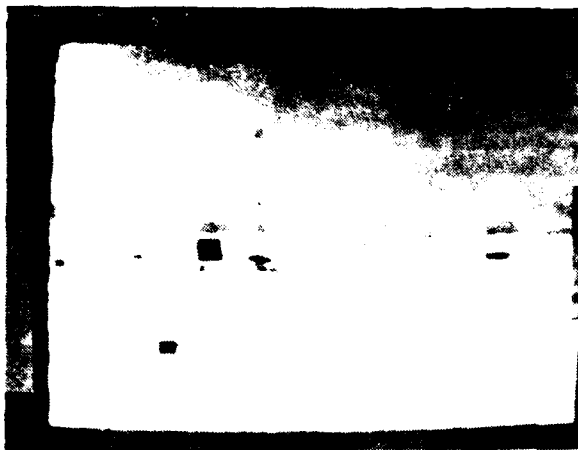
a) D-TV original   b) D-FLIR original
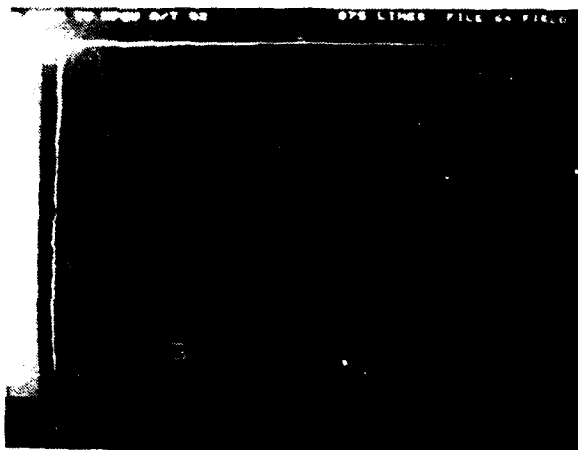
c) Prewitt (3 x 3)   d) Prewitt (3 x 3)
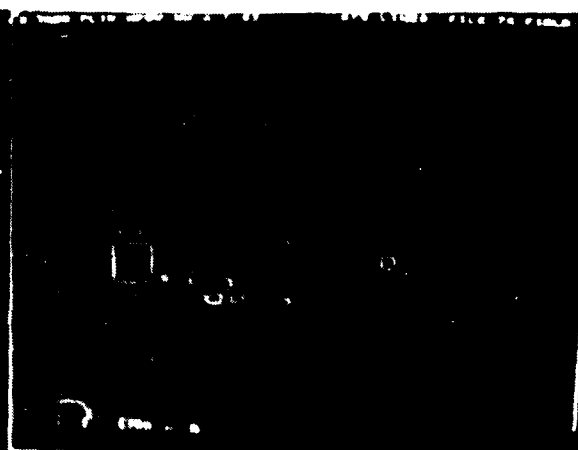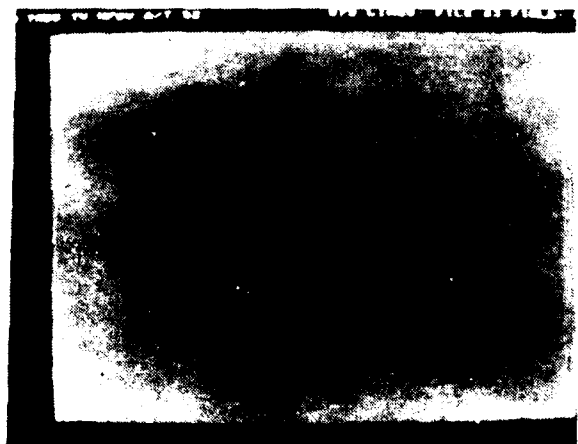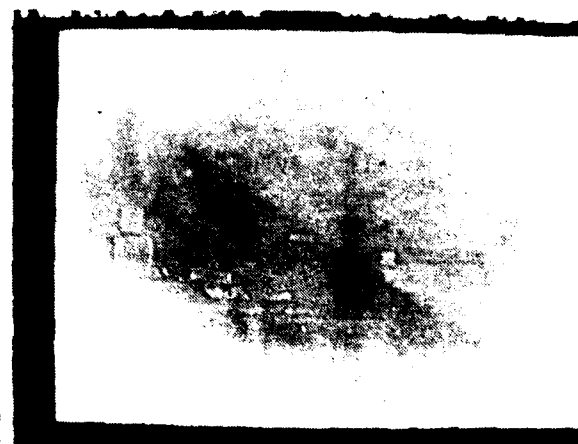
e) Unsharp mask (3 x 3)   f) Unsharp mask (3 x 3)

Figure 4.28   D-TV & FLIR Image gradients

55
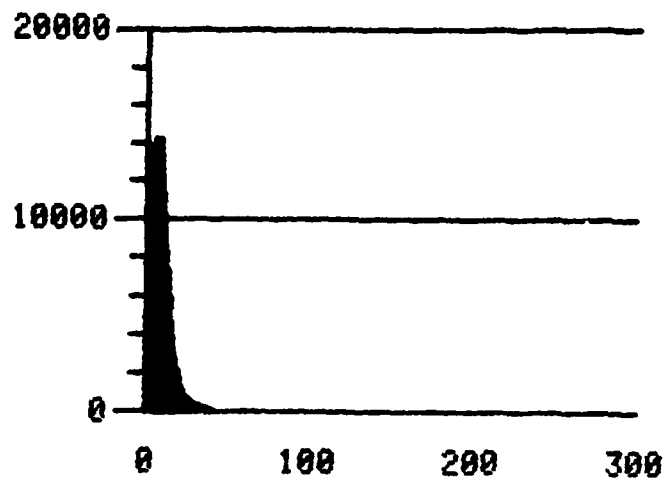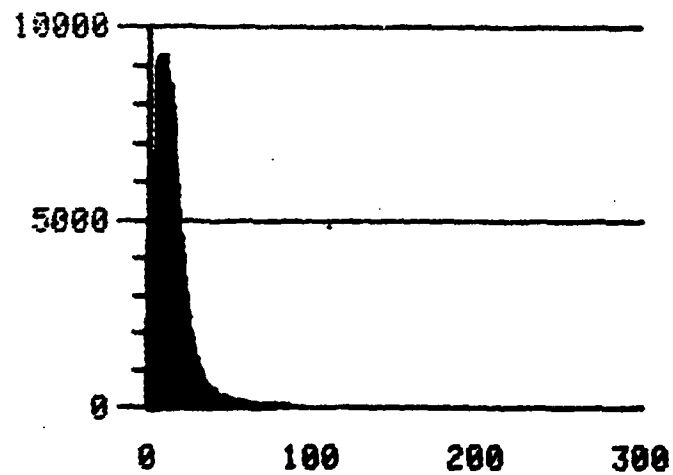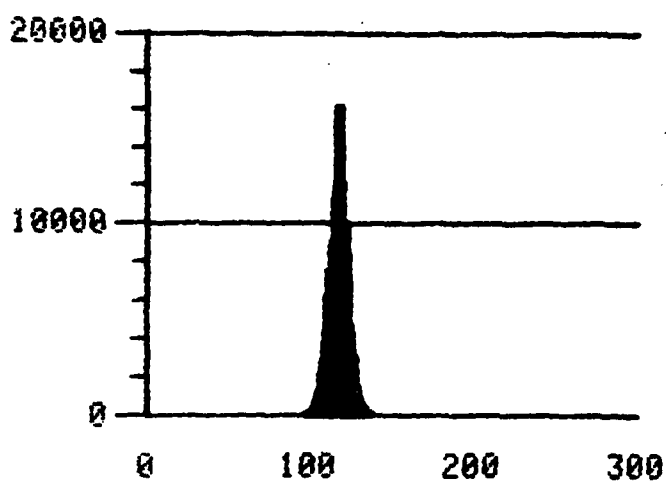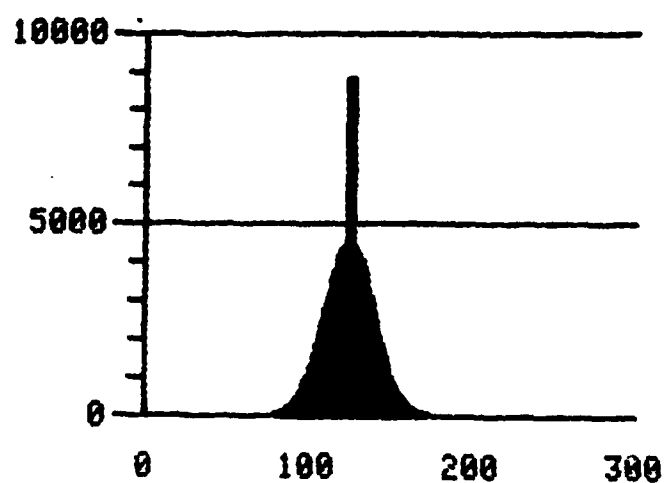
Figure 4.29   Histograms for figure 4.28

56
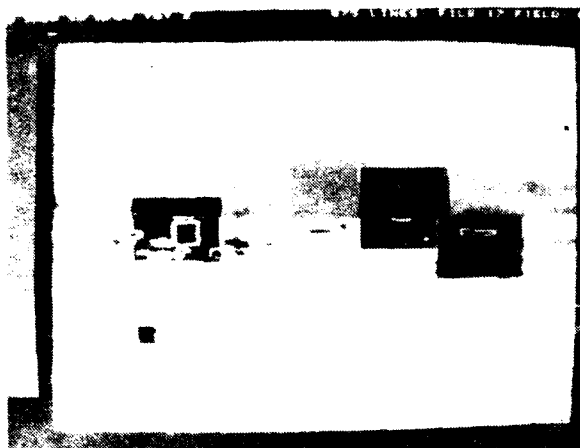
a) Prewitt (global mean)
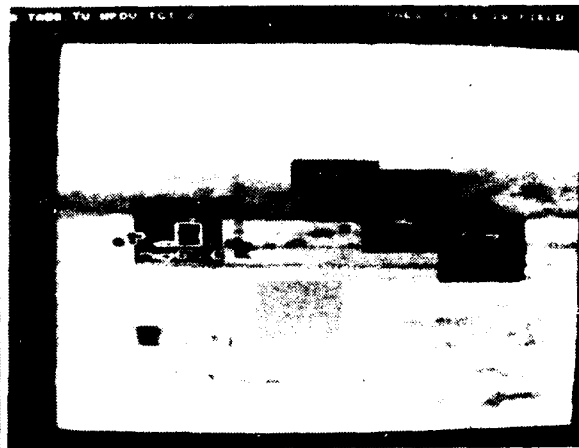
b) Sobel (global mean)
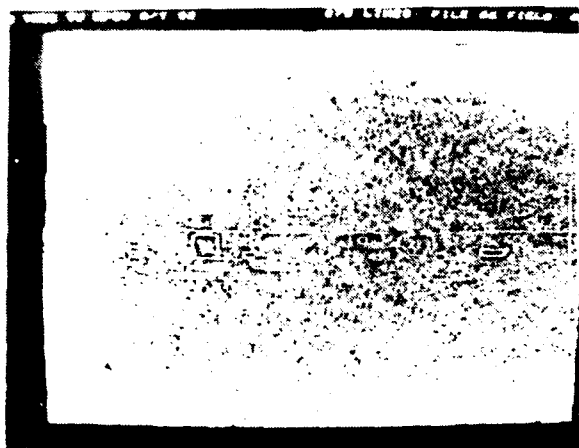
c) Prewitt (3 x 3 local mean)
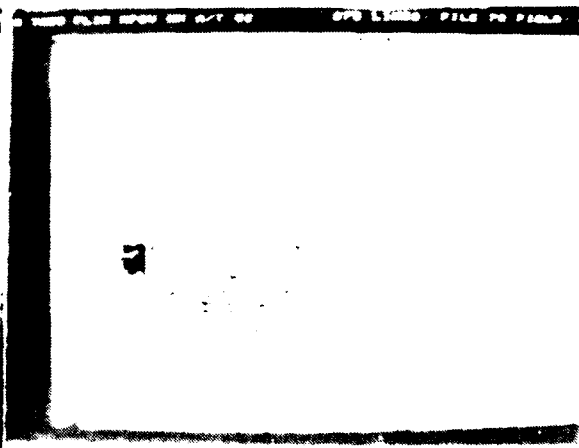
d) Sobel (3 x 3 local mean)

Figure 4.30   Edge images - global mean threshold

PERCENT EDGES

c) 49.08%   d) 49.41%

Figure 4.31 Histograms for figure 4.30
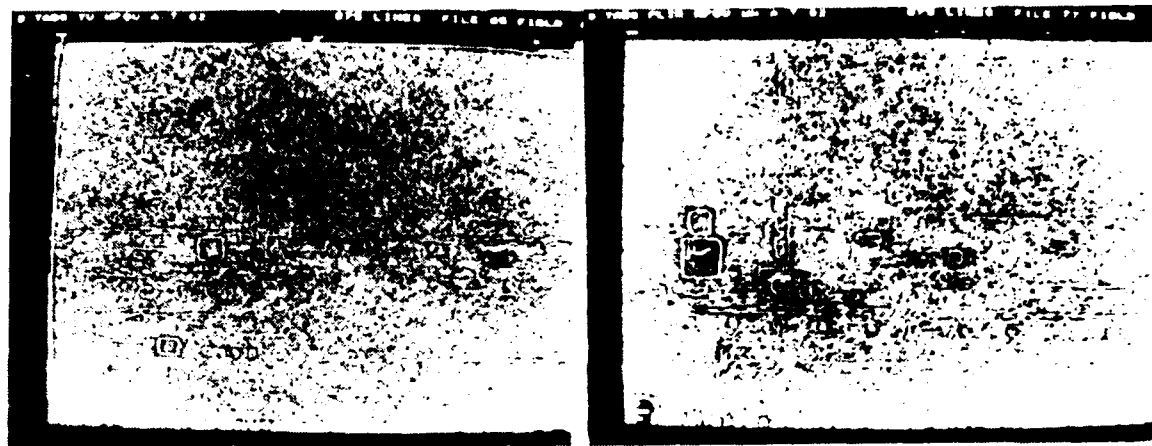
a) Prewitt local, T = μ+.5σ   b) Prewitt local, T = μ+ .5σ
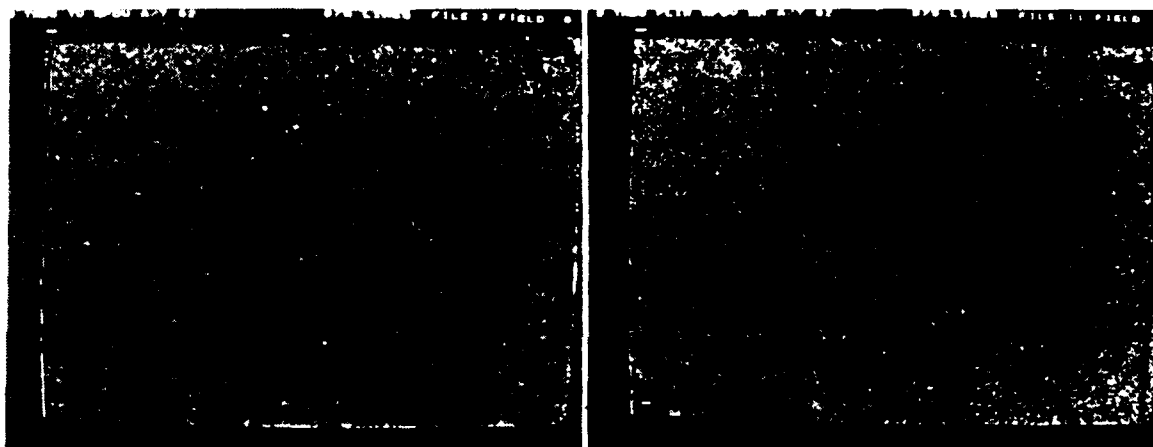
c) Prewitt local, T = μ+ σ   d) Prewitt local, T = μ + σ
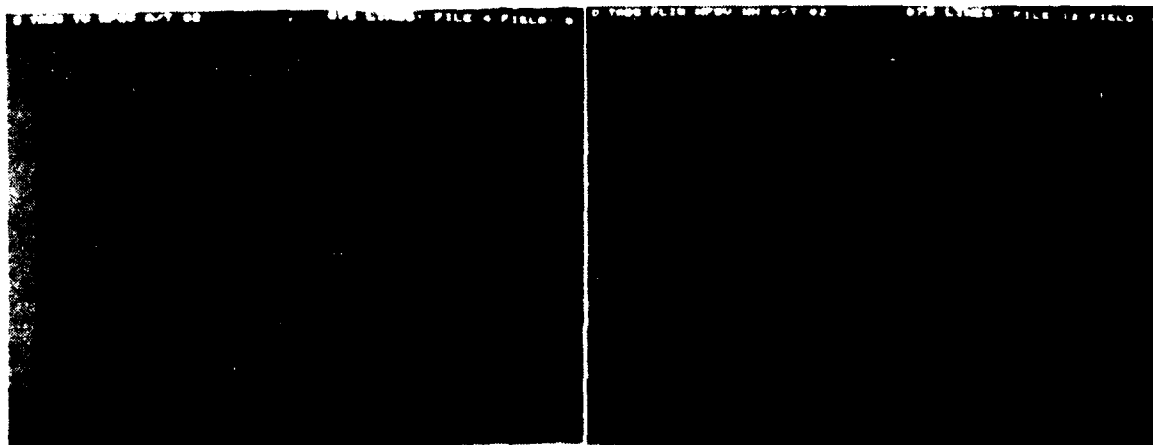
e) Prewitt local, T = μ + 2σ   f) Prewitt local, T = μ + 2σ

Figure 4.32   Edge images - 3 x 3 local thresholds

PERCENT EDGES

a)   29.91%   b)   29.33%

c)   14.86%   d)   14.18%

e)   0.58%   f)   0.43%

Figure 4.33 Histograms for figure 4.32
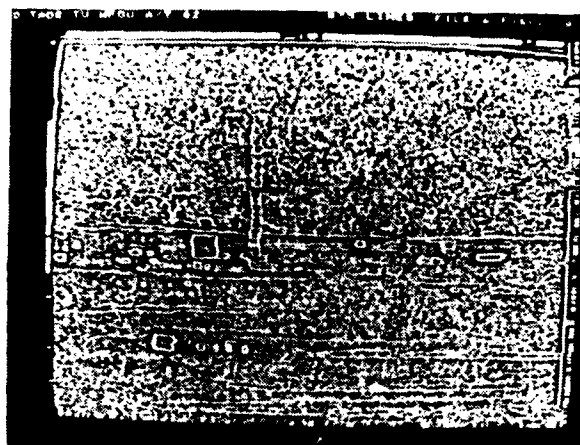
a) 7 x 7 local, T = μ
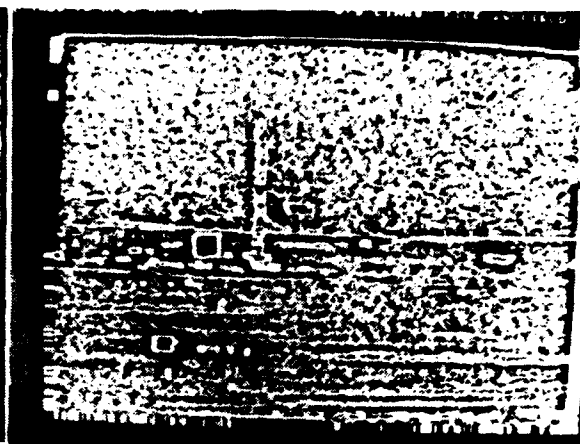
b) 15 x 15 local, T = μ
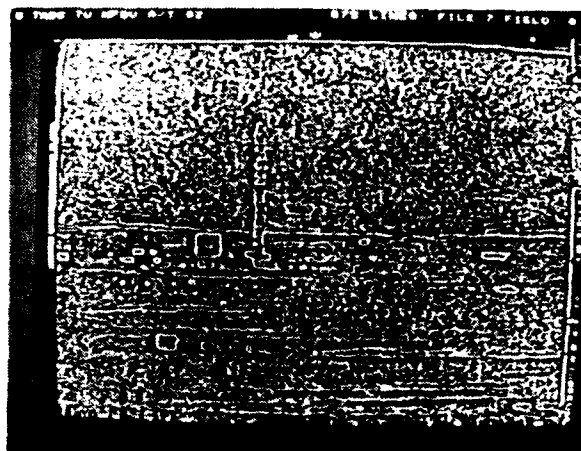
c) 7 x 7 local, T = μ + .5σ
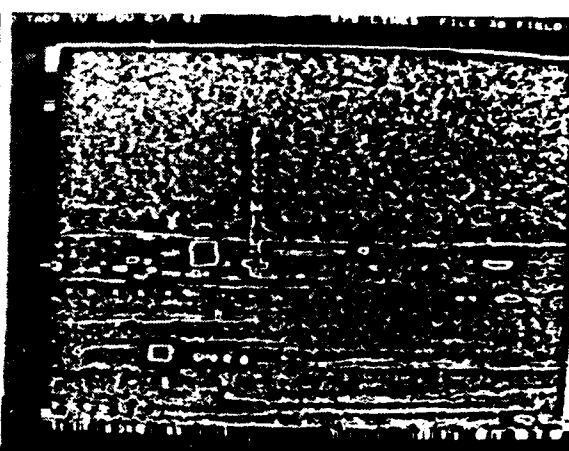
d) 15 x 15 local. T = μ + .5σ
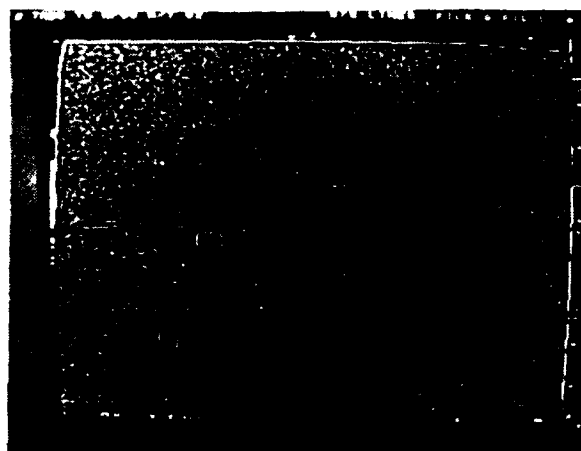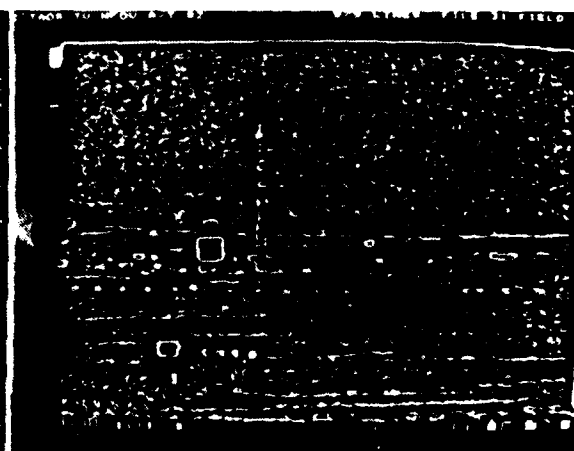
e) 7 x 7 local, T = μ + σ

f) 15 x 15 local, T = μ + σ

Figure 4.34   D-TV edge images - 7 x 7 & 15 x 15 local
thresholds

61

PERCENT EDGES

a)   45.20%   .   b)   41.52%

c)   27.75%   d)   26.14%

e)   15.66%   f)   15.54%

Figure 4.35   Histograms for figure 4.34
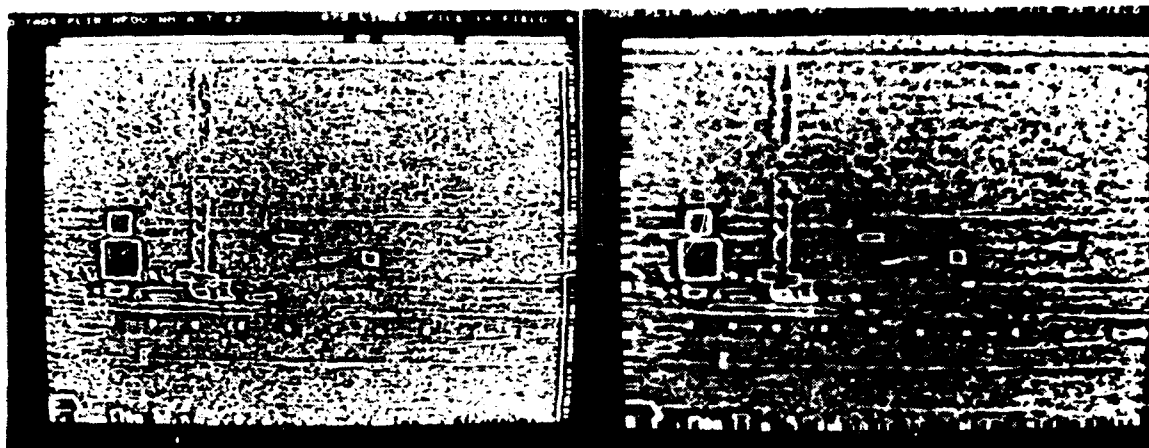
62

a) 7 x 7 local, T = μ   b) 15 x 15 local, T = μ
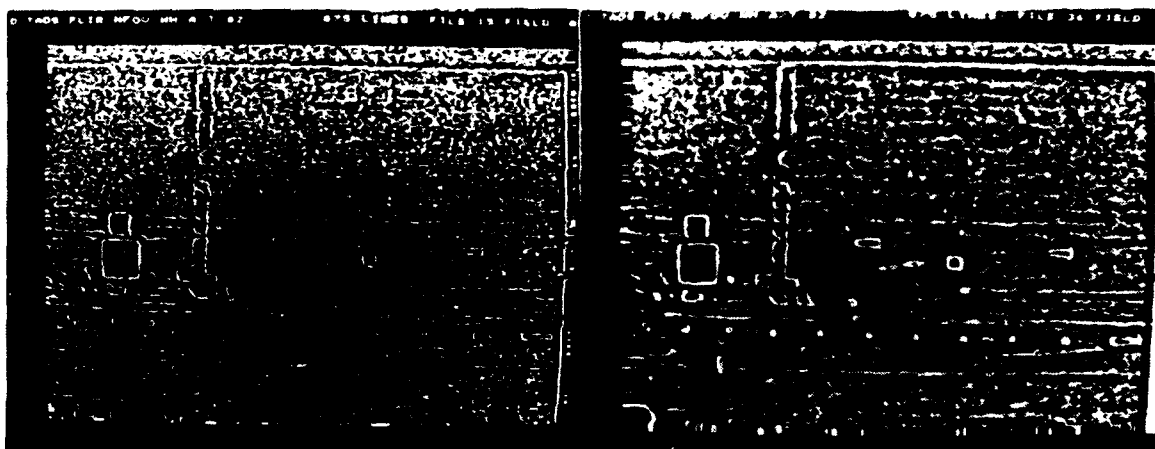
c) 7 x 7 local, T = μ + .5σ   d) 15 x 15 local, T = μ + .5σ
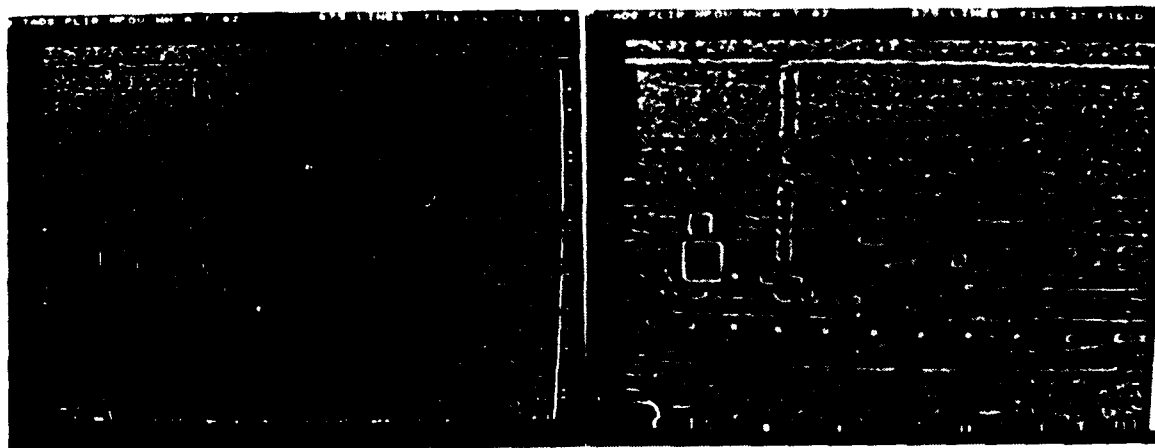
e) 7 x 7 local, T = μ + σ   f) 15 x 15 local, T = μ + σ

Figure 4.36   D-FLIR edge images – 7 x 7 & 15 x 15 local thresholds

63

<u>PERCENT EDGES</u>

a)   45.66%   b)   42.69%

c)   27.90%   d)   27.26%

e)   15.45%   f)   16.47%

Figure 4.37   Histograms for figure 4.36
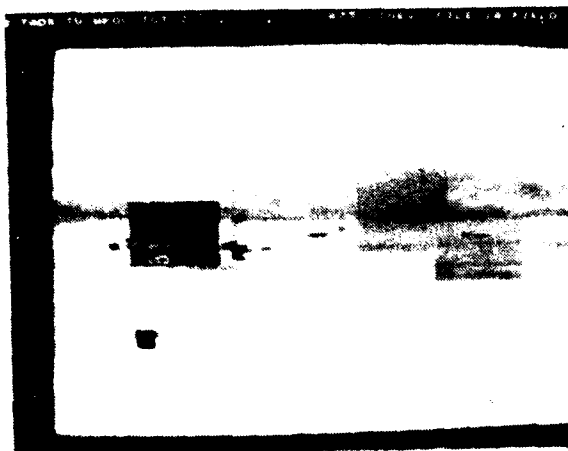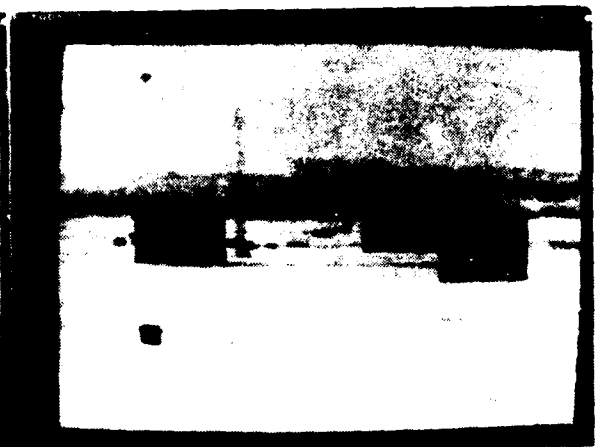
a) Prewitt b) Sobel
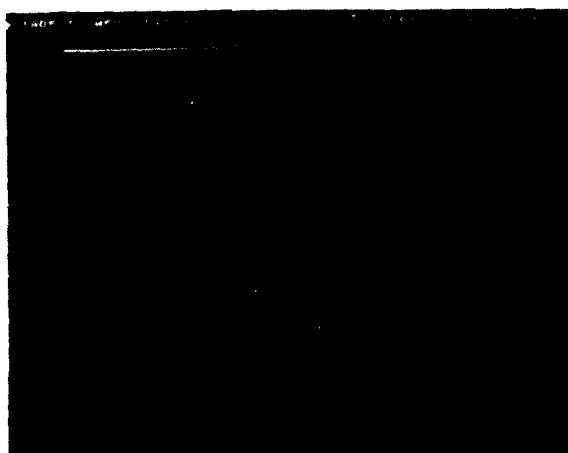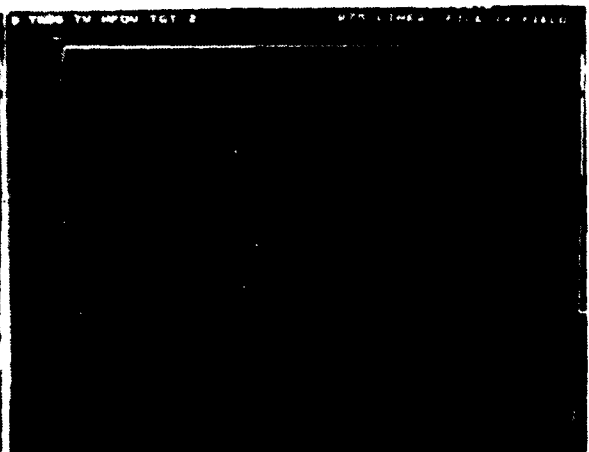
c) Prewitt d) Sobel

Figure 4.38 B-TV original plus gradients
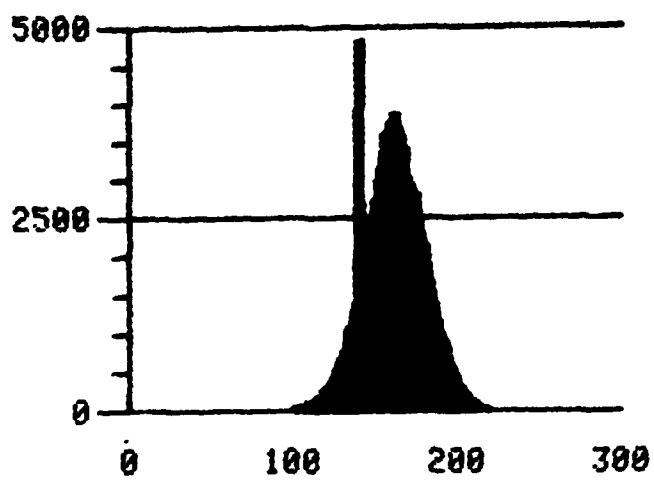
c)
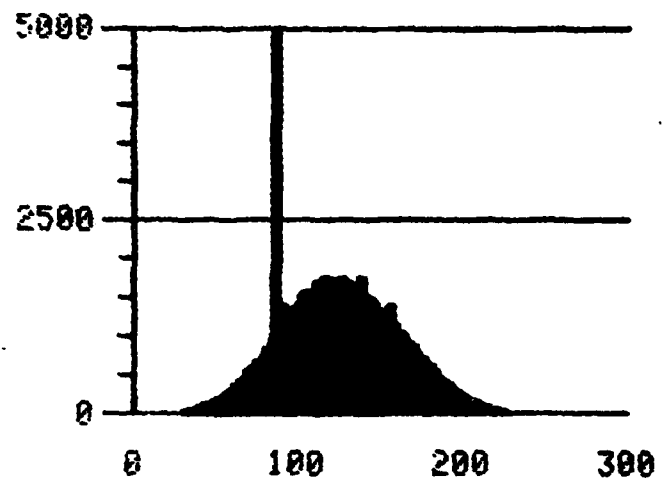
d)

Figure 4.39   Histograms for figure 4.38

66

a) 3 x 3, T = $\mu + \sigma$ b) 3 x 3, T = $\mu + \sigma$

c) 7 x 7, T = $\mu + \sigma$ d) 7 x 7, T = $\mu + \sigma$
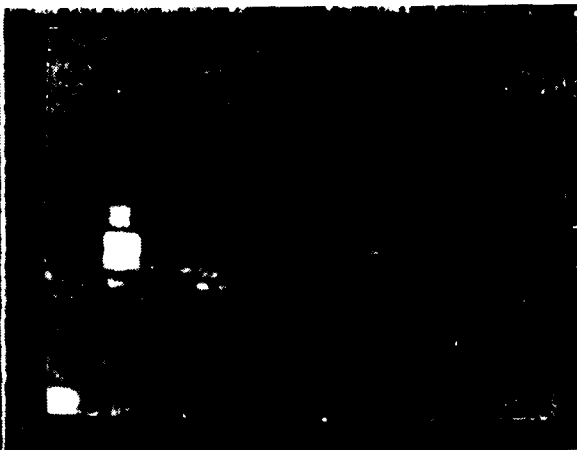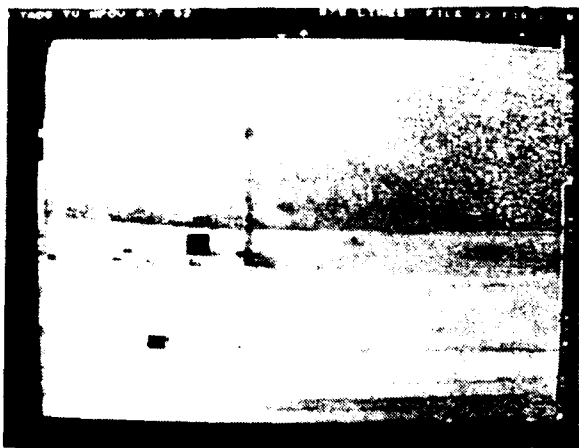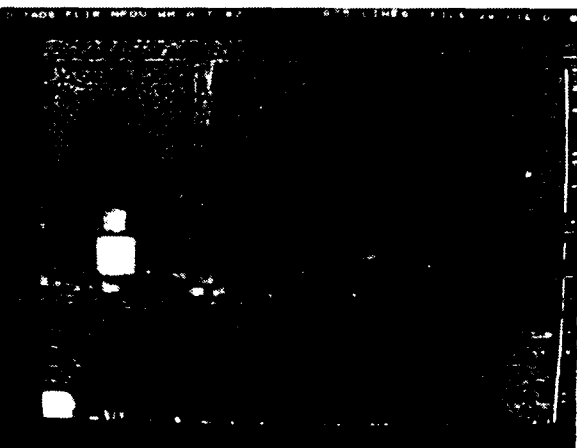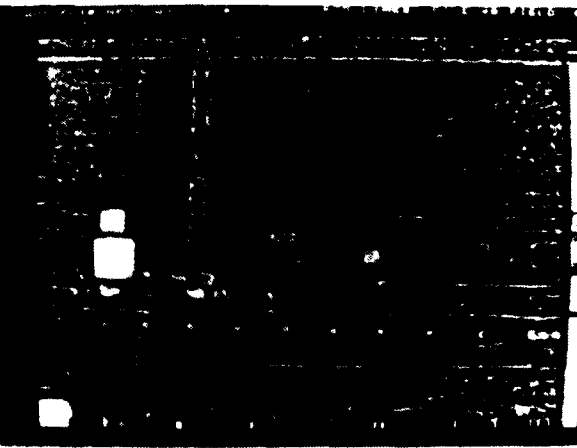
e) 15 x 15, T = $\mu + \sigma$ f) 15 x 15, T = $\mu + \sigma$

Figure 4.40 Original with edge replacement – 3 x 3, 7 x 7 & 15 x 15
local threshold
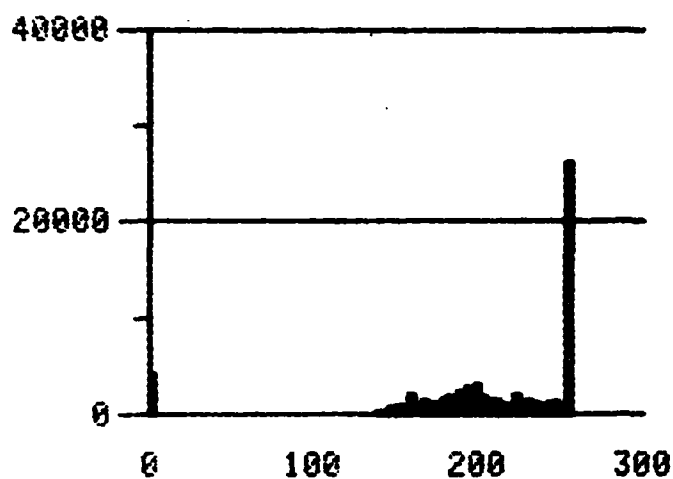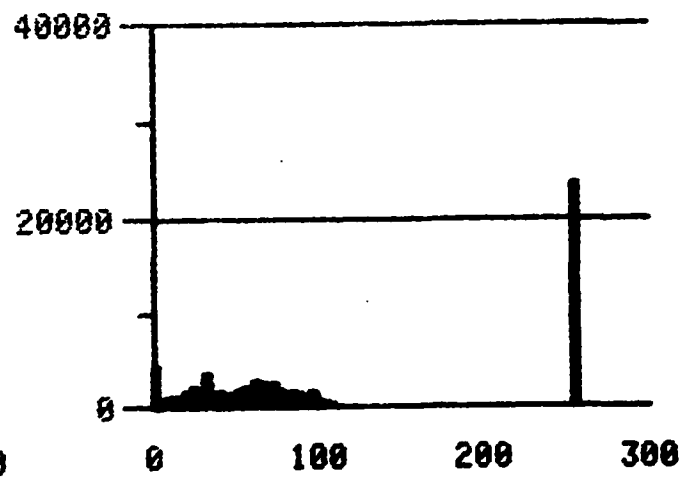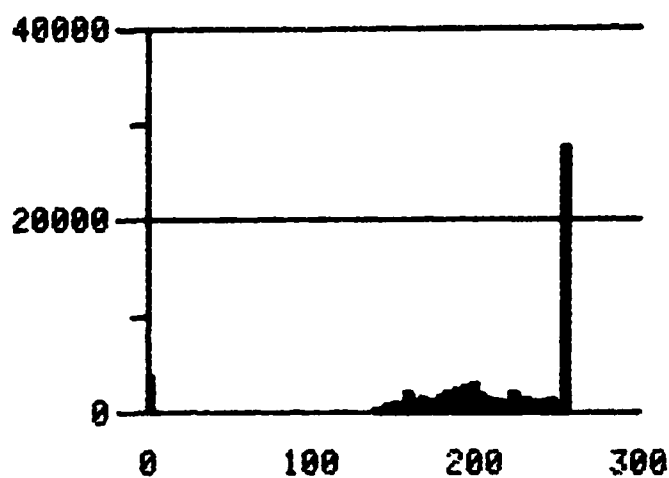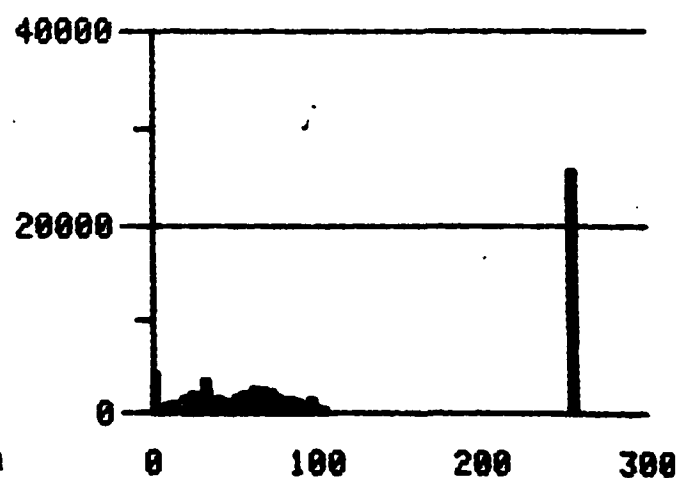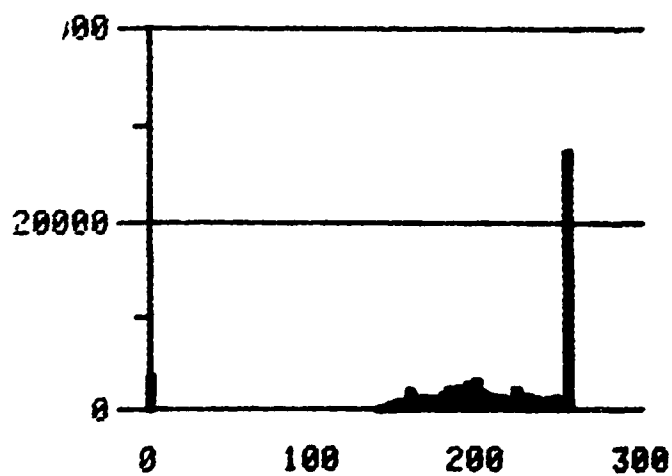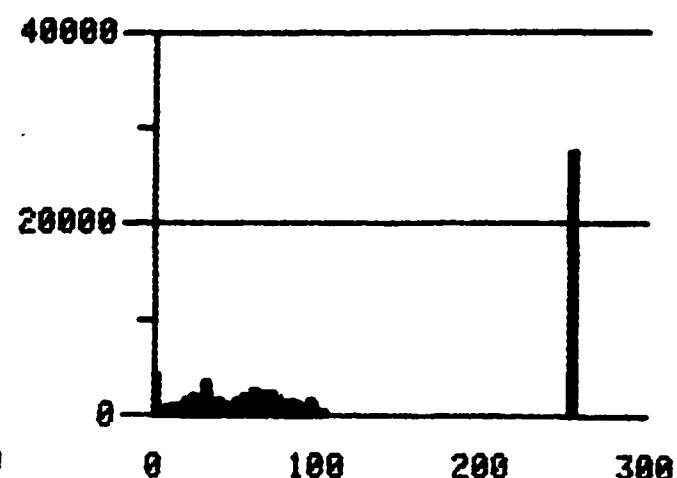
Figure 4.41 Histograms for figure 4.40

68
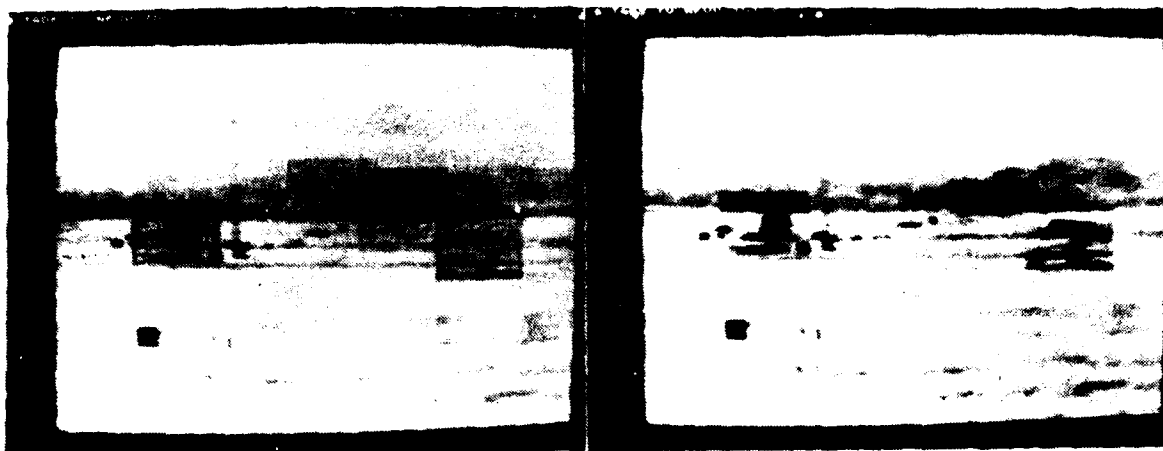
a) LAGC (5 x 5) $\longrightarrow$ Median (5x5)   b) Average (5 x 5) $\longrightarrow$ Histogram equal
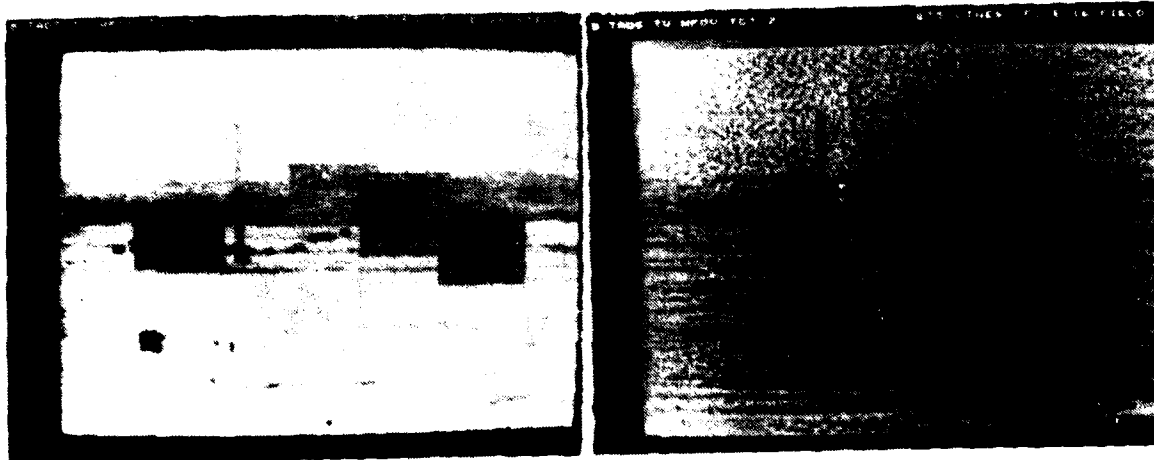
c) Median (5 x 5) $\longrightarrow$ LAGC (5 x 5)   d) Median (5 x 5) $\longrightarrow$ LAGC (5 x 5)

Figure 4.42   B- TV serial processing

69
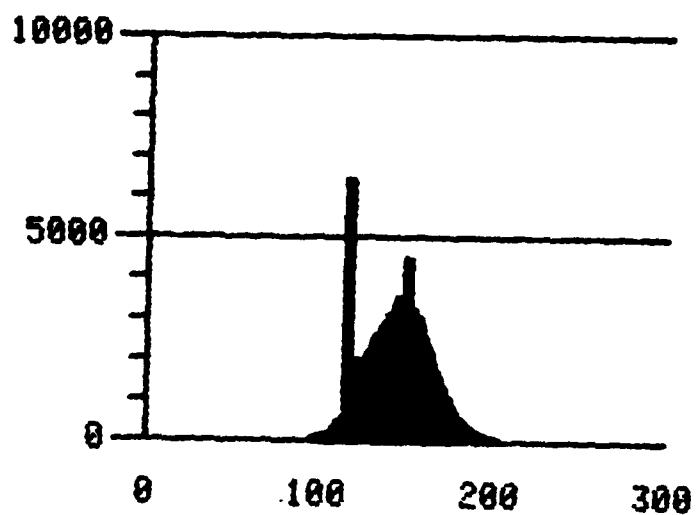
d)

Figure 4.43   Histograms for figure 4.42
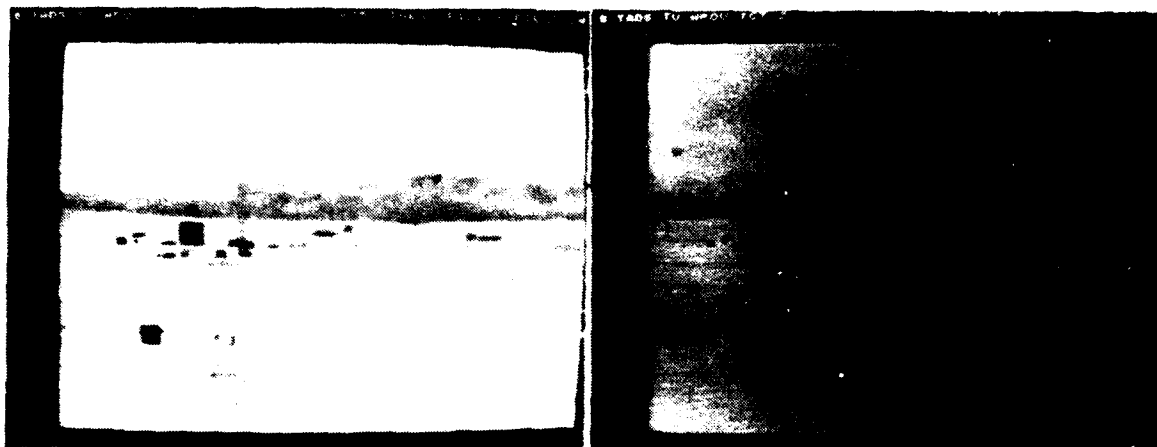
a) B-TV original

b) Median $(\frac{1}{3})$ + LAGC $(\frac{1}{3})$ + Prewitt $(\frac{1}{3})$
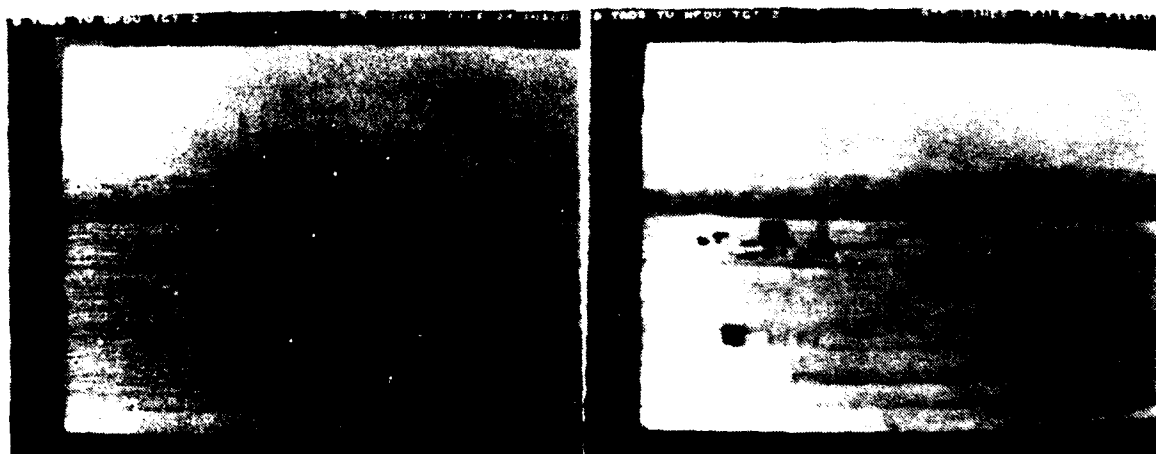
c) Median (.25) + LAGC (.75)

d) Median (.75) + LAGC (.25)

Figure 4.44 B-TV parallel processing

71
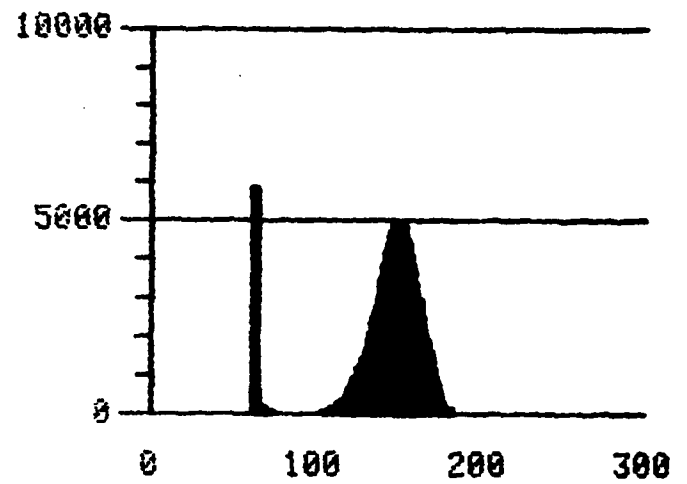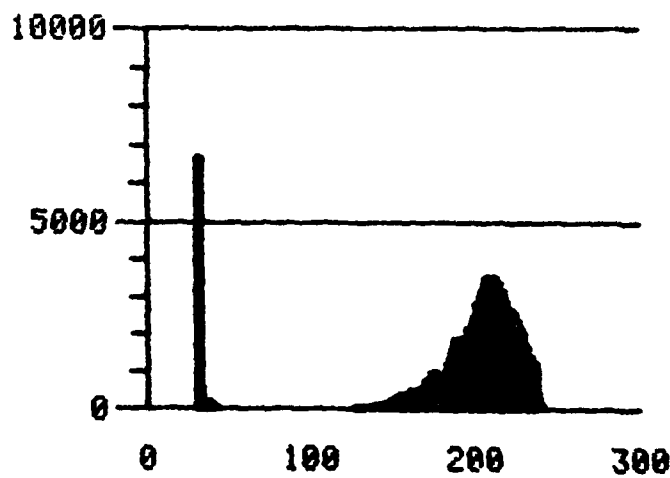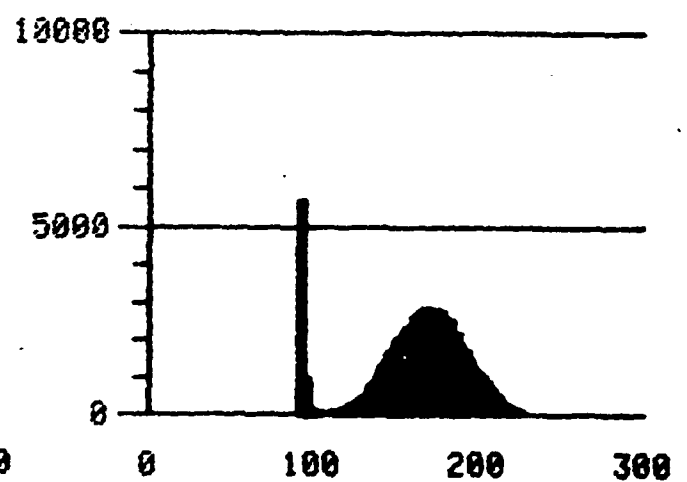
Figure 4.45 Histograms for figure 4.44

a) B-FLIR original   b) Median $(\frac{1}{3})$ + LAGC $(\frac{1}{3})$ + Prewitt $(\frac{1}{3})$
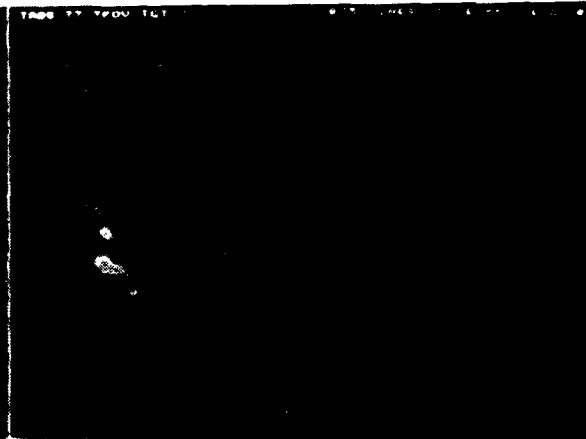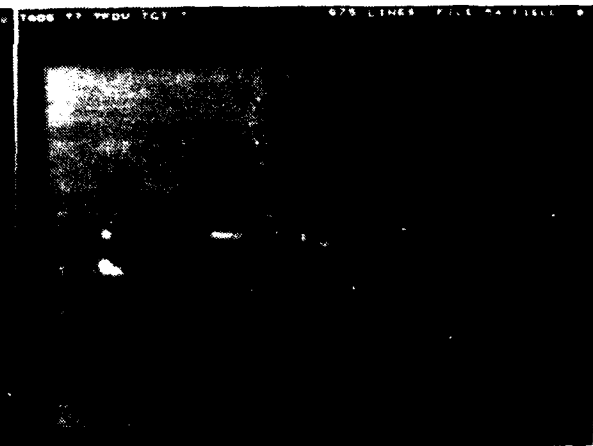
c) Median (.25) + LAGC (.75)   d) Median (.75) + LAGC (.25)

Figure 4.46   FLIR parallel processing
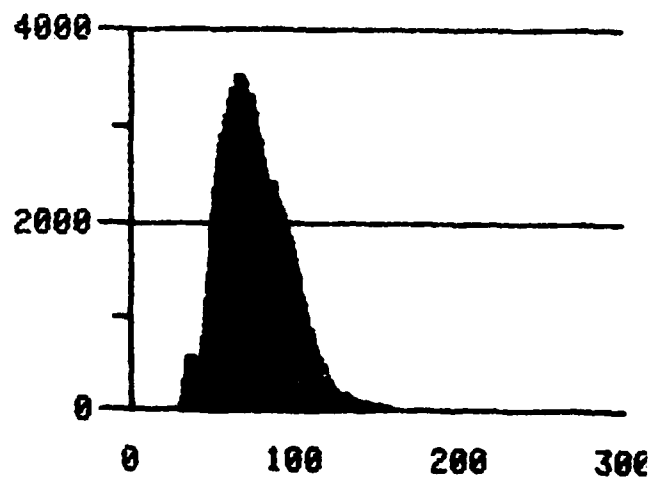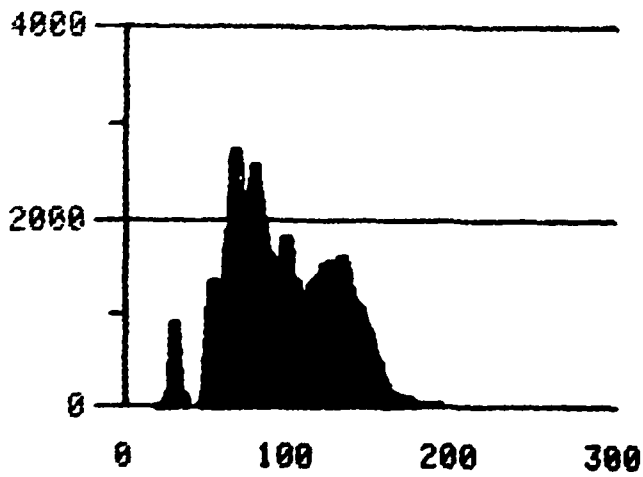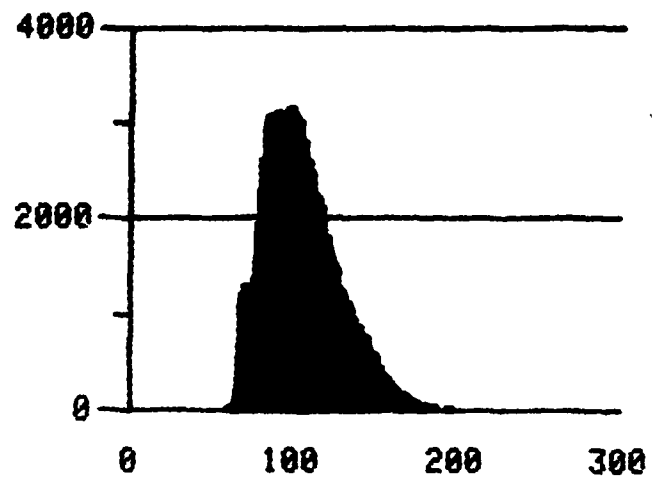
Figure 4.47   Histograms for figure 4.46

74

TABLE 4.3 IMAGE CHARACTERIZATION - PROCESSED IMAGES

PROCESSED - NOISE REDUCTION

IMAGE	STATISTICS				SIGNAL/ NOISE	SIGNAL/ CLUTTER	FFT RESOLUTION	CONTRAST	FIGURE
	MEAN	STD	SKEW	KURTOSIS					
1. B-TV (Segments)									
A. MEDIAN (3 x 3)									
- TARGET/FIELD	197.1	23.5	-2.25	10.2	9.3	6.12	7	0.66	4.12b
- TARGET/TREES	189.6	26.4	-0.2	3.09	10.3	4.04	4	0.73	
- TARGET/FIELD-TREES	199.6	30.5	-0.48	2.5	10.9	3.8	3	0.79	
- TREE BACK-GROUND	206.5	25.8	0.208	1.77	9.36	1.84	3	0.175	
- FIELD BACK-GROUND	235.2	6.76	0.18	2.64	1.98	2.99	8	0.38	
- LARGE TARGET BOARD	177.5	54.7	-0.69	2.6	20.6	3.4	8	0.82	
B. MEDIAN (5 x 5)									
- TARGET/FIELD	193.3	24.3	-2.17	9.67	10.4	6.2	5	0.63	4.12c
- TARGET/TREES	184.4	26.8	-0.18	2.85	12.1	4.05	4	0.67	
- TARGET/FIELD-TREES	193.4	30.8	-0.44	2.3	13.2	3.9	3	0.70	
- TREE BACK-GROUND	206.6	25.7	0.231	1.74	9.59	1.87	3	0.163	

IMAGE	MEAN	STATISTICS STD	SKEW	KURTOSIS	SIGNAL/ NOISE	SIGNAL/ CLUTTER	FFT RESOLUTION	CONTRAST	FIGURE
- FIELD BACK-GROUND	235.1	6.43	0.34	2.83	2.15	3.21	6	0.268	
- LARGE TARGET BOARD	172.1	57.5	-0.72	2.7	24.5	3.5	8	0.74	4.12d
C. AVERAGE(3 x 3)									
- TARGET/FIELD	196.7	23.0	-2.2	9.6	10.8	6.2	5	0.65	
- TARGET/TREES	189.5	26.1	-0.23	2.99	12.0	4.09	4	0.73	
-TARGET/FIELD-TREES	189.8	31.6	-0.38	2.1	15.0	3.97	3	0.71	
- TREE BACK-GROUND	206.2	25.6	0.227	1.75	10.4	1.87	3	0.167	
- FIELD BACK-GROUND	235.3	6.40	0.14	2.77	2.14	3.17	7	0.37	
- LARGE TARGET BOARD	177.1	53.0	-0.68	2.69	23.5	3.53	8	0.8	
D. AVERAGE (5 x 5)									
- TARGET/FIELD	191.0	24.2	-1.92	8.1	11.7	6.2	5	0.62	
- TARGET/TREES	180.6	27.5	-0.12	2.69	13.6	4.17	4	0.66	
- TARGET/FIELD TREES	199.3	30.2	-0.45	2.4	12.8	3.87	3	0.79	4.12e
- TARGET BACK GROUND	206.7	25.2	0.25	1.72	9.84	1.92	3	0.152	
- FIELD BACK-GROUND	235.3	6.12	0.27	3.03	2.12	3.37	5	0.24	
- LARGE TARGET BOARD	169.5	54.4	-0.66	2.8	23.4	3.6	8	0.68	

IMAGE	MEAN	STATISTICS STD	SKEW	KURTOSIS	SIGNAL/ NOISE	SIGNAL/ CLUTTER	FFT RESOLUTION	CONTRAST	FIGURE
2. B-TV and FLIR TOTAL IMAGES									
A. MEDIAN (TV) (5x5)	206.7	56.6	-2.7	9.8	11.2	6.15	6	0.64	4.14c
B. AVERAGE(TV) (5x5)	206.4	54.8	-2.6	9.5	12.1	6.12	6	0.63	4.14e
C. MEDIAN (FLIR) (5 x 5)	93.8	38.1	0.21	2.6	11.3	6.23	5	0.66	4.14d
D. AVERAGE (FLIR) (5 x 5)	93.8	37.9	0.20	2.5	12.3	6.17	5	0.66	4.14f
3. D-TV and FLIR									
A. TV MEDIAN (5x5)	190.2	47.7	-2.0	8.8	11.3	6.17	6	0.65	4.16c
B. FLIR MEDIAN(5x5)	55.3	36.2	1.8	10.4	12.4	6.14	5	0.60	4.16d

PROCESSED - CONTRAST ENHANCEMENT

IMAGE	MEAN	STATISTICS STD	SKEW	KURTOSIS	SIGNAL/ NOISE	SIGNAL/ CLUTTER	FFT RESOLUTION	CONTRAST	FIGURE
4. B-TV and FLIR									
A. TV-HIST (EQ.)									
- TARGET/FIELD	152.3	48.4	-3.0E-2	1.8	4.7	3.8	5	0.77	4.18a
- TARGET/TREES	172.3	48.2	-2.4 -2	1.8	4.77	2.59	4	0.95	
- TARGET/FIELD TREES	168.8	46.5	-6.1E-2	1.8	4.57	3.2	3	0.89	
- FIELD BACK GROUND	232.7	13.2	-7.3E-2	1.84	1.37	1.7	22	1.0	
B. TV-HIST (HY.)									
- TARGET/FIELD	99.2	42.2	1.59	4.6	4.7	4.4	6	0.67	4.18b
- TARGET/TREES	118.2	40.9	1.6	4.7	4.7	4.1	4	0.4	
- TARGET/FIELD- TREES	117.6	40.1	1.6	4.4	4.5	4.1	4	0.77	

77

IMAGE	MEAN	STATISTICS STD	SKEW	KURTOSIS	SIGNAL/ NOISE	SIGNAL/ CLUTTER	FFT RESOLUTION	CONTRAST	FIGURE
- FIELD BACK-GROUND	217.9	11.6	1.5	4.4	1.31	3.4	22	1.0	
C. TV-LAGC (3x3)									
- TARGET/FIELD	146.5	25.2	2.1E-2	3.3	5.2	5.0	4	0.59	4.18c
- TARGET/TREES	167.8	25.7	3.85	3.04	5.32	3.69	7	0.81	
- TARGET/FIELD TREES	164.9	23.6	0.12	3.11	5.02	4.28	4	0.67	
- FIELD BACK-GROUND	231.7	7.9	8.0E-2	2.6	1.49	2.85	2	0.82	
- TREE BACK-GROUND	204.2	14.9	9.6E-2	3.09	3.16	3.36	3	0.839	
D. TV-LAGC (5x5)	152.2	25.4	5.2E-2	3.17	5.31	4.29	5	0.71	4.18d
E. FLIR-UNPROC.	93.8	38.8	0.23	2.64	5.25	4.37	5	0.76	4.18e
F. FLIR-LAGC (5x5)	109.7	21.8	0.71	4.19	5.18	4.35	5	0.74	4.18f
5. D-LAGC (1/σ)									
A. TV-UNPROC.	190.0	48.1	-1.97	8.61	5.02	4.96	6	0.75	4.20a
B. FLIR-UNPROC.	55.5	37.1	1.78	9.90	5.30	4.31	5	0.75	4.20b
C. TV-LAGC (5x5)	189.8	47.2	-1.9	8.55	5.09	4.94	7	0.77	4.20c
D. FLIR-LAGC (5x5)	55.6	36.4	1.8	10.2	5.28	4.32	5	0.76	4.20d
E. TV-LAGC (15x15)	187.9	45.8	-1.84	8.45	4.92	4.98	9	0.79	4.20e
F. FLIR-LAGC (15x15)	56.1	35.7	1.86	11.2	5.19	4.27	8	0.78	4.20f

IMAGE	STATISTICS MEAN	STD	SKEW	KURTOSIS	SIGNAL/ NOISE	SIGNAL/ CLUTTER	FFT RESOLUTION	CONTRAST	FIGURE
6. D-LAGC (μ/σ)									
A. TV-UNPROC.	190.0	48.1	-1.97	8.61	5.02	4.96	6	0.75	4.22a
B. FLIR-UNPROC.	55.5	37.1	1.78	9.90	5.30	4.31	5	0.75	4.22b
C. TV-LAGC (5x5)	187.6	49.5	-1.92	8.56	5.04	4.93	6	0.77	4.22c
D. FLIR-LAGC (5x5)	55.0	36.0	1.9	10.3	5.28	4.37	6	0.77	4.22d
E. TV-LAGC (15x15)	182.3	46.3	-1.89	8.51	4.99	4.97	10	0.79	4.22e
F. FLIR-LAGC (15x15)	55.1	36.1	2.0	11.7	5.20	4.29	9	0.78	4.22f
7. B-TV GRADIENT									
A. PREWITT (3x3)									
- TARGET/FIELD	101.3	31.0	1.66	5.3	5.6	2.9	16	0.8	4.24a
- TARGET/TREES	111.9	27.1	2.6	9.0	6.3	4.8	15	1.0	
- TARGET/FIELD-TREES	111.6	26.1	2.3	7.8	5.7	3.2	15	0.92	
- FIELD BACKGROUND	215.7	9.6	3.3	12.8	2.2	4.3	21	0.11	
- TREE BACKGROUND	173.2	20.1	2.7	9.9	4.3	4.5	17	0.77	
- LARGE TARGET BACKGROUND	64.1	40.8	1.57	5.2	7.39	4.9	14	0.67	
B. SOBEL (3x3)									
- TARGET/FIELD	98.8	26.5	1.6	6.0	3.9	3.5	16	0.8	4.24b
- TARGET/TREES	111.1	22.6	2.4	9.5	4.3	5.7	13	1.0	
- TARGET/FIELD-TREES	110.7	22.1	2.1	8.2	3.9	3.7	13	0.92	

79

IMAGE	MEAN	STATISTICS STD	SKEW	KURTOSIS	SIGNAL/ NOISE	SIGNAL/ CLUTTER	FFT RESOLUTION	CONTRAST	FIGURE
- FIELD BACK-GROUND	217.3	9.5	2.9	11.2	1.9	4.2	21	0.22	
- TREE BACK-GROUND	175.2	18.5	2.24	7.59	3.05	4.79	17	0.217	
- LARGE TARGET BACKGROUND	60.5	38.0	1.74	6.1	6.37	5.33	14	0.61	4.24c
C. UNSHARP MASK (3x3)									
- TARGET/FIELD	196.6	23.0	-2.1	9.6	10.8	6.2	5	0.65	
- TARGET/TREE	189.2	27.3	-6.7E-2	2.9	12.3	4.0	4	0.62	
- TARGET/FIELD-TREE	199.3	30.2	-0.4	2.4	12.8	3.87	3	0.79	
- FIELD BACK-GROUND	253.4	6.39	0.14	2.76	2.14	3.17	7	0.36	
- TREE BACK-GROUND	207.8	25.3	0.15	1.79	5.5	1.8	3	0.21	
- LARGE TARGET BACKGROUND	177.0	52.9	-0.67	2.69	23.5	3.52	8	0.81	4.24d
D. UNSHARP MASK (5x5)									
- TARGET/FIELD	199.8	21.6	-2.4	10.7	5.4	6.2	7	0.65	
- TARGET/TREE	191.5	26.2	-0.2	3.2	6.7	3.9	4	0.58	
- TARGET/FIELD-TREE	198.1	28.1	-0.57	2.7	6.8	4.1	4	0.73	
- FIELD BACK-GROUND	237.8	6.56	-0.3	2.7	1.56	2.69	8	0.83	
- TREE BACK-GROUND	207.9	25.2	0.13	1.79	5.6	1.9	3	0.2	

IMAGE	MEAN	STATISTICS STD	SKEW	KURTOSIS	SIGNAL/NOISE	SIGNAL/CLUTTER	FFT RESOLUTION	CONTRAST	FIGURE
- LARGE TARGET BACKGROUND	177.7	51.7	-0.73	2.7	12.6	3.5	8	0.69	
8. B-TV and FLIR GRAD.									
A. TV-UNPROC.	206.4	57.2	-2.6	9.5	4.99	5.02	6	0.74	4.26a
B. FLIR-UNPROC.	93.8	38.8	9.23	2.64	5.25	4.37	5	0.76	4.26b
C. TV-PREWITT (3x3)	11.1	23.8	6.4	51.7	5.07	5.0	7	0.77	4.26c
D. FLIR-PREWITT (3x3)	26.5	25.2	2.9	14.2	5.3	4.34	6	0.78	4.26d
E. TV-U. MASK (3x3)	112.6	7.3	0.44	58.6	5.16	4.97	8	0.67	4.26e
F. FLIR U. MASK(3x3)	132.3	19.1	1.1E-2	3.7	5.34	4.28	6	0.65	4.26f
9. D-TV and FLIR GRAD.									
A. TV-UNPROC.	190.0	48.1	-0197	8.61	5.02	4.96	6	0.75	r.28a
B. FLIR-UNPROC.	55.5	37.1	1.78	9.90	5.30	4.31	5	0.75	4.28b
C. TV-PREWITT(3x3)	11.5	20.5	6.5	53.9	5.08	4.91	7	0.73	4.28c
D. FLIR-PREWITT(3x3)	15.4	17.4	4.2	27.7	5.32	4.28	6	0.79	4.28d
E. TV-U.MASK(3x3)	116.8	7.4	-2.1	35.1	5.14	4.86	7	0.68	4.28e
F. FLIR-U.MASK(3x3)	125.4	15.5	8.2	6.1	5.39	4.22	5	0.71	4.28f

PROCESSED - EDGES

IMAGE	MEAN	STATISTICS STD	SKEW	KURTOSIS	SIGNAL/NOISE	SIGNAL/CLUTTER	FFT RESOLUTION	CONTRAST	FIGURE
10. MEAN THRESHOLD									
A. B-TV (GLOBAL) PREWITT									
- TARGET/FIELD	76.8	37.2	3.9	16.9	4.0	3.1	20	0.8	
- TARGET/TREE	95.9	35.6	4.2	18.9	3.7	4.6	5	1.0	4.30a

IMAGE	MEAN	STATISTICS STD	SKEW	KURTOSIS	SIGNAL/ NOISE	SIGNAL/ CLUTTER	FFT RESOLUTION	CONTRAST	FIGURE
- TARGET/FIELD-TREE	94.2	30.8	4.8	24.1	3.3	3.9	18	0.92	
- FIELD BACK-GROUND	211.8	11.0	3.6	14.3	0.8	4.2	21	0.0	
- TREE BACK-GROUND	160.8	21.3	41.8	18.5	2.1	4.0	10	0.0	
- LARGE TARGET BACKGROUND	60.4	85.4	1.84	4.39	8.0	2.52	18	1.0	4.30b
B. B-TV (GLOBAL) SOBEL									
- TARGET/FIELD	80.1	43.1	3.3	11.8	3.4	1.7	18	0.8	
- TARGET/TREE	97.7	38.9	3.8	15.4	3.1	3.5	8	1.0	
- TARGET/FIELD-TREE	95.7	34.4	4.2	18.7	2.7	2.0	18	0.92	
- FIELD BACK-GROUND	211.8	11.0	3.7	14.3	0.6	4.2	21	0.0	
- TREE BACK-GROUND	160.8	21.3	41.8	18.5	1.6	4.6	10	0.0	
- LARGE TARGET BACKGROUND	70.2	96.2	1.35	2.82	6.41	2.11	14	1.0	
C. D-TV (LOCAL) PREWITT	125.2	127.6	3.5E-2	1.0	4.2	3.5	6	0.92	4.30c
D. D-FLIR (LOCAL) PREWITT	126.1	126.5	2.2E-2	1.0	4.15	3.6	6	0.92	4.30d
11. D-TV and FLIR (LOCAL) PREWITT (T IN 3 x 3 WINDOW)									
A. TV - T = μ + .5σ	76.3	116.7	0.88	1.77	4.37	3.46	8	0.92	4.32a
B. FLIR-T - μ + .5σ	74.8	116.2	0.90	1.82	4.21	3.53	8	0.92	4.32b

IMAGE	MEAN	STATISTICS STD	SKEW	KURTOSIS	SIGNAL/ NOISE	SIGNAL/ CLUTTER	FFT RESOLUTION	CONTRAST	FIGURE
C. TV - T = μ + σ	199.2	51.4	-1.8	7.7	4.49	3.41	10	1.0	4.32c
D. FLIR - T = μ + σ	84.0	77.9	1.4	3.7	4.29	3.47	12	1.0	4.32d
E. TV - T = μ + 2σ	190.4	48.2	-1.9	8.6	4.32	3.47	16	1.0	4.32e
F. FLIR - T = μ + 2σ	56.4	39.2	2.00	10.6	4.22	3.50	18	1.0	4.32f
12. D-TV (LOCAL) PREWITT (T in 7 x 7 and 15 x 15 WINDOWS)									
A. T(7 x 7) = μ	217.6	51.7	-2.12	8.9	4.39	3.45	8	0.92	4.34a
B. T(15 x 15) = μ	105.9	125.8	0.34	1.1	4.23	3.54	8	0.92	4.34b
C. T(7 x 7) = μ+.5σ	208.1	51.1	-1.8	8.0	4.52	3.39	14	1.0	4.34c
D. T(15 x 15) = μ+.5σ	66.7	112.1	1.1	2.2	4.31	3.44	16	1.0	4.34d
E. T(7 x 7) = μ +σ	200.8	49.7	-1.8	8.0	4.35	3.45	17	1.0	4.34e
F. T(15 x 15) = μ +σ	39.6	92.4	1.9	4.6	4.24	3.50	20	1.0	4.34f
13. D-FLIR (LOCAL) PREWITT (T IN 7 x 7 and 15 x 15 WINDOWS)									
A. T(7 x 7) = μ	143.6	103.8	5.1E-2	1.2	4.45	3.41	8	0.92	4.36a
B. T(15 x 15) = μ	108.9	126.1	0.30	1.1	4.29	3.50	10	0.92	4.36b
C. T(7 x 7) = μ+.5σ	110.9	95.3	0.7	1.8	4.36	3.49	14	1.0	4.36c
D. T(15x15) = μ+.5σ	69.5	113.6	1.02	2.04	4.18	3.59	16	1.0	4.36d
E. T(7 x 7) = μ +σ	86.2	80.0	1.3	3.4	4.24	3.52	18	1.0	4.36e
F. T(15x15) = μ +σ	42.0	94.6	1.8	4.26	4.00	3.63	20	1.0	4.36f

ORIGINAL PLUS GRADIENT

| 14. B-TV | | | | | | | | | 4.38a |

IMAGE	STATISTICS MEAN	STD	SKEW	KURTOSIS	SIGNAL/NOISE	SIGNAL/CLUTTER	FFT RESOLUTION	CONTRAST	FIGURE
A. PREWITT(SEG.)									4.38a
- TARGET/FIELD	161.1	15.1	-1.6	10.9	2.4	7.7	9	0.8	
- TARGET/TREE	160.7	18.9	4.4E-2	3.5	2.7	6.5	5	1.0	
- TARGET/FIELD-TREE	160.2	18.9	-0.3	3.0	2.7	5.9	4	0.92	
- LARGE TARGET BACKGROUND	96.7	29.9	0.79	6.0	6.28	6.78	14	0.65	
B. SOBEL (SEG.)									4.38b
- TARGET/FIELD	131.5	12.6	1.7	19.2	2.4	8.7	16	0.8	
- TARGET/TREE	139.5	14.3	1.3	10.6	2.1	8.8	5	1.0	
- TARGET/FIELD TREE	13.0	14.1	0.8	8.9	2.0	7.2	5	0.92	
- LARGE TARGET BACKGROUND	79.1	29.5	1.79	8.3	5.95	7.04	17	0.60	
C. PREWITT	161.0	15.9	-1.1	8.1	2.5	7.3	8	0.8	4.38c
D. SOBEL	138.1	13.2	1.5	16.7	2.3	8.5	7	0.8	4.38d

ORIGINAL WITH EDGE REPLACEMNT

IMAGE	STATISTICS MEAN	STD	SKEW	KURTOSIS	SIGNAL/NOISE	SIGNAL/CLUTTER	FFT RESOLUTION	CONTRAST	FIGURE
15. D-TV and FLIR (LOCAL) PREWITT									
A. TV-T(3 x 3) = μ+σ	199.2	51.4	-1.8	7.7	5.54	6.47	8	0.8	4.40a
B. FLIR-T(3x3) =μ+σ	84.0	77.9	1.4	3.7	5.55	6.37	7	0.78	4.40b
C. TV-T(7x7)= μ+σ	200.8	49.7	-1.8	8.0	5.98	5.87	9	0.92	4.40c
D. FLIR-T(7x7)= μ+σ	86.2	80.1	1.3	3.4	5.92	5.80	9	0.91	4.40d
E. TV-T(15x15= μ+σ	202.5	47.6	-1.8	8.7	6.31	5.49	11	1.0	4.40e
F. FLIR-T(15x15)=μ+σ	88.3	81.6	1.3	3.2	6.27	5.48	10	1.0	4.40f

SERIAL PROCESSING

| IMAGE | MEAN | STATISTICS | | | SIGNAL/ NOISE | SIGNAL/ CLUTTER | FFT RESOLUTION | CONTRAST | FIGURE |
		STD	SKEW	KURTOSIS					
16. B-TV									
A. LAGC (5) MEDIAN (5)									
- TARGET/FIELD	159.5	26.6	-0.4	2.9	13.3	5.5	8	0.57	4.42a
- TARGET/TREE	160.8	22.4	-8.5E-2	2.9	12.1	4.8	11	0.48	
- TARGET/FIELD-TREE	169.4	26.9	-9.8E-2	2.8	12.2	4.4	9	0.75	
- FIELD BACK-GROUND	232.3	6.8	-7.9E-3	3.5	2.7	3.1	24	0.7	
- TREE BACK-GROUND	202.5	13.9	-3.1E-2	3.4	6.9	3.1	10	0.47	
- LARGE TARGET BACKGROUND	126.4	50.4	-5.1E-2	2.2	23.0	4.22	8	0.645	
B. AVG(5) HIST(EQ.)									
- TARGET/FIELD	152.1	48.4	-2.6E-2	1.8	4.7	3.8	5	0.62	4.42b
- TARGET/TREE	172.0	48.2	-1.9E-2	1.8	4.8	3.2	4	0.64	
- TARGET/FIELD-TREE	168.6	46.5	-2.4E-3	1.8	4.6	3.3	3	0.74	
- FIELD BACK-GROUND	217.9	11.7	1.6	4.5	1.3	3.6	5	0.16	
- TREE BACK-GROUND	205.9	28.5	-2.4E-3	1.8	2.8	1.5	3	0.18	
- LARGE TARGET BACKGROUND	64.8	57.3	1.65	4.8	6.5	4.0	7	0.123	

END
DATE
FILMED
9 81
DTIC

IMAGE	MEAN	STATISTICS STD	SKEW	KURTOSIS	SIGNAL/ NOISE	SIGNAL/ CLUTTER	FFT RESOLUTION	CONTRAST	FIGURE
C. MED(5) LAGC (5)									4.42c
- TARGET/FIELD	128.9	16.6	3.1E-2	3.5	4.1	8.8	10	0.21	
- TARGET/TREE	165.6	20.2	0.15	3.9	4.0	4.8	22	0.46	
- TARGET/FIELD-TREE	170.9	12.2	0.23	4.4	3.7	7.7	20	0.40	
- FIELD BACK-GROUND	231.4	4.5	0.1	4.5	1.3	4.8	6	0.5	
- TREE BACK-GROUND	206.8	10.3	0.11	5.1	2.5	4.1	23	0.5	
- LARGE TARGET BACKGROUND	112.7	30.0	0.43	3.06	5.1	6.0	11	0.322	
D. MED(5) LAGC(5)	145.2	19.5	0.15	3.51	4.15	4.74	12	0.42	4.42d

PARALLEL PROCESSING

IMAGE	MEAN	STATISTICS STD	SKEW	KURTOSIS	SIGNAL/ NOISE	SIGNAL/ CLUTTER	FFT RESOLUTION	CONTRAST	FIGURE
17. B-TV									
A. UNPROC.	206.4	57.2	-2.6	9.5	4.99	5.02	6	0.74	4.44a
B. MED+LAGC+GRAD.	144.4	22.7	-2.1	8.3	4.10	5.31	8	0.49	4.44b
C. MED(.25)+LAGC (.75)	193.4	45.0	-2.6	9.4	4.8	5.2	7	0.46	4.44c
D. MED(.75)+LAGC (.25)	166.1	27.2	-0.76	3.9	4.6	5.4	7	0.47	4.44d

18. B-FLIR

IMAGE	MEAN	STATISTICS STD	SKEW	KURTOSIS	SIGNAL/ NOISE	SIGNAL/ CLUTTER	FFT RESOLUTION	CONTRAST	FIGURE
A. UNPROCESSED	93.8	38.8	0.23	2.64	5.25	4.37	5	0.76	4.46a
B. MED+LAGC+GRAD.	76.0	20.2	0.77	4.20	4.0	5.34	7	0.50	4.46b
C. MED(.25)+LAGC (.75)	97.5	31.7	0.30	2.72	3.95	5.27	6	0.49	4.46c
D. MED(.75)+LAGC (.25)	105.4	22.6	0.80	3.50	3.90	5.43	6	0.50	4.46d

5. DISCUSSION OF RESULTS AND RECOMMENDATIONS

5.1 Results comparison. A number of comparisons can be made among the simulation results for the three general processor categories: noise reduction, contrast enhancement and clutter reduction. Of the noise reduction methods investigated, the median filter offered the most improvement without image degradation (blurring of detail). Window sizes of 3 x 3 and 5 x 5 were simulated; very little difference in image quality was observable between the two. However, the 5 x 5 window did produce a slightly smoother image.

The LAGC method ($G=1/\sigma$) for contrast enhancement had the problem that it increased high frequency noise and added clutter to the scene. Modification of the gain term to include the mean value ($G = \mu/\sigma$) greatly reduced the high frequency noise and appeared to improve contrast.

Based on the analysis in Appendix A, the optimum window size for LAGC is equal to the object size which is being emphasized. For the case of long standoff detection range, targets typically subtend only 2-5 pixels. Therefore, if the LAGC is to be implemented it should be only for those cases where the target size is small (2-5 pixels) and should use a 3 x 3 or 5 x 5 window at most. Simulations with a larger 15 x 15 window showed significant blurring of smaller image details for the $G = \mu/\sigma$ algorithm.

Of the edge detection methods investigated similar results were obtained with Prewitt and Sobel gradient operators. Local edge detection thresholds offered promise of pulling out weaker edges but showed sensitivity to the window size used in threshold calculation.

Serial combinations of processors typically produced results which suffered from bad features of each processor used. For example an averaging window (improved S/N, blurred image) in series with LAGC (enhanced contrast/resolution, increased noise level) produced an image with blurred detail and higher noise.

The serial processing option did not produce improved images in most cases.

Parallel combinations of processors did produce enhanced imagery considered to be a desirable approach for real-time enhancement of image quality (for target acquisition).

5.2 Recommended processor(s). Based on analyses and simulation results conducted during this contract effort, the following processor options are recommended for implementation into a target acquisition/target handoff system.

Figure 5.1 is a block diagram of the recommended processor option. The input image f(x,y) is median filtered to reduce noice without blurring edges. The noise cleaned image can then be processed to produce gradient or edge images and to produce an LAGC image. Output options include all possible combinations of the noise cleaned image, the LAGC image and the gradient or edge image.

For target acquisition by a human observer, all options should be available to the operator. Additionally the operator should have control of window size for median filtering for edge detection and for LAGC. The coefficients a, b & c allow output display of any processed image above or in combination with other images.
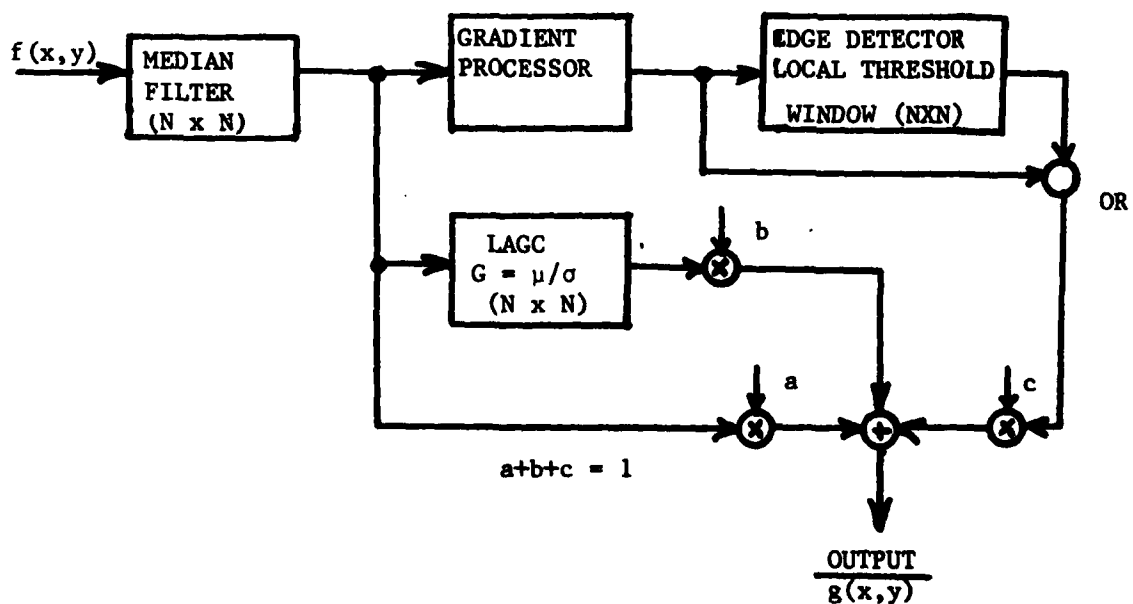
Figure 5.1   Recommended processor options

89

BIBLIOGRAPHY

1. Pinson, L. J. & Baumann, J. L. "Image Enhancement for Man-in-Loop Target Acquisition Systems," Presented at MICOM Conference on Autonomous Acquisition for Missile Guidance, Redstone Arsenal, AL. Nov. 19-20, 1979.

2. Bailey, H., "Target Detection, Through Visual Recognition: A Quantitative Model", RM6158-PR, RAND Corp., Feb. 1970.

3. Nahin, Paul J., "A Simplified, Derivation of Frei's Histogram Hyperbolization for Image Enhancement", IEEE Trans. on Pattern Analysis and Machine Intelligence, Vol. PAMI - 1, No. 4, Oct. 1979.

4. "Automated FLIR Enhancement Techniques for Second Generation FLIR", Honeywell Final Report 77SRC93, Dec. 1977 (Contract No. DAAG53-76-C-0195).

APPENDIX A: LAGC ANALYSIS

Local area gain control is a method whereby the gain applied to the center pixel within a window varies with statistics of all pixel values within the window. Variations of this method have been applied to forward looking infrared (FLIR) imagery and analyzed for application to TV imagery. This Appendix presents a quanitative parametric analysis and evaluation of one version of the local area gain control processing method.

If the input image $f(x,y)$ is processed using the LAGC to give output image $g(x,y)$ then the following relationship results.

$$g(x,y) = G\left[f(x,y) - m_{AB}(x,y)\right] + km_{AB}(x,y) \qquad (A-1)$$

where: $-m_{AB}(x,y)$ is the mean pixel value within an A x B window centered about pixel (x,y).

- $G = C/S_{AB}(x,y)$ is the adaptive gain applied to the center pixel with mean value removed.

$-S_{AB}(x,y)$ is the standard deviation of pixel values within the A x B window.

−C and k are constants which control the gain magnitude and relative mean value added back to the signal.

Steps in the procedure are shown in Figure A.1 . LAGC is a non-linear adaptive processor which enhances low contrast sub-regions in an image without causing high contrast regions to saturate the display dynamic range. For analysis of certain parametric effects a one-dimensional model (input $f(x)$, output $g(x)$ and window length L) is used with simple sinusoidal and square wave patterns as input images. This allows the evaluation of otherwise complicated analytical expressions and gives results which are easily relatable to standard MTF and bar pattern contrast measures.

91
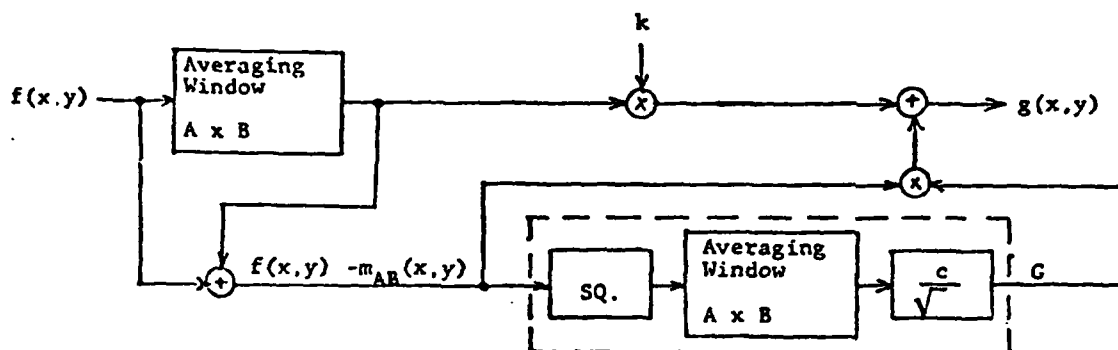
Figure A.1. Local area gain control (LAGC) method.

For the LAGC method the following evaluations were accomplised:

- Gain (or sigma) dependence on window size (L) and position (x) for sine and square wave images

- Contrast transfer computed as the ratio of modulation contrast of $g(x)$ and $f(x)$ for sine and square wave images (peak and average values over one period) as functions of window size (L).

- Simulation with known simple image waveforms (sine and square). Plot of $f(x)$ and $g(x)$. (Various L values.)

- Simulation with typical TADS imagery.

Further needed evaluation includes an analysis of the effects of noise and development of relationships showing depandence on scene spectral content.

Gain (Sigma) Analysis

For the one-dimensional model equation(A-1)becomes

$$g(x) = \frac{1}{s_L(x)} \left[f(x) - m_L(x) \right] + m_L(x) \quad . \tag{A-2}$$

For a sine or square wave, it is convenient to define the window size (L) in terms of fractions of a period as shown in Figure A.2 . Then the averaging window and its Fourier transform are given by

$$w(x) = \frac{1}{a} \text{ rect } \frac{x}{a} \tag{A-3}$$

and $\quad W(\beta) = \text{sinc } (\beta a) = \text{sinc}\left(\frac{\beta}{\beta_0} L\right) \tag{A-4}$

Calculation and removal of the mean value is a linear operation so that sinusoidal frequency content is preserved and we get for the sine wave input

$$f(x) - m_L(x) = \left[1 - \text{sinc } (L)\right] \sin 2\pi\beta_0 x \tag{A-5}$$

which is a sine wave at the same frequency with a magnitude determined by the window length (L). Integer values of L (i.e. multiple periods) give correct mean value estimates $f(x) = 0$ and $f(x) - m_L(x) = f(x)$. Most significant errors in $m_L(x)$ occur for L a small fraction of the sine wave period.

Computation of sigma for the sine wave input is accomplished by

$$s_L(x) = \left\{\left[f(x) - m_L(x)\right]^2 * w(x)\right\}^{\frac{1}{2}} \tag{A-6}$$

Using (A-3) and (A-5) in (A-6) gives for the standard deviation

$$s_L(x) = \left[1 - \text{sinc } (L)\right] \left[\frac{1}{2} - \frac{1}{2} \cos\left(2\pi \left(2\beta_0\right) x\right) \text{sinc } (2L)\right]^{\frac{1}{2}} \tag{A-7}$$

and the gain for sine wave input is the reciprocal of equation (A-7).

$$G_L(x) = 1/s_L(x) \tag{A-8}$$

A two dimensional perspective plot of $s_L(x)$ vs. L and x is shown in Figure A.3. The surface is relatively smooth and approaches a value of $\sqrt{2}$ for large L. The figure shows only slight dependence on x. More detailed dependence is shown if Figure A.4 where $s_L(x)$ is plotted vs. L for selected values of x. The gain $(1/s_L(x))$ tends to blow up for small values of L which may cause some processing difficulty. It is expected from this analysis that the gain may need to be limited to some maximum value even though, in computing $g(x)$, the high gain will usually be partially compensated by multiplication with a small difference signal $f(x) - m_L(x)$. This compensating effect is apparent in the simulations to be shown later.
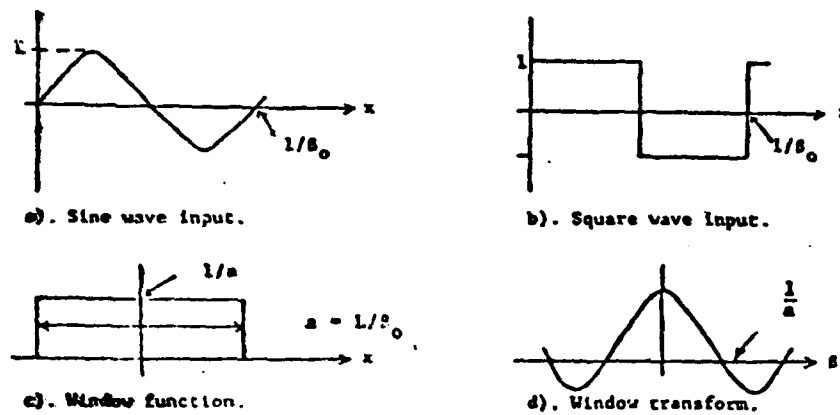
93

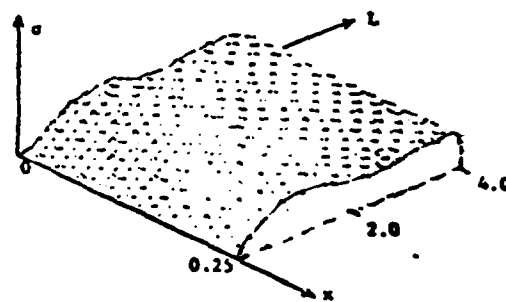Figure A.2   Input waveforms and window function
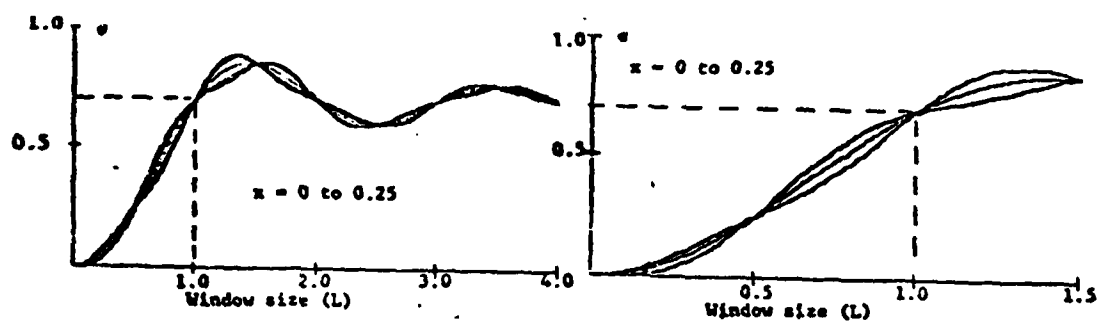

Figure A.3   Sigma for sine wave input

Figure A.4   Sigma versus window size (sine)

94

For the square wave input waveform a similar analysis is performed; the major difference is that the harmonic frequency content of the square wave complicates expressions for $s_L(x)$ and $G_L(x)$. A linear analysis gives the mean removed signal for the square wave.

$$f(x) - m_L(x) = \sum_{\substack{n=1 \\ n \text{ odd only}}}^{\infty} \frac{4}{n\pi} \left[1 - \text{sinc}(L) \right] \sin 2\pi n \beta_0 x \qquad \text{(A-9)}$$

Then using (A-3) and (A-9) and (A-6) gives after some manipulation the square wave standard deviation

$$s_L(x) = \sum_{\substack{n=1 \\ n,m \text{ odd only}}}^{\infty} \sum_{m=1}^{\infty} \frac{8}{nm\pi^2} \left[1 - \text{sinc}(nL) \right] \left[1 - \text{sinc}(mL) \right]$$

$$\left\{ \left[\text{sinc}(n-m)L \cos\left(2\pi\beta_0 (n-m) \ x \right) - \text{sinc}(n+m)L \cos 2\pi\beta_0 (n+m)x \right] \right\}^{\frac{1}{2}} \qquad \text{(A-10)}$$

Figure A.5 shows $s_L(x)$ for the square wave input as a function of L for various x. Harmonics through n,m=9 were used in the computation.
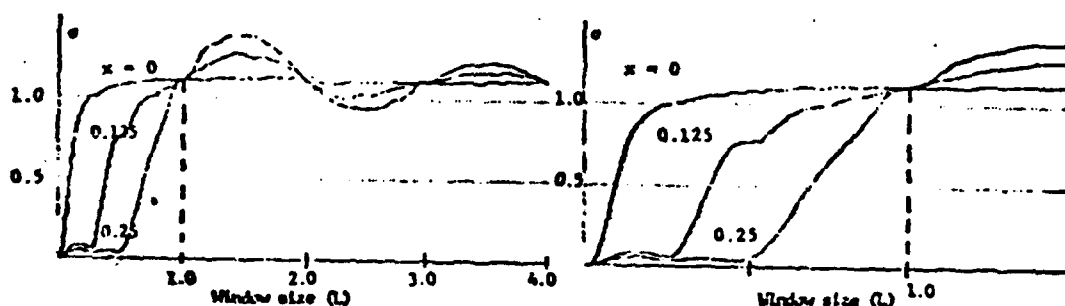

Figure A.5 Sigma for square wave

Modulation Contrast Transfer

For the input signal $f(x)$, we define peak and average modulation contrast in a window (L) by

$$M_p(L) \triangleq \left(\frac{f_{max} - f_{min}}{f_{max} + f_{min}} \right)_L \qquad \text{(A-11)}$$

95

and

$$M_a(L) \triangleq \left(\frac{f_1 - f_2}{f_1 + f_2}\right)_L \tag{A-12}$$

where f_{max} and f_{min} are the maximum and minimum pixel values in window L. Definitions for f_1 and f_2 are based on averages over equal areas of light and dark. For the sine or square wave signals f_1 is the average pixel value over the positive half period and f_2 is the average pixel value over the negative half period.

Using these definitions for modulation contrast it is possible to define the contrast transfer ratios

$$R_p(L) = \frac{M_p(L) \text{ output}}{M_p(L) \text{ input}} \tag{A-13}$$

$$R_a(L) = \frac{M_a(L) \text{ output}}{M_a(L) \text{ input}} \tag{A-14}$$

Equations for $R_p(L)$ and $R_a(L)$ were simulated on a small computer. Results are shown in Figure A.6 for both the sine and square wave inputs. Significant features of the result are that even for small values of L, there is an increase in both peak and average modulation contrast $(R_p, R_a > 1)$ and this increase levels off at a stable value for large L.
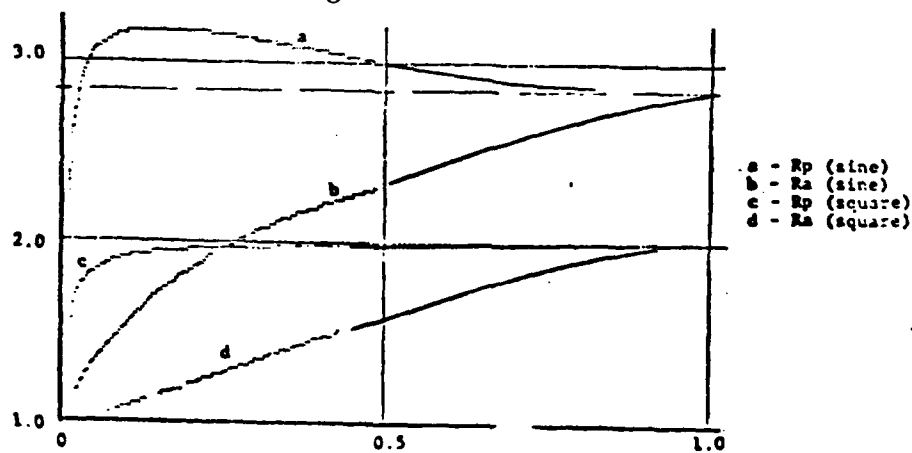
Figure A.6 Transfer of modulation contrast

a). L = 0.016   b). L = 0.125   c). L = 0.25

d). L = 0.5   e). L = 0.75   f). L = 1.0
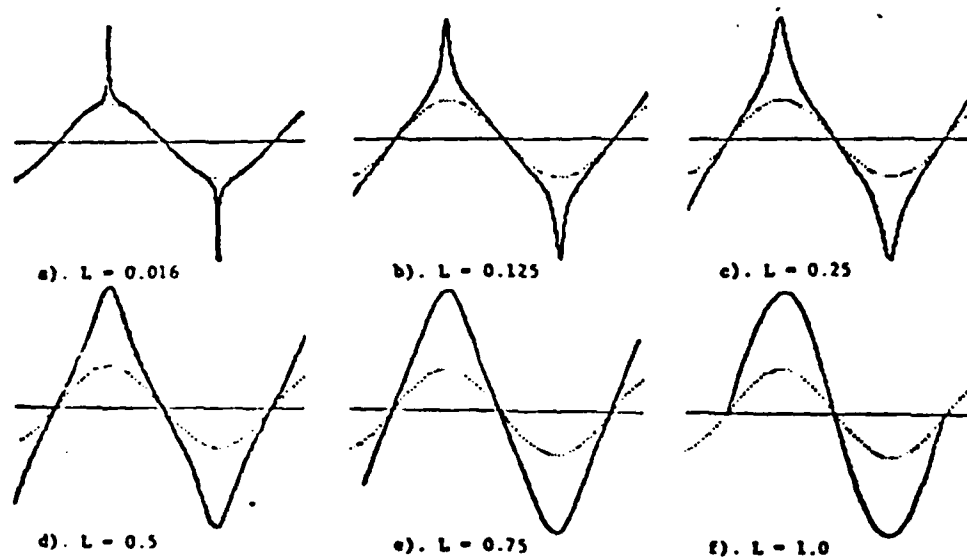
Figure A.7 LAGC output (solid line) for sine input
(dotted line) of amplitude 1.0

Simulation Results

Computer implementation of the LAGC method was accomplished and the method
was applied to simple (sine and square) waveforms for various window sizes (L).

Figure A.7 shows the simulation reslults for six different L values for the
sine input. Both input and output waveforms are shown (input is lower magnitude
in every case). Figure A.8 shows similar results for the square wave input.

97

Conclusions

From the analysis and simulation results it is evident that the LAGC image processing method improves modulation contrast and thus offers the potential for improving target detection/recognition by an observer. It is also clear that the non-linear nature of the method produces frequency distortion which depends on window size. Optimization of the value of L dependent on expected target size is recommended.

a). L - 0.0.16   b). L - 0.125   c). L - 0.25

d). L - 0.5   e). L - 0.75   f). L - 1.0
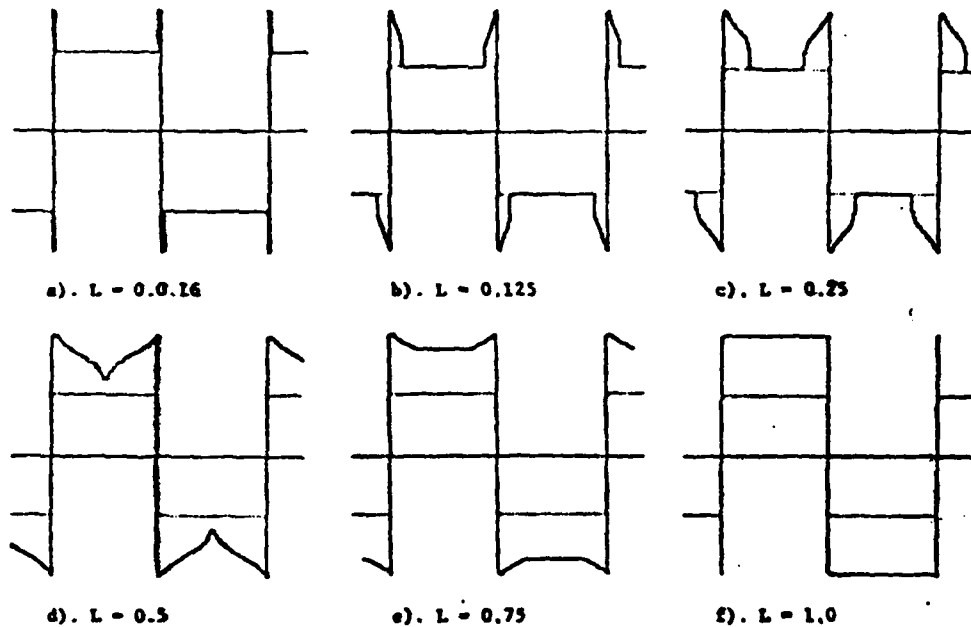
Figure A.8   LAGC output (solid line) for square wave input (dotted line)
of amplitude 1.0

DISTRIBUTION

No of Copies

Program Manager Advanced Attack Helicopter
ATTN: DRCPM-AAH, MG E. Browne   1
4300 Goodfellow Blvd
St Louis, MO 63120

Project Manager
TADS/PNVS
ATTN: DRCPM-AAH-TP, COL D. Wray   1
                    S. Smith   1
4300 Goodfellow Blvd
St Louis, MO 63120

Commander
US Army Aviation Systems Command
ATTN: DRSAV-EV, D. Weller   1
4300 Goodfellow Blvd
St Louis, MO 63120

Commander
US Army Aviation Center
ATTN: ATZQ-TSM-S   1
       ATZQ-TSM-A   1
       ATZQ-D-MS   1
Ft Rucker, AL 36360

Commander
Headquarters TCATA   1
ATTN: ATCAT-CAD-TA
Ft Hood, TX 76544

Commander
Headquarters TRADOC
ATTN: ATCD-CM   1
Ft Monroe, VA 23351

Program Manager
Advanced Scout Helicopter
ATTN: M. Jackson   1
4300 Goodfellow Blvd
St Louis, MO 63120

IIT Research Institute
ATTN: GACIAC   1
10 West 35th Street
Chicago, IL 60616

```
Commander US Army Armament R&D Command
Picatinny Arsenal
ATTN:   Dr. Gyorog                                            1
        DRDAR-FCD-W                                           1
Dover, NJ  07801


Commander US Army Electronics R&D Command
ATTN:   DRSEL-TL-I, Dr. Jacobs                                1
        DRSEL-CT, Dr. R. Buser                               1
        DELET-M, Mr. Walt Gelnovatch                         1
                Mr. N. Wilson                                1
        Ft Monmouth, NJ  07703


Commander
US Army Electronics Command
NV&EOL
ATTN:   DELNV-SI, John Johnson                               1
Ft Belvoir, VA  22060


Commander
US Army Training and Doctrine Command
Ft Monroe, VA  23341                                         1


Commander
US Army Combined Arms Combat Development Activity            1
Ft Leavenworth, Kansas  66027


Commander
US Army Armor Center
Directorate for Armor Aviation
ATTN:   ATSB-AADO-MS, LTC Don Smart                          1
Ft Knox, KY  40121


Headquarters
Department of the Army
ATTN:   DAMA, WSM, MAJ Belch                                 1
Washington, DC  20310
```

DRSMI-IYB, Mr. Ingram   1

University of Tennessee Space Institute   10
ATTN: L. J. Pinson
Tullahoma, TN 37388

Texas Instruments
ATTN: Dr. Jack Pridgen   1
PO Box 6015
Dallas, TX 75222

Goodyear Aerospace Corporation
ATTN: H. Pfeiffer   2
Akron, Ohio 44315

Lockheed Missiles and Space Company
ATTN: Dr. James Pearson   1
3251 Hanover Street
Palo Alto, CA 94304

Martin Marietta Aerospace
ATTN: Charles R. Layne MP 142   1
       Max W. Farrow, MP 544   1
PO Box 5837
Orlando, FL 32855

RCA Government Systems Division
ATTN: Richard Foley   1
Camden, NJ 08102

TASC
ATTN: Martin Svedlow   1
6 Jacob Way
Reading, MA 01867